AD631407

Department of Industrial Metallurgy.

University of Birmingham.

Research on Hot Working of Metals, with particular

reference to microstructure, mechanical properties and texture

by   I.L. Dillamore and W.T. Roberts.

Technical Report   (Final)

January 1961 - April 1964.

(i)
CONTENTS

SECTION 1.

(ii)

CONTENTS (contd)

Best
Available
Copy

1. Structure and Mechanical Properties of Deformed Copper.

1.1. Introduction.

The inhomogeneous nature of plastic deformation of metals on a microscopic scale is well known. Manifestations of this inhomogeneity are slip lines, deformation bands, deformation twins and subgrains. Observations of the structure of deformed metal have been made by various methods summarised in Table 1.

Table 1.

Technique	Indications	Limitations.
Optical microscopy of metal surface	Surface steps due to emergence of slip lines, surface tilts due to deformation bands and twins.	Surface behaviour may not be representative of interior.
Optical microscopy of etched sections.	Various types of markings related to those observed on surface.	Difficult to reveal some Types of markings, especially in pure metals.
X-ray microscopy.	Regions of misorientation – especially deformation bands.	Very limited linear resolution.
X-ray microbeam diffraction	Subgrains-linear dimensions, angular misorientations and degree of distortion.	Resolution difficult below about 1 micron.
Thin film transmission electron microscopy.	Dislocation distributions. Sub-grains, types of boundaries. Twins.	Possible changes in distribution during thinning.

The observations pertinent to the deformation of copper will be discussed below, but in some instances it may be necessary to quote work on other metals.

Slip bands, deformation twins and deformation bands.

A systematic study of the markings observed on etched deformed copper and copper-base alloys has been made by Samuels[1] and Hatherly[2]. The type 1 markings referred to by Samuels[1] are straight parallel lines spaced at a distance apart of about one micron, and these correspond with the slip lines observed on the surface. Type III markings observed in copper appear to be due to slip on two sets of planes, but the author is less definite about the

nature of these markings. Type IV markings are faint surface undulations which are probably deformation bands. Kuhlmann-Wilsdorf and Wilsdorf[3] have suggested that the differential etching occurs because the slip areas are thermodynamically unstable owing to the presence of piled-up dislocations.

Hatherly[2] examined polycrystalline copper deformed by hammering at -183°C and observed very wide strain markings reminiscent of the deformation twins observed by Blewitt et al[4] in single crystals of copper strained at 77°K and 4.2°K. Similar features have been observed by Smith[5] in copper at room temperature subjected to plane shock waves of high intensity. There now seems quite a body of evidence that deformation twinning is frequent in copper deformed at very high rates of strain at moderate temperatures and in copper deformed more slowly at low temperatures.

Blewitt et al[4] observed an orientation dependence of twinning, crystals with the tension axis close to $\langle 111 \rangle$ twinning more readily than other orientations. They concluded that the critical resolved shear stress law does not operate for twinning under their conditions, but Venables[6] quotes a critical shear stress of 15 kg/mm^2 for twinning in copper at 77°K. Both workers agree that copper twins mainly on the primary slip plane, but Blewitt observed twins on the conjugate plane in irradiated copper, and Venables observed twins on the primary, conjugate and critical planes in copper alloys.

Deformation bands are lamellar regions within different orientations have arisen as a result of slip, the orientation difference between adjacent bands increasing as deformation proceeds[7]. Honeycombe[8] makes a distinction between two different types of deformation bands, - kink bands and bands of secondary slip.

Investigations into the nature of deformation bands have been made on single crystals and X-ray microscopy has often been used to reveal the presence of bands. It has generally been observed that f.c.c. crystals deforming by primary slip show kink bands[8,9,10], the boundaries of which are parallel to (110) planes lying perpendicular to the primary slip plane. Bands of secondary slip were observed by Honeycombe[8] in most orientations, but they were particularly prominent in orientations initially favourable for duplex slip. It would therefore appear likely that this type of band will occur more frequently in polycrystalline material, although there is no direct evidence for this statement.

The appearance of deformation bands varies with changing deformation temperature. Sawkill & Honeycombe[11] observed that in single crystals of gold, the prominence and spacing of kink bands increased with increasing temperature, and Andrade and Aboav[12] made a similar observation on copper single crystals.

There is no information on the temperature dependence of bands of secondary slip.

Substructure.

The first quantitative estimates of the size of sub grains formed in worked metal were made from measurements of the broadening of X-ray diffraction lines[13]. The method was very indirect and subsequent measurements have indicated that the values obtained by this method were generally too low. A more direct method for the study of substructure became available with the development of X-ray microbeam diffraction techniques[14], when it was possible to resolve reflection spots from individual subgrains. Mean sub grain diameters were determined by counting spots on a Debye ring, the mean boundary angle could be roughly estimated and in some instances, the distortion within the subgrains could be determined. For all metals, the mean subgrain diameter decreased rapidly to a lower limiting value with increasing deformation, provided that recrystallisation did not occur at room temperature after deformation.

The results for copper[15] with an initial grain size of 0.02mm deformed by rolling at room temperature indicated that the mean subgrain diameter decreased to about 4μ after 3% deformation, to 2.8μ after 7% deformation and to a limiting value of about 0.6μ. The total angular misorientation within one original grain increased from about $1\frac{1}{2}^{\circ}$ after 3% deformation to about 15° after 50% deformation, but the relative misorientation of two subgrains contributing to adjacent reflections was more difficult to estimate. A value of about $\frac{1}{2}^{\circ}$ misorientation after 10% deformation increasing to about $1\frac{1}{2}^{\circ}$ after 50% deformation was calculated[16].

The subgrains in these investigations were interpreted as the regions between dislocation pile-ups locked on the active slip systems, in kink bands or against sessile dislocations[17]. The implication that the mean subgrain diameter should be the same as the limiting slip band spacing was experimentally verified for a number of metals.

The advent of transmission electron microscopy of metals[18] provided a direct method for the study of dislocation distributions in cold worked metals. In general, the results obtained by this technique have confirmed the results of X-ray microbeam diffraction experiments. Because of the many advantages of the electron microscope method, it has now largely superceded the X-ray diffraction method, and the recent observations of substructure in copper which will be referred to in the following paragraphs have been made by electron microscopy.

Warrington[19] studied the substructure in copper deformed over a range of temperatures from -196°C to 750°C. In any single specimen, subgrain dimensions varied by a factor of ten at the lower deformation temperature, and a statistical mean diameter is quoted in addition to the range. His results are summarised in table 2.

Table 2.

Deformation Temp. °C		-196	0	100	200	300	400	650	750
Subgrain Size (μ)	Max.	1.5	2.0	2.0	3.3	3.0	3.3.	10.5	
	Min.	0.2	0.3	0.4	0.5	0.5	0.8	4.0	
	Average	0.6	0.9	1.0	1.2	1.4	1.8	7.0	15
Estimated boundary width (Å)		1500	1500	1250	1000	750	500	-	-

The subgrain boundary walls tend to lie parallel to low index crystallographic planes. Warrington found walls parallel to (100), (110) and, to a lesser extent (111), the alignment becoming more pronounced at higher deformation temperatures. On the other hand, Howie[20] reports that the walls are more often parallel to the primary and conjugate slip planes during stage III of the deformation of copper single crystals. The dislocations in the subgrain walls are arranged in an irregular manner and a general observation is that small subgrain diameters are associated with more ragged walls.

A detailed study of dislocation configurations in copper single crystals at various stages of the tensile stress-strain curve has been made by Steeds[21]. In the easy glide region, patches of dipoles parallel to $\langle 112 \rangle$ were observed. The dipoles were about 1 micron long and 100 Å wide. At the beginning of Stage II, marked local activity on the secondary planes were observed, with evidence on interactions between primary and secondary dislocations. Tangles of dipoles and forest dislocations later became aligned along traces of secondary planes, but as deformation proceeds, there is an increasing tendency for the tangles to become more irregular and to lie out of the slip planes. At the end of stage II, the tangles form a ragged subgrain structure of about 5 microns diameter. In Stage III, subgrains are formed with boundaries parallel to the primary slip plane spaced at about one or two microns apart, with other boundaries perpendicular to the slip plane.

- 5 -

Relation between structure and mechanical properties.

The effectiveness of deformation bands and subgrain boundaries as
barriers to plastic deformation has been studied by a number of workers.
Many[7,8,22] suggest that deformation bands contribute greatly to work harden-
ing, acting in much the same way as grain boundaries. On the other hand
Mott[23] considers that deformation bands should have little or no effect on
hardening.

More quantitative evidence is available on the relation between subgrain
size and work-hardening. Gay, Hirsch and Kelly[14] first suggested that the
subgrain size and the flow stress are related by

$$\sigma = Kt^{-\frac{1}{2}}$$

where σ is the flow stress, K is a constant and t is the subgrain diameter.
Ball[24] arrived at the rather surprising result that in α-iron the
angular misorientation across a subgrain boundary does not seem to affect its
strength. In these experiments, the angular misorientation and the subgrain
size were varied simultaneously and a multiple linear regression analysis was
made. Although the statistical analysis is valid and leads to a small partial
correlation coefficient between angle of misorientation and yield strength,
the method for determination of angles is very approximate and more precise
measurements of this variable are desirable.

It is evident, however, that subgrain boundaries are less effective
barriers to slip than large angle boundaries. Ball reports a value of k,
the slope of the line $t^{-\frac{1}{2}}$ plotted against flow strength, for sub boundaries
in polygonised iron which is about half of that for high angle boundaries. A
more recent investigation[25] indicates that the contribution of sub boundaries
to strength in zone refined iron is small compared with the effect of
interstitial-substructure interaction.

An alternative expression for the flow strength

$$\sigma = kN^{\frac{1}{2}}$$

where K is a constant and N is the dislocation density expressed in lines per
sq.cm, has been proposed by Blewitt et al[26]. This relation has been verified
for polycrystalline silver by Bailey and Hirsch[27] by direct counting of
dislocation lines in the electron microscope.

Since N and t are related, the two expressions may both be valid; further discussion of the point occurs later.

1.2. Experimental.

In all of the experiments described in this section, the material used was OF.H.C copper. Most of the work was carried out using $\frac{5}{8}$" diameter extruded rod which, in the as-received condition, was slightly work-hardened. This rod was cut into cylinders $\frac{5}{8}$" high before annealing in vacuo for one hour at 800°C. This treatment was to ensure that a large stable grain size was obtained so that subsequent reheating to the testing temperature would cause no change in the grain structure. The average grain size was 8 grains/mm^2.

Smaller cylinders were required for flow stress determinations after deformation, and these were obtained by swaging the as-received rod to 0.271" diameter with two intermediate anneals of half an hour at 500°C. The swaged rod was cut to give parallel ended cylinders 0.271" high before finally annealing in vacuo for one hour at 800°C. The grain size obtained by this treatment, 8 grains/mm^2, was the same as for the larger cylinders.

The cylinders of both sizes had a pronounced $\langle 111 \rangle$ fibre texture in the final condition, and in all cases of uniaxial compression, the compression axis was parallel to the fibre axis.

A small section of the investigations was concerned with rolled material. This was received in the form of one inch thick hot-rolled slab which was subsequently rolled down to 0.1" thickness with two intermediate anneals each of half an hour at 500°C and a final anneal of one hour at 650°C. The grain size obtained in this way was 250 grains/mm^2.

High strain rate deformation by forging.

High strain rate compression was carried out on a drop-hammer. The construction of the drop-hammer is shown in Fig.1. An 84 lb.weight is raised by means of a cable and connected to the cable by an electro-magnet. Cutting off the current to the electro-magnet releases the weight and allows it to fall and strike a punch. The punch is supported on a spring and retained in a cast iron case (Fig.2.) and, on being struck by the weight, is projected downwards to make contact with the cylindrical specimen which rests on an anvil.

The weight is a lead-filled welded steel can to which is attached at the lower end by high tensile bolts an alloy steel striker piece, a cylinder 6" long by 4" diameter. The punch is of EN.24 steel hardened

and tempered at $500^{\circ}C$ to give an optimum blend of strength and toughness. The section of the punch, as shown in Fig.2, is three coaxial cylinders. The lower cylinder, that of the smaller diameter, is the impacter; the central cylinder rests on the spring and the upper section, which is too large to enter the cast iron case, enables stops limiting the amount of deformation to be bolted to the top of the cast iron case. The spring supporting the punch is strong enough to prevent the punch from striking the specimen a second time after rebounding. The anvil is made of a high tungsten steel and is bolted to a base plate sunk into a reinforced concrete block resting on shock absorbers.

A quenching device, used for rapidly cooling the specimens deformed at high temperatures, is incorporated with the drop-hammer. An electromagnet is used to hold a water-pipe against the opposing action of a coil spring, so as to direct the water jet to one side of the anvil. Cutting off the current to the electromagnet allows the spring to contract and deflect the water jet on to the anvil. The jet sweeps the specimen off the anvil into the surrounding water-containing can. For deformation at room temperature, the water jet was played on the specimen throughout the deformation to minimise the heating effect of deformation.

For deformation at elevated temperatures the specimen was heated to the required temperature in a small tube furnace, withdrawn and placed on the anvil, and at the same time the power was cut off from the electromagnet supporting the weight. The power was also cut off from the quenching device electromagnet immediately upon impact in order to give a rapid quench. A few specimens were deformed at liquid nitrogen temperature and for these the specimen was cooled in a bath of liquid nitrogen immediately before being deformed. No quenching was used in this case.

In all of the experiments, the anvil and the punch were coated with graphite, applied in the form of a colloidal suspension in acetone. This was found to give very good lubrication and to minimise the inhomogeneity of deformation.

The height of drop of the weight before making contact with the punch was standardised at 10 feet, and the amount of deformation was varied by bolting hard rolled brass rings of various thicknesses to the top of the cast-iron punch housing.

The strain-rate in drop forging was measured by high-speed cine photography, the details of which are described later.

Slow strain rate deformation by compression.

Slow strain rate deformation was carried out on a hydraulic press using the compression jig shown in figure 3. This was constructed with a long lower platen so that a tube furnace could be placed around the specimen position on the lower platen during deformation, and so that the furnace could be lowered clear of the specimen to allow its rapid removal. The furnace is supported at either side by wires which run over pulleys and are connected at the other end to weights which counterbalance the furnace.

For deformation at high temperatures, the furnace was raised into position around the specimen and a thermo-couple introduced via a silica tube running perpendicular to the furnace tube, and placed such that the axis of the silica tube bisected the furnace tube axis. The thermo-couple was placed in contact with the specimen and, when it showed that the specimen had reached the furnace temperature, the hydraulic press was switched on and deformation commenced.

The rate of oil feed to the hydraulic press was the same for deformation at all temperatures. The amount of deformation could be judged from a dial-gauge and, just before the required deformation was reached, the furnace was lowered clear of the specimen. When the pressure was removed, the specimen was impelled manually into a water bath.

For deformation at liquid nitrogen temperature, a container was placed on the lower platen and around the upper platen. This was kept topped up with liquid nitrogen during deformation.

It was found that efficient lubrication was obtained by coating the specimen with graphite before pre-heating, except at the highest temperature of deformation, $600^{\circ}C$, when the graphite coating started to break down.

Deformation by rolling.

Samples 6" long by 1" wide by 0.1" thick were heated to the required temperature in a tube furnace, rapidly withdrawn and passed between the rolls. On emerging from the rolls, the strip was quenched. A Taylor and Challen two high 10" mill running at 100 ft/min. peripheral roll speed was used, giving a strain rate of 20"/ $\cdot$ /sec.

Strain-rate determination.

The strain-rate in compression on the hydraulic press was obtained by plotting displacement-time curves obtained directly by taking dial gauge readings at 30 second intervals. The instantaneous strain rate, the slope of the displacement-time curve divided by the specimen height at that instant, was determined over the

full range of deformation at each of the temperatures used. Graphical summation gave mean strain rate versus percentage deformation curves.

In order to determine the strain-rates in drop-forging, high speed cine films were taken showing the interaction between the punch and the specimen at the five deformation temperatures. A 16 mm. Fastax high speed cine camera capable of a maximum framing speed of about 5000 frames per second was used. In a single experiment 100 feet of film were used in 1.1 sec., the camera attaining its maximum speed 1/3 or $\frac{1}{2}$ sec. after starting. The camera was started when the current was cut off from the electromagnet supporting the weight, and the film was then moving at almost full speed when the weight struck the punch. An internal calibration of the speed of the film was provided by a neon lamp inside the camera which flashed 100 times per second. Illumination was obtained by placing a diffusing screen between the object and a xenon filled cold cathode discharge lamp operating at 1 kw. Kodak Tri-X film was used, with the lens aperture set at f.8.

Five films taken at the five deformation temperatures were supplemented by a sixth showing the interaction between the weight and the punch when the specimen being deformed was at room temperature. The displacement-time curve obtained from this last mentioned film is reproduced in figure 4 and serves to indicate the sequence of events. Zero displacement corresponds to the position of the punch at rest. The weight approaches the punch, meeting it at A. The weight and punch meet on one frame and are apart again on the next, the time interval corresponding to an elastic wave reflection from the first shoulder of the punch.

The punch then carries on and strikes the specimen at B. When deformation has proceeded to the point C, the energy of the punch has been absorbed, and the punch comes to rest until the weight catches up with it. Punch and weight then carry on together until, at point D, all the energy has been absorbed. The punch, anvil and spring recoil, and subsequently the weight and punch bounce on the spring several times before coming to rest. Punch and specimen do not come in contact again, even if the specimen is not swept from the anvil by the water jet.

The displacement-time curves for the six films were obtained by projecting the film onto a screen at 50x magnification and by measuring frame by frame with a ruler. Strain-rate versus deformation curves were obtained from the displacement-time curves in the same way as for the slow strain rate deformation. The forging strain-rate versus percentage deformation curves showed a break due to the double impact. The break occurred at 25% at 196°C, 28% at 20°C, 29% at 300°C, 31% at 450°C and 33% at 600°C.

The curves of mean strain rate versus percentage deformation for both forging and slow compression are reproduced in Fig. 5.

Flow-Stress determination.

In order to determine the flow-stress subsequent to deformation, either on the drop-hammer or the hydraulic press, it was necessary to use the small compression specimens. Deformation was carried out in exactly the same way as for the larger specimens, except that a smaller drop-height was used to retain the same initial strain-rate in the case of forging.

The flow-stress was determined at room-temperature on a Hounsfield tensometer. It was taken to be the point of intersection of the elastic line with a straight line drawn through the first few points in the plastic region of the stress-strain curve. When work-softening occurred, the upper yield stress was taken for the flow-stress value.

Metallography.

Deformed compression specimens were sectioned parallel to the compression axis, half being used for metallography and the other half for hardness measurements. The section used for metallography was ground on waterproof emery paper and electro-polished in Jacquet's[28] ortho-phosphoric acid bath. This bath, consisting of 70% orthophosphoric acid and 30% water, is operated at about 9 amps/dm^2 and 2 volts. A polishing time of about 15 minutes is required. Jacquet also recommends this bath for electro-etching for a short time under much reduced voltage, 0.15 volts, and later with the anode and cathode shorted across. It was found, however, that better results were obtained if etching was carried out in the polish-attack regions, i.e. with the voltage reduced to just below the polishing plateau. A time of 30 seconds was used for etching.

Electron Microscopy.

Rolled material which was examined under the electron microscope was initially thinned .080" to .002" in a chemical polishing solution of 20% HNO_3, 10% HCl, 20% H_3PO_4 and 50% CH_3COOH. The solution was maintained at $60^{o}C$ during thinning from .080" to .020", but at this stage the edges were blanked off with "lacomit" and polishing continued with the solution cold. The specimen was repeatedly inverted during thinning to avoid uneven thinning, and each time perforation appeared at the edge of the stopping-off medium,

a further coating was applied to cover the perforation. On reaching .002"
thickness, the thinning procedure was continued by electro-polishing in a
70% phosphoric acid bath. This was initially operated at 4 volts, but after
the first perforation the edges of the specimen were again blanked off and
the specimen returned to the bath, which was now operated at 2 volts. Thinning
was continued using the window technique, and foils were cut from the centre
of the specimen.

In the case of forged specimens, a disc .050" thick was machined from
the centre of the deformed specimen. Almost half of the thickness was
machined from either end of the cylinder on a lathe taking cuts of .001"
under a copious flow of coolant. The .050" thick disc was thinned in the
same way as the rolled material.

The foils were examined on a Phillips E.M.75 electron microscope
operating at 75kV. This instrument is not entirely suitable for thin film
electron microscopy of metals, but was adequate for the determination of
sub-grain dimensions and for more general observations on the sub-grain
structure. The lack of selected area di fraction facilities did not prevent
orientation determinations in the present work; since most of the foils had a
grain size of 8 grains/mm^2, the electron beam only rarely covered more than
one grain, and it was possible to infer to within a few degrees the orientation
of the area under observation.

A few foils were examined for particular features on a Metropolitan-Vickers
E.M.6. electron microscope operating at 100 kV.

Microbeam X-ray diffraction.

The method first described by Hirsch and Kellar[14] was used to determine
the sub-grain sizes of material rolled at the four different temperatures.

A Hilger microbeam X-ray unit with a copper target was the source of
X-rays. A beam divergence of 3×10^{-3} radians was obtained by having a focal
spot size of 100 μ and taking off X-rays at an angle of 6° through a 50 μ pinhole.
A specimen-film distance of 1.98 cm was used. The method recommended by
Gay and Kelly[15], in w.ich the cassette is loaded with two films to avoid
inaccuracies due to different conditions when two seperate exposures are made,
was employed and the factor $ln \frac{t_1}{t_0}$ in the expression:-

$$N_1 - N_0 = \frac{A.p. \cos\theta \quad (d\theta + \Delta)}{2.v.\mu. \quad (1-\sec 2\theta)} \log \frac{t_1}{t_0}$$

was given numerically as 2.5.

In the above expression, N is the number of spots on the particular Debye
ring under consideration. The suffixes 1 and 0 refer to the films nearer to

the specimen and further from the specimen respectively.   v is the sub-grain volume, A is the area of specimen in the X-ray beam, Θ is the Bragg angle, μ is the linear absorption coefficient, dΘ is the beam divergence, p is the multiplicity factor, and Δ is a term, assumed to be negligible, which takes into account the range of reflection due to distortion in the metal and wave-length spread of reflection.

In order to facilitate counting of spots on the films, the emulsion on the back of each film was removed by washing with sodium hypochlorite solution.

The average sub-grain diameter, t $(=v^{\frac{1}{3}})$ was obtained by counting spots on the 331 and 420 rings.

1.3. Results.

Strain rate as a function of deformation.

The strain-rate versus deformation curves for both drop-forging and slow compression at five different temperatures are reproduced in Fig. 5.   These curves show the average strain-rate over any deformation.   In both cases the strain-rate varied through the deformation, and in drop forging there is a discontinuity which arises from the separate impacts of the punch and the weight.   Since the power supplied in both forging and slow-compression was not varied with deformation temperature, the strain rate was higher at high deformation temperatures than at low ones.

4.2. Stess-strain curves.

For slow compression, stress-strain curves were plotted from load-strain measurements, making the assumption of constant volume to determine the stress.

A less direct method was necessary for determining the stress-strain curves in drop forging.   Estimates of the energy transfer during deformation were made from the displacement-time curves obtained by the high speed cine film method.   The constants in idealised stress-strain relationships were then derived by the following analysis:-

The energy required to produce deformation corresponding to a punch displacement x is given by

$$E = \tfrac{1}{2} m \left(V_o^2 - V_x^2 \right) \qquad\qquad 1.$$

where Vo is the velocity of the punch on striking the specimen, V_x is the velocity of the punch at the end of the displacement x, and m is the mass of

the punch. This expression applies to the part of the deformation between
B and C in Fig. 4. Between B and D, the expression for the energy is:-

$$E = \tfrac{1}{2} m V_o^2 + \tfrac{1}{2} (M + m) (V_1^2 - V_x^2) \qquad 2.$$

where V_1 is the velocity of weight and punch when the weight strikes the punch.
a second time. M is the mass of the weight. The total energy available for
deformation is

$$E = \tfrac{1}{2} m V_o^2 + \tfrac{1}{2} (M + m) V_2^2 \qquad 3.$$

It is assumed that the elastic energy stored in the spring, weight, punch,
anvil and specimen is negligible compared with the energy irreversibly expended
in deforming the specimen, and the energy stored in the specimen. An
indication of the validity of this assumption is given from the displacement-time
curves by the velocity of throw-off of the punch and weight. This was
invariably low in comparison with the impact velocity, and the above assumption
will introduce an overestimate of the available energy of less than 10%.

Energy-displacement curves obtained from the above equations can now
be used to determine the idealised stress-strain curves.

It is assumed that the stress-strain relationship of the material is given
by :

$$\sigma = K E^n \qquad 4.$$

where σ is true stress and ϵ true strain.

The problem then resolves into determining the constants K and n for
different temperatures of deformation.

The true strain, ϵ, is by deformation

$$\epsilon = \ln \left(\frac{H}{H - x.} \right) \qquad 5.$$

where H is the initial specimen height and x the displacement.

The work done during deformation is given by the product of force and
displacement. The force, however, varies continuously due to work-hardening
and increasing specimen cross-sectional area. If the specimen volume V is
assumed to remain constant, the cross-sectional are A is given by :-

$$A = \frac{V}{H - x} \qquad 6.$$

and the deforming force at any instant (F) is given by:-

$$F = \frac{\sigma V}{H-x} g = \frac{K \epsilon^n V g}{H-x} \qquad 7.$$

The energy expended in deforming through an increment of displacement dx is

$$dE = \frac{K\epsilon^n}{H - x} \, Vg. \, dx. \qquad\qquad 8.$$

This is a continuously varying function which can be integrated:-

$$E = K \, Vg. \int_0^x \frac{\epsilon^n}{H - x} \, dx \qquad\qquad 9.$$

Using equation 5. to substitute for ϵ, we obtain

$$E = \frac{K \, Vg}{n + 1} \left(\ln \frac{H}{H - x} \right)^{n + 1} \qquad\qquad 10.$$

Equating the expression 10 with the energy values given by equations 1 and 2 at various values of x, the unknown constants K and n can be evaluated.

Table 3 lists the values of K and n obtained for the five deformation temperatures.

<div align="center">Table 3.</div>

Deformation Temperature $^{\circ}$C	K Tons/in^2	n
-196	53.6	0.44
20	48.8	0.50
300	42.8	0.55
450	38.5	0.53
600	14.3	0.31

Curves of $\sigma = K\epsilon^n$ inserting the appropriate values of K and n are plotted in Fig.6. alongside the stress-strain curves obtained in slow rate compression.

Flow stress as a function of deformation.

The flow-stress curves for specimens deformed by different amounts and at different temperatures on the drop hammer and subsequently tested in compression at room temperature are shown in Fig.7, and for specimens deformed on the hydraulic press in Fig.8. It will be noticed that at the slow strain rate there is a greater difference between the retained work-hardening in specimens deformed at 20°C and 300°C than there is between these two temperatures for rapid deformation. In the latter case, at a given strain, retained work-hardening apparently varies linearly with temperature up to about 450°C. At 600°C the flow stress is lower than would be expected from this linear relationship.

Hardness as a function of deformation.

The hardness versus deformation curves are shown in Fig.9 for the forged material in Fig. 10 for the slowly compressed material. There are no data for specimens deformed at -196°C. For the four temperatures considered, the results supplement the information obtained from flow-stress measurements.

The indications from the hardness curves are that softening occurs at high deformations at $600^{\circ}C$, but that no softening is apparent at the other deformation temperatures. The pronounced softening observed at $600^{\circ}C$ is at deformations higher than those investigated by flow-stress determinations.

Flow-stress recovery and ratios.

From the stress-strain curves shown in Fig. 6 and the room temperature flow-stress versus percentage deformation curves of Figs 7 and 8 it was possible to obtain information about the strain-rate and temperature dependence of the flow stress.

The notation used in deriving these relationships is illustrated in Fig.11. E_1 is the drop-hammer strain-rate and $\dot{E}_2$ is the hydraulic press strain-rate which is of the same order of magnitude as the strain-rate on the Hounsfield tensometer. It is assumed here that these two slow strain-rates are the same. T_1 is the comparison temperature. This is taken to be $-196^{\circ}C$ and the room temperature flow-stress measurements were normalised to this temperature using the procedure of Cottrell and Stokes[29]. T_2 is the temperature of deformation. In the notation of Fig.11, σ_0' is the stress after strain ϵ on the drop-hammer at the comparison temperature. Interrupting the test at this stage and changing the strain rate to the lower one, a flow-stress σ_0 is obtained. The stress σ_0'' is the stress which would have been reached in the deformation had been entirely at the lower strain rate. In the case of a specimen deformed initially at a high temperature and the high strain-rate a stress σ_1'. is reached after strain ϵ . Stopping the test and subsequently determining the flow stress involves changing both the temperature and the strain-rate, the flow-stress then being σ_2 . It is necessary to know the stress level reached on changing each of the variables, strain-rate and temperature, seperately. Changing the temperature alone would give the flow-stress σ_2' and changing the strain-rate would give σ_1 . For deformation entirely at the low strain rate, the stress at strain ϵ and temperature T_2 is σ_1 and the flow-stress at the comparison temperature T_1 is σ_2 The values of σ_1, σ_0, σ_0', σ_2, σ_1', σ_2' and σ_1' are known from the curves of Figs. 6, 7, and 8 but σ_1'' and σ_1 are not known directly. It is possible to deduce σ_1'' by invoking the Cottrell-Stokes law at the slow strain-rate if the Cottrell-Stokes law is obeyed.

$$\frac{\sigma_1}{\sigma_2} = \frac{\sigma_1''}{\sigma_2'}$$
Similarly σ_2' can be obtained by invoking the constancy of the strain-rate dependence with strain (88) at the comparison temperature, so that

$$\frac{\sigma_2'}{\sigma_2} = \frac{\sigma_0'}{\sigma_0}$$

The Cottrell-Stokes ratios were corrected for changes in the elastic moduli with temperatures using the values of Koster (30) for the variation of Young's modulus with temperature.

The flow-stress ratios $\frac{\sigma_1'}{\sigma_1}$ used as an indication of the strain-rate dependence, $\frac{\sigma_1'}{\sigma_2}$, the Cottrell-Stokes ratio at high strain rate and $\frac{\sigma}{\sigma_2}$, the Cottrell-Stokes ratio at low strain rates are shown plotted against temperature of deformation in Fig.12. These were obtained from averages of values computed from interpolations on the curves of Figs. 6,7, and 8 at every 5% deformation from 5 to 25%

The strain rate dependence is shown to reach a maximum around $450^{\circ}C$ and to decrease at $600^{\circ}C$. The Cottrell-Stokes ratio for the high strain rate varies with temperature slightly less rapidly than for the slow strain rate.

Recovery ratios of the type plotted by Bullen and Hutchinson[31] were obtained and are plotted against prestrain. The recovery ratio R, at strain-rate $\dot{\epsilon}_1$ if given by:-

$$R_1 = \frac{\sigma_0' - \sigma_2'}{\sigma_0'}$$

at $\dot{\epsilon}_2$ the ratio is

$$R_2 = \frac{\sigma_0'' - \sigma_2'}{\sigma_0''}$$

and the recovery ratio between strain-rates

$$R_{12} = \frac{\sigma_0'' - \sigma_2}{\sigma_0'}$$

R_{12} is the ratio obtained by comparing the flow stress at $-196^{\circ}C$ of a sample prestrained on the drop-hammer with that of a sample which has been strained throughout at the slow strain rate and low temperature.

The ratios are plotted in Figs.13,14 and 15 respectively and will be discussed later.

Metallographic observations.

A number of interesting features were observed metallographically after polishing in Jacquet's orthophosphoric acid solution and etching, using the same solution in the polish attack region. An investigation was made of the strain-rate and temperature sensitivity of the various metallographic features.

Fig.16. shows a type of marking which is observed at both strain rates and is more frequent at low temperatures than at high temperatures. There appears to be no significant difference between the scale or frequency of these markings at the two strain rates. The major variables affecting its occurrence are strain and orientation. By no means all of the grains of

a specimen show this type of structure but the 'step-ladder' effect shown in Fig.16 was often observed.   It is clear that the markings have the appearance of deformation bands, probably bands of secondary slip.   The cause of the 'step-ladder' effect is likely to lie in the constraint between the annealing twins and the matrix.

Fig.16 also shows some markings on a fine scale and Figs.17 and 18 show some better examples of these;   Fig.17 is a micrograph of a specimen deformed 10% by forging at $300^{o}C$ and Fig.18 of a specimen compressed 10% at $300^{o}C$.   These micrographs illustrate the main features of the fine markings, which from their appearance are tentatively identified with slip bands.   The lines are either straight or wavy and may occur in a single approximately parallel set or as two crossed sets of lines.   From observations or a large number of micrographs over the full range of temperatures investigated the following conclusions (regarding the fine markings) have been reached:

(1)   At a given strain and temperature the markings are finer at the strain rate.

(2)   There is a greater tendency for the markings to be wavy at the high strain rate (c.f. Figs 17 and 18).

(3)   For a given temperature and strain rate the scale of the markings is finer the higher the strain.

(4)   For a given strain and strain-rate the scale of the markings is coarser the higher the temperature.

Examination of the fine markings at a high magnification shows them as seen in Fig. 19.   This is clearly indicative of a cellular appearance, which is associated with wavy markings.   Straight markings give a cross-hatched appearance under high magnification.

Deformation at the high strain-rate and at sub-zero temperatures gives rise to profuse deformation twinning, as instanced by Fig.20, a micrograph of a sample deformed 40% in liquid nitrogen.

There is some contrast between the metallography of specimens deformed at the two strain rates at high temperatures.   Figs. 21 and 22 are of sample both deformed 14% at 600, the sample of Fig.21 by forging and that of Fig.22 by slow compression.   At the high strain rate there is some recrystallisation apparent at the grain boundaries and the typical slip like markings are seen within the grains.   In the specimen deformed at the slow strain rate the slip like markings are less readily detectable and there is clear evidence of grain boundary migration as shown by the 'Ghost' grain boundaries being

displaced from the site of the migrant grain boundaries.   Some recrystallisation
is also evident.

The 'ghost' grain boundaries are useful metallographic markers   as shown
by Fig.23, from a sample deformed by forging 55% at 600°C.   Recrystallisation is
obviously started at grain boundaries and some instances are seen of re-
crystallisation twins ending on the site of the old grain boundary.

Electron microscope studies.

The dislocation structure observed under the electron microscope was
similar in type over the whole temperature range for deformation at the high
strain-rate and was similar to the low temperature structure obtained in copper
at a low strain rate by Warrington[19].   Examples are shown in Fig.24,
a sample forged 9% at 20°C, Fig.25, from a sample forged 24% at 20°C, Fig.26 -
a specimen forged 12% at 600°C and Fig.27 from a specimen forged at 600°C.

These selected micrographs indicate the variation of dislocation
structure with strain and with temperature.   A tangled cell structure is found at
all strains and temperatures at the high strain rate but the cell size
decreases with increasing strain at the same temperature and with decreasing
temperature at the same strain.   The dislocation walls are cleaner at higher
deformation temperatures.

The same pattern obtains at the low strain rate but the cell size is
larger for equal strain and temperature then at the high strain rate.   At
600°C there is a marked difference between the cell structure found at low and
high strain rates, as may be seen by comparison of Figs. 28 and 29 with Fig.27.
The two micrographs of copper deformed at the low strain-rate show clean
dislocation structures (Figs. 28 and 29) while that from the forged sample has
a tangled structure with much higher dislocation density (Fig.27).

A feature observed at high strain rates but not found at low strain
rates is shown in Fig.30.   The associated electron diffraction pattern of
this area showed streaking of diffraction spots, indicating a stacking fault.
Such effects were observed in forging at temperatures up to and including
450°C.   From the evidence of electron micrographs there is an incubation strain
at each temperature before stacking faults were observed.   This was about 14%
at room temperature, 24% at 300°C and 30% at 450°C.   The corresponding stresses
are all about 21 or 22 tons/in^2 - corresponding to a maximum shear stress on the
most favourable twinning system of $\sim$ 10-11 tons/in or approximately 16 kg/mm^2 which
is very close to the twinning stress found by Venables[6] for copper deformed at liq

helium temperature. It is clear that stacking faults form by a similar mechanism to twins and it appears that the stress for this is not very much dependent on temperature.

Fig.31 shows a rarely observed configuration; a pile-up of extended edge dislocations against a sub-boundary is shown in a specimen deformed 24% at 20°C. The extended dislocations were formed during preparation, running in from a hole in the foil to the left of the area. Extended dislocations are also seen leaving the sub-boundary on the opposite side.

Estimation of sub-grain dimensions.

The variation of subgrain size with strains was determined for the forged material at the four temperatures 20°C, 300°C, 450°C and 600°C. The determination was made from electron micrographs using the line intercept method and taking an average of ten areas for measurement of each condition. The results are shown in Fig.32. In Fig. 32 the limiting subgrain sizes are compared with those of Warrington[19] obtained at a low strain rate (10^{-4}/sec) and the subgrain size at 20% deformation by rolling, the results being plotted against deformation temperature.

For the rolled material a comparison was made between the subgrain size determined by electron microscopy and by the X-ray microbeam method with the dimensions of the fine etching structure illustrated by Fig.19. The results are shown in Table 4.

Table 4.

Subgrain size of OFHC copper rolled at various temperatures.

Deformation	Subgrain size (microns)		
Temperature °C.	Optical Micrography	X-ray Microbeam	Electron Microscopy
20	0.3	0.5	0.1 - 1.0
300	0.6	-	0.2 - 2.0
450	0.6	0.6	0.2 - 2.0
600	0.7	0.7	0.5 - 4.0

The trend of all the results in Table 4 is the same and it is felt that this is the best indication which can be obtained to indicate that the etched structure is the same as that observed under the electron microscope. The dislocation structure is apparently etched preferentially. The one to one relationship between subgrain size and slip-band spacing noted by Gay, Hirsch

and Kelly[17] and the similarity of the etched structure to slip markings
encourages the conclusion that the fine etched markings correspond to both slip
bands and dislocation boundaries.

1.4. Discussion.
Mechanisms of deformation.

The deformation bands found in the optical micrographs have no counterpart
in the electron micrographs but it is probable from the evidence of Table II that
the fine etching structure is related to the cell structure found under the
electron microscope. It is also clear that the appearance of the fine etched
markings is very similar to that of surface slip lines. Assuming that this
correspondence is real, some interesting observations can be made about the
relationship between surface slip lines and the cell structure.

Where the fine slip markings are straight the high magnification appearance
is for cross-hatching and for the low deformation temperatures and low strains
at which this type of structure is most frequently found, the electron
micrographs show ill-developed cell structures, (e.g. Fig.24). At high
strains and at high temperatures the fine slip markings are wavy and under
these conditions the cell structure is well developed (see Fig. 25, 26 and 27).
Clearly the waviness of the slip markings is due to cross-slip and we may thus
infer that cross-slip is necessary for cell formation. An experimental
observation in agreement with these suggestions is that at high temperatures
the cell structure is well formed at very low strains (as low as 5% at
$600^{\circ}C$) while at low temperatures well formed cell-structures are first found
at higher strains (above 10% at $20^{\circ}C$).

Comparing the structures between strain rates it has been noted that straight
slip lines were more common at the low rate than at the high rate and this is
in agreement with the present electron microscope observations and those of
Warrington[19]. For instance at $20^{\circ}C$ a well formed cell structure is found
at above 10% strain at the high strain rate but higher strains ($\sim 20\%$) are
necessary for the formation of similarly developed structures at the low strain rate.

The interpretation relating the fine etching structure to the dislocation
structure is thus in agreement with all of the experimental evidence and leads
to the conclusion that cross-slip is essential for the formation of a well-
developed cell structure. A further conclusion is that since the wavy
metallographic structure is more prevalent at the high strain rate and the cell

structure is better developed at low strains, cross-slip is more prevalent at the high strain rate. This is in agreement with the findings of Dieter [32] that shock-loaded nickel showed more cross-slip than statically loaded nickel.

Comparison of the stress-strain curves of Fig.6. indicates that the stress reached for a given deformation is between 60% and 100% higher for forging than for slow compression. The difference is probably overestimated by about 10% because of the indirect stress measurements at high strain rates and a more realistic range of differences is 45% to 80%.

In comparing the stress-strain curves between temperatures at the high strain rate, it is sufficient to compare the coefficients K and n in the expression: $\sigma = K\epsilon^n$. . These are listed in Table 3.

K shows an approximately linear variation with temperature up to $450^{\circ}C$, but at $600^{\circ}C$ the value is some way below this linear plot, indicating a much lower resistance to deformation. The n values may be interpreted as indicating that the stress-strain curves are roughly parabolic at $20^{\circ}C$, $300^{\circ}C$ and $450^{\circ}C$, but that the deformation mechanisms are different at $600^{\circ}C$ and $-196^{\circ}C$ the strain hardening exponents being less than 0.5.

The lower strain hardening exponent at $-196^{\circ}C$ is probably due to twinning occurring, while at $600^{\circ}C$ it is likely that recrystallisation is occurring during deformation.

In Fig.12 three flow stress ratios are plotted. The strain-rate sensitivity is σ_1'/σ_1, the temperature sensitivity (the Cottrell-Stokes ratio) at the forging strain rate is σ_1'/σ_1' and at the slow strain rate it is σ_1''/σ_2'. . Only the last of the ratios is known from direct measurement. The calculated variation with temperature of the strain rate sensitivity ratio is based on the assumption of the Cottrell Stokes law to determine σ_1; this has been repeatedly shown to be valid. The value of may be about 10% too high but this does not affect the trend of the results. It will, however, affect the relative magnitudes of the Cottrell-Stokes ratios at the high and low strain rates and it seems probable that these do not differ greatly from each other.

From the results of Hirsch and Warrington [33] it was expected that the Cottrell-Stokes ratio versus temperature curve at low strain-rates would show a region of increasing variation at temperatures above $450^{\circ}C$. The Cottrell-Stokes ratio at $600^{\circ}C$ is, however, rather higher than would be expected and this will be caused by the method used here of averaging the ratio over 25% prestrain.

At $600^{\circ}C$ recrystallisation occurs after less than 25% deformation, and the resultant softening affects the low temperature flow stress, with the net effect of increasing the flow stress ratio.

The variation of the strain rate dependence with temperature is generally as would be expected from the flow-stress ratio versus temperature curves of Hirsch and Warrington[33], (Fig.10) except in the return to a lower value at $600^{\circ}C$. This can again be attributed to the onset of recrystallisation during deformation. In general terms the variation of the strain-rate dependence with temperature can be described in the terms of the greater importance of thermal aid to slip processes at the low strain-rate. At the high strain-rate, a greater part of the energy required to overcome the obstacles to slip has to be supplied by the applied stress. The rapid increase of the strain-rate dependence at temperatures above $300^{\circ}C$, assuming the $600^{\circ}C$ ratio to be affected by a change in dislocation structure and so to be a spurious effect in this context, is most likely to be associated with the great importance of self-diffusion above this temperature.

The importance of self-diffusion is shown by the contribution of grain-boundary migration to deformation at the slow strain-rate at $450^{\circ}C$ and $600^{\circ}C$, as instanced by Fig.22.

Recovery Ratios.

The recovery ratios (Figs.13,14, and 15) measure the difference in retained work-hardening as determined by measuring the flow stress at $-196^{\circ}C$ between specimens prestrained by the same amount at the test temperature and at $-196^{\circ}C$. A positive value of the recovery ratio indicates the material to be softer after deformation at the test temperature than at $-196^{\circ}C$.

R_1 (Fig.13) is the recovery ratio when deformation at both the test temperature and $-196^{\circ}C$ is carried out on the drop-hammer.

The variation of R_1 with prestrain is not likely to have any significance in view of the methods used to determined the variables. The only conclusion that can be drawn from Fig.13 is that the retained work-hardening is greater for lower deformation temperatures.

The variables used in determining, R_2, the recovery ratio at the slow strain-rate, are all independently determined and it is considered that the relationship between R_2 and prestrain is reasonably established. The variation obtained is different from that found by Bullen and Hutchison[31] who found that the recovery ratio changed linearly with prestrain for the polycrystalline copper.

These workers also found that the linear plots of recovery ratio against prestrain, for all test temperatures, extrapolated back to a common point. The behaviour found in the present work indicates that the recovery ratio is not a simple function of either prestrain or temperature. The room temperature recovery ratio is approximately independent of prestrain. At the higher temperatures the recovery ratio increases with prestrain but apparently approaches a constant value asymptotically. The recovery ratio is larger at any given prestrain for a higher temperature.

A physical picture of the processes contributing to the observed recovery effects may be drawn as follows: at each temperature there will be a mean free dislocation path which a dislocation can traverse before finally becoming pinned. This path will be longer for high temperatures than for low temperatures. If we assume that this mean free path varies with prestrain in the same way at each temperature in the absence of any recovery processes, then we can write after Blewitt et al[26] $\sigma = KN^{\frac{1}{2}}$ and Bailey and Hirsch[27], where σ is the flow stress and N is the dislocation density in lines/cm^2.

For a prestrain ϵ at the comparison temperature

$$\epsilon = b \, A \, N$$

where $A = F^2$; F is the mean free path of a dislocation at the comparison temperature and b is the Burgers vector of the dislocation.

Hence the flow stress at $-196^{\circ}C$, the comparison temperature, is given by

$$\sigma = K \left(\frac{\epsilon}{bA}\right)^{\frac{1}{2}}$$

A prestrain at the test temperature, where the mean free path of the dislocations is F_1, introduces N_1 dislocations given by the expression $\epsilon = b \, A_1 N_1$, where $A_1 = E_1^2$

This dislocation density will give a flow stress at the comparison temperature.

$$\sigma_1 = K \left(\frac{\epsilon}{bA_1}\right)^{\frac{1}{2}}$$

The recovery ratio will be :-

$$R_2 = \frac{K \left(\frac{\epsilon}{bA}\right)^{\frac{1}{2}} - K \left(\frac{\epsilon}{bA_1}\right)^{\frac{1}{2}}}{K \left(\frac{\epsilon}{bA}\right)^{\frac{1}{2}}}$$

$$= 1 - \left(\frac{A}{A_1}\right)^{\frac{1}{2}}$$

$$= 1 - F/F_1$$

It is seen from this result that if only the scale of the dislocation
structure is different at different temperatures for the same prestrain, that
is to say that the variation of the mean free path with prestrain at each temperature
obeys the same laws exhibiting a temperature dependence only through a constant factor,
the recovery ratio should be independent of prestrain.   It is found that R_2 is
practically independent of prestrain at room temperature and below, and
it may thus be inferred that the assumption made is in this case valid. i.e.
no recovery processes occur and the mean free path varies with prestrain in
the same way at $-196^{\circ}C$ as at room temperature.   At the higher temperatures it
is found that the recovery ratio increases with prestrain so that the above
assumption is not valid.   This indicates that some of the dislocations created
during deformation are annihilated by some recovery process, and that the
intrusion of this process alters the function relating the mean free path to the
prestrain.

This simple analysis accounts for the main features of the observed
variations of R_2 with temperature and prestrain but is not completely rigorous.
The prestrain at which stage III and the associated cross-slip commences will
not be the same at $-196^{\circ}C$ and $20^{\circ}C$, and this will invalidate the postulate
concerning the variation of mean free path with temperatures.   It seems likely
however, that the deformation processes at $-196^{\circ}C$ and $20^{\circ}C$ differ only in scale,
since at these temperatures the mutual annihilation of dislocations will occur
mainly by chance meetings.   When the extra degree of freedom of dislocation
climb is available, dislocation of opposite signs will be able to come together
by a stress aided process so that the number of annihilations will be greater than
expected from random chance.

The recovery ratio between strain rates R_{12} gives a measure of the
retained work-hardening after high strain rate deformation.   An immediate
conclusion is that prestrain on the drop-hammer at about $150^{\circ}C$ would produce
similar hardening to prestrain at the slow rate at $-196^{\circ}C$.

It is not possible, however, to be sure of the significance of the
initial downward trend in the plot of R_{12} against prestrain at the two high
temperatures since the accuracy of the measurements is low in this region.

On the basis of the foregoing analysis concerning the dislocation mean
free path at any temperature, it may be inferred that at the high strain-rate very
little recovery has occurred at even the highest temperature.   Since all of
the curves may be drawn, allowing for scatter, almost parallel to the prestrain
axis, it seems that the simple analysis in terms of mean free path length will

describe the operative processes. The higher recovery ratio at high temperatures indicates a lower dislocation density and a longer mean free path. Since stress activated cross-slip occurs at all temperatures in deformation on the drop-hammer, it is quite possible that the deformation processes differ only in scale at the different temperatures.

No evidence has been found in support of the analysis made by Bullen and Hutchison of the variation of the recovery ratio with prestrain and temperature, and further examination of the plots made by Bullen and Hutchison[31] suggests that a parabola could equally well be drawn through the prestrain-recovery ratio points. If this is so much of the analysis of Bullen and Hutchison is invalidated and the interpretation is similar to that of the present work when recovery is occurring. In the more sensitive measurements of Bullen and Hutchison at very low strain rates $(\sim 10^{-5}/\text{sec})$ the differences in the prestrain at which cross-slip sets in will contibute to the parabolic shape of the curves.

Relationship between Mechanical Properties and Substructure.

It was suggested in the preceeding section that in deformation on the drop-hammer only the scale of the structure varied with temperature but that the type of structure was essentially the same. This suggestion was made on the basis of the recovery ratio measurements without any regard for the structure that is actually observed, and it is interesting to see how well this interpretation ties in with actual structural observations.

The electron micrographs of the drop-forged material show that the subgrain size is larger at high temperatures and that the subgrain boundaries are less dense the higher the deformation temperature. Fig.32 shows the variation in subgrain size with prestrain and it would appear that the subgrain size varies in approximately the same way at each of the deformation temperatures. Fig.33 shows that at the high strain-rate the limiting subgrain size varies only slowly with temperature and thus with the other observations listed above indicates the analysis on the basis of the recovery ratios to be reasonable.

At the low strain-rate, comparison of the electron microscope observations with the recovery ratio analysis shows that here there is a variation in addition to the expected scale variation. A high deformation temperatures the subgrain size increases rapidly over a fairly small temperature range and the cleanliness of the boundaries is increased at high temperatures. The recovery ratio R_2 was found to vary rapidly with prestrain in the same temperature range and this led to the conclusion that some additional

recovery process was available in this range. This is in agreement with
the conclusions of Warrington[27] that a large, clean substructure results when
dislocation climbs occur.

It may thus be concluded that the interpretation of the recovery ratio
curves and the structural evidence is in excellent agreement.

The two expressions for the flow-stress, $\sigma = KN^{\frac{1}{2}}$, proposed by
Blewitt et al[26], and $\sigma = Kt^{-\frac{1}{2}}$, proposed by Gay et al[17] appear to be
to some extent conflicting, particularly in view of the results of Ball[24]
and Warrington[19] showing there to be no dependence of flow stress on the
angle across the sub-boundaries. It must be noted, however, that both of
these workers used a technique of prestraining to obtain the required
subgrain size and subsequently annealing at a low temperature prior to testing.
This procedure has been shown by Kelly[34] to sharpen up to sub-boundaries
while leaving the subgrain size about the same. This probably indicates that
unlike dislocations in the boundary become paired off annihilate each
and it may be that in materials of all subgrain diameters the boundaries
were of approximately the same angle.

In the present work no accurate correlations between subgrain diameter
or dislocation density and flow stress were attempted but crude estimates
indicate that both relationships could be applied.

Bailey and Hirsch[27] suggested that in the expression $\sigma = KN^{\frac{1}{2}}$ the
dislocation density that is measured should be that in the sub-boundaries.
This implies a certain boundary strength. Fig.31, an electron micrograph
obtained under fortuitous circumstances, clearly demonstrated that sub-
boundaries have a certain strength and also hints at the importance of sub-grain
diameter. The physical picture drawn from Fig.31 is of a stress
concentration at the head of a regular pile-up of edge-dislocations either forcing
a dislocation at the head of the pile-up to bow out through gaps between
boundary dislocations and emit a loop on the other side of the sub-boundary
or forcing dislocations away from the other side of the boundary. For the
first alternative it is possible to obtain some value for the strength
of the boundary using the general ideas of the "mesh-length" theory of
Kuhlmann-Wilsdorf[35] but in the second case it is not readily possible to take
account of the masking effect of dislocations between the head of the pile-up
and the emitted dislocation or the short range and long range forces tending
to retain dislocations in the boundary. For either alternative it is

possible to write an expression of the Petch type to express the flow stress,

$$\sigma_f = \sigma_0 + kt^{-\frac{1}{2}}$$

where σ_f is a friction stress, and this may be considered negligible in
f.c.c. metals, t is the sub-grain or grain diameter and k is a term dependent
on boundary strength and on an orientation factor m across the grain boundary.
For small angle boundaries the orientation factor will be near to unity.
The strength of a boundary for the first alternative can be written in the form:-

$$\sigma_b = \alpha \frac{Gb}{l}$$

where l is the largest boundary gap and is given by

$$l = \frac{c}{N N_1}$$

N here is the dislocation density in the boundary.

$$\therefore \sigma_b = \frac{\alpha Gb\, N N_1}{c}$$

The flow stress is then given by

$$f = Kt^{-\frac{1}{2}}N_1^{\frac{1}{2}}$$

This result will probably also hold for the second model for propagation
of slip across the sub-boundary and it indicates that there must be some
constant relationship between the dislocation density in the boundaries and the
boundary dimensions in order for the two equations:

$$\sigma = KN^{\frac{1}{2}}$$

and $\sigma = Kt^{-\frac{1}{2}}$ to be satisfied simultaneously. It is readily seen that
the average dislocation density N is related to the dislocation density in the
boundary, N_1, by the expression:-

$$N = \frac{N_1}{t}$$

so that the expression:-
$$\sigma_f = Kt^{-\frac{1}{2}}N_1^{\frac{1}{2}}$$
reduces to $\quad \sigma_f = KN^{\frac{1}{2}}$

or if N_1 does not vary with t, as is probably the case in the experiments
of Ball[24] and Warrington[19] then it reduces to:- $\sigma_f = Kt^{-\frac{1}{2}}$.

It is concluded that the expression $\sigma_f = KN^{\frac{1}{2}}$ is probably the more
fundamental relationship.

Work-hardening theories.

Figure 31 confirms the feasibility of the basic idea of the long-range stress theory, that of a pile-up of dislocations acting as a super dislocation to overcome obstacles to slip. The pile-up of figure 31 is approximately regular, as far as can be determined from the few extended dislocations in the field of view. The extension of the dislocations seen here is far greater than is normally found in copper, but the dislocations in copper are known to be slightly extended so that the difference will be only one of degree.

The extended dislocations in figure 31 are in the edge orientation so that the leading dislocation will be unable to cross slip, even if fully constricted. Since it is not a pile-up of screw dislocations, there is also no likelihood of its being irregular because of anchoring by dissociated vacancy jogs.

The subgrain diameter is clearly an important factor in determining the flow stress, as is illustrated by the stress-concentration effect in figure 31. No means of rationalising this observation have been proposed on the basis of the mesh-length, forest, or jog theories of work-hardening, but a rationalisation on the basis of the long-range stress theory has been proposed by Petch for the grain size dependence of the flow stress. This is equally applicable to the effect of subgrain size. Any account of the grain size dependence of the flow stress on the forest, mesh-length, or jog theories must depend ultimately on a back stress on the source being caused by the original dislocation loop having expanded to a limiting radius dependent on the grain size. This then reduces the theory to the same terms as the long-range stress theory.

The metallographic evidence from the specimens slowly strained at 450°C and 600°C has a bearing on the high-temperature work-hardening theory of Hirsch and Warrington[33]. These workers suggested that the high temperature drop in the flow-stress ratio was caused by the ability of vacancies produced by moving screw dislocations intersecting forest dislocations to diffuse away in the very process of production. At low temperatures the vacancies do not diffuse away, according to Hirsch and Warrington, but remain in the form of vacancy jogs which retard the dislocation line.

From the micrographs of the specimen slowly compressed at 450°C and 600°C (e.g. Fig. 22) it is clear that at high temperatures the grain boundaries can readily yield to the applied stress by migrating. This is probably the reason for the drop in the flow-stress ratio at high temperatures. Such behaviour would not be expected in single crystals but there are no results available to confirm or deny this.

Summary and Conclusions.

1. The structure of O.F.H.C. copper deformed over a wide range of temperature and at two strain-rates, approximately 5×10^{-3}/sec and 5×10^{2}/sec. respectively, has been examined. Both optical and electron-microscopy have been used in this study.

2. It has been possible to correlate the structure seen under the optical microscope with that seen in the electron microscope. The metallographic appearance was found to bear a close relationship to the type of structure found on external surfaces and has been interpreted in terms of slip-bands.

3. It is concluded that most of the dislocation boundaries found in deformed copper over the full-range of temperature at the higher strain-rate are formed by the trapping of dislocations in slip bands.

4. Stress-aided cross-slip is an important mode of deformation at all temperatures and strains at the higher strain-rate. This is the conclusion drawn from the predominance of wavy slip-bands in the metallographic structure of the rapidly strained material. At the low strain-rate straight slip bands were found in material deformed to strains above 10% at room temperature and 300°C.

5. Dislocation substructures over the full temperature range at high strain rates, and at low temperatures and low strain-rates are most probably formed in the way suggested by Gay, Hirsch and Kelly[17]. That is, the cell boundaries are formed by dislocations locked in slip-bands. To form a complete cell structure it is necessary for slip bands to be formed on three intersecting slip planes. This condition is satisfied after the onset of cross-slip. The correlation between cell-formation and the onset of stage III of the stress-strain curve is thus explained.

6. Deformation induced stacking faults have been observed at the high strain-rate. It was found that the shear stress to initiate faulting was very close to that found for twinning at low strain rates at 4°K and 77°K. It is concluded that twinning is a temperature and strain-rate independent process except in so far as the greater inertia of slip processes at low temperatures and high strain-rates allowes a sufficiently high stress level to be reached.

7. Imposing an increased strain-rate causes the dislocations to move faster and also causes an increase in the number of dislocations. The dislocation path is thus shortened in reaching a given strain.

8. At the high strain rate the deformation only varies in scale between the different temperatures.   Thermally activated recovery processes do not play a great part in the deformation.   There is some indication from the mechanical properties and metallography that recrystallisation may occur during deformation at the highest temperature used and at both strain-rates.   At low strain rates, however, thermally activated recovery processes result in much lower retained work-hardening from the high deformation temperatures.

9. It is concluded that high temperature variation in the curve of flow-stress ratio against temperatures obtained by Hirsch and Warrington[33] is caused by thermally activated mass transport.

SECTION II.

Introduction.

The determination of deformation modes has normally been carried out from surface observations of deformed metals. At high temperatures and high strain rates such methods are not readily applicable. It was hoped, therefore, to obtain information about the deformation modes from the preferred orientations resulting from deformation at a number of temperatures.

In the course of this investigation, it was found that the state of the theories relating preferred orientation to deformation modes left much to be desired, and a number of experiments were initiated in order to resolve some of the outstanding problems. The theories evolved and the application of these theories are presented in four sections. The material contained in each of these sections has been published as follows:

1. "Rolling Textures in f.c.c. and b.c.c. Metals" by I.L. Dillamore and W.T. Roberts, Acta Met. 1964.

2. "The Rolling Texture and Stacking Fault Energy of Thorium, Cerium and some Thorium-Cerium Alloys" By I.L. Dillamore, I.R. Harris and R.E. Smallman; Acta Met. 1964.

3. "A Determination of the Stacking Fault Energy of some Pure f.c.c. Metals", by I.L. Dillamore, R.E. Smallman and W.T. Roberts; Phil. Mag. 1964.

4. "The variation of Crystallographic Preferred Orientation through Rolled Aluminium and Copper Sheet" by I.L. Dillamore and W.T. Roberts, J. Inst. Metals, 1964.

2.   <u>Rolling Textures in f.c.c. and b.c.c. metals.</u>

2. 1. Introduction.

Previous theories of rolling textures have either ignored the processes whereby material takes up the predicted orientation [36-38] or have assumed that the rotations leading to the development of tension textures and compression textures can be combined to explain the development of rolling textures [39-41]. The theories of Wever and Schmid [36] Pickus and Mathewson [37] and Hibbard and Yen [38] predict from stability considerations a (110) [1$\bar{1}$2] end texture for f.c.c. metals. Calnan and Clews [39], considering the rolling texture to consist of those orientations which satisfy simultaneously the requirements of the tension and compression textures, predict a pole figure for f.c.c. metals consisting of (110) [1$\bar{1}$2] with spread towards (131) [$\bar{1}$12] plus minor components of (110) [$\bar{1}$1$\bar{1}$] and (110) [001]. A more recent theory by Haessner [41] based on the Calnan and Clews model is discussed in detail in a later section.

In considering texture development from the slip rotations occurring during deformation most workers have assumed that between three and five slip systems are necessary to ensure continuity across the grain boundaries. There is evidence [42,43], however, that at least in large grained aluminium multiple slip systems are required to operate only in the immediate vicinity of the grain boundary, while in the body of the grains slip occurs on only one or two planes. It is likely therefore that multiple slip in the boundary regions can be largely ignored from the point of view of texture development, since the slip rotations in the body of the grain will be more rapid and will be the dominant process. On this basis the deformation of individual grains in a polycrystal can be considered as being closely similar to the deformation of single crystals of the same orientation.

The concept introduced by Calnan and Clews [39] of an effective stress axis removed from the true stress axis by the constraints imposed by surrounding grains is useful when considering only one stress axis, but it does not lend itself readily to the case of rolling where two stress axes are involved and must be considered to act together.

Tucker[44] has suggested that slip rotations during rolling should
be considered to be due to a triaxial stress system in which the three
stresses are σ, a compressive stress parallel to the normal to the
rolling plane, $n\sigma$, a tensile stress parallel to the rolling direction
and $\left\{\dfrac{\sigma - n\sigma}{2}\right\}$, a stress the sign of which depends on the value
of n, parallel to the transverse direction. No development of this
suggestion has been published with application to rolling but Tucker[45]
has used a bi-axial stress system to predict the earing behaviour of
textured-sheet.

2. 2. Theory.

(a) Rotations due to primary and conjugate slip.

A stress system is assumed to operate in rolling in which σ is equal
to the compressive stress parallel to the rolling plane normal and $-\sigma$ is
equal to the tensile stress parallel to the rolling direction.   The
transverse stress is thus zero.   If the direction cosines of the normal
direction with respect to a slip plane normal and a corresponding slip
direction in any grain are a_c and b_c, and those of the rolling direction
with respect to the same slip plane normal and slip direction are a_t and b_t,
the total resolved shear stress acting on the slip system is given by:

$$\tau = \sigma(a_c b_c - a_t b_t). \qquad\qquad 1$$

It is well established that when only one stress axis is considered, a
tensile stress axis rotates towards the slip direction and a compression
stress axis towards the slip plane normal.   In rolling, where the two
axes must be considered to act together, the rotations will take the
tensile axis towards the operative slip direction and the compression axis
towards the slip plane normal, these directions being orthogonal.

It is now assumed that the slip systems for which τ, given by
equation 1, is greatest will operate, and that any stresses due to
intergranular constraints are relieved by slip on other systems, but that
this accommodating deformation constitutes only a small percentage of the
total deformation and does not contribute in any systematic way to
texture development.

In figure 34, the well-known diagram indicating the operative slip
system for any position of an uniaxial stress is reproduced.   Under a
biaxial stress system, we can assume with complete generality that one
stress axis lies somewhere in the unit triangle 001, 111, 011,   The other
stress axis must then lie in the region bounded by the (001), (111) and
(011) great circles.

The slip system which operates in any grain will be determined by
the orientation of the grain relative to the stress axes as indicated by
equation 1 and can be indicated by diagrams similar to figure 1 but
drawn to fit the requirements of a biaxial stress system.

Figures 35a, b and c have been drawn to show the operative slip systems
when one stress axis lies in one of the three sections of the unit
triangle indicated.   The three sections are bounded by 113, 111, 133,
123; 013, 123, 133, 011 and 001, 113, 123, 013.   The operative slip
system is indicated for each position of the second stress axis when the
first stress axis is in the base triangle 001, 111, 011.   The diagrams
in figure 35 were plotted from computations of τ for ten positions of
the second stress axis for each of five positions of the first one per
sub-area of the unit triangle.   Figure 35 was drawn by superimposing
figures 35a, b and c to determine the regions where the slip system does
not depend on the exact position of the stress axis in the base unit
triangle apart from the limitation that it must be 90° from the second axis.

The total number of computations from which figure 35d is plotted,
about 100, is not sufficient for complete accuracy and some interpolations
were necessary.   The boundaries between regions in which different slip
systems operate have been represented as sharp lines, although they will in
fact be diffuse owing to a dependence on the exact position of the stress
axis in the base triangle.   Nevertheless, the diagram gives a reasonable
indication of the slip systems which will operate for the possible
orientation of the second stress axis relative to the first stress axis
lying in the base unit triangle.

Consider now the rotations which a grain in a polycrystalline
aggregate will follow under the operation of the slip system shown in
figure 35d.   It is necessary, when considering the rotations taking place
due to slip on any system, to specify which axis is situated in the base

unit triangle.   Reference to equation 1 will show that there are two
positions of the stress axes relative to a slip system for which that
system will have the same resolved shear stress.   The two positions are
given by the condition that the direction cosines a_c and b_c in equation 1
are interchanged with the direction cosines a_t and b_t.   The rotations
which occur for the two cases can be described by considering first the
tensile axis to lie in the base triangle and second the compression axis
to have this position.   Most of the grains in a random aggregate will be
oriented for single slip but there will be some oriented for duplex slip
or slip on three or more systems.

The rotations occurring in a grain initially oriented for single
slip on the system A_3 ((111) $[\bar{1}01]$), for the case when the tensile
axis lies in the base unit triangle, are shown in figure 36.   The paths of
rotation for one starting position of the tensile axis and three positions
of the compression axis have been indicated.   The shear stress on the
system A3 initially increases, remains almost constant as the tensile axis
enters the unit triangle 001, 011, $\bar{1}11$ and the compression axis approaches
the unit triangle 100, 110, 111.   When the tensile axis approaches the
(110) great circle and the compression axis approaches a line drawn in
figure 36 to represent the boundary between re ions where A3 and C2 are the
operative slip systems, the resolved shear stress on A3 is decreasing and
that on C2 is increasing.   When the two systems have equal components of
resolved shear stress, the slip rotations cause the orientation to move to
a position where the net rotation is zero.   In figure 36 this position is
the (110) $[\bar{1}12]$ orientation.

Table I summarises all possible slip systems, the associated
secondary system and the resulting end positions.

TABLE 5.

Primary System	Tensile axis lying in the 001,111,011 unit triangle		Compression axis lying in 001,111,001, unit triangle	
	Secondary System	End Orientation	Secondary System	End Orien...
A3 (111)[101]	C2 (1̄1̄1)[011]	(110)[112]	B6 (1̄11)[110]	(011)[2...
A4 (111)[011]	C2 (1̄1̄1)[011]	(110)[001]	D6 (1̄1̄1)[110]	(101)[...
B1 (1̄11)[101]	D2 (1̄1̄1)[011]	(11̄0)[112]	A5 (111)[1̄10]	(011)[2...
B4 (1̄11)[011]	D2 (1̄11)[011]	(11̄0)[001]	C5 (1̄1̄1)[1̄10]	(1̄01)[...
B6 (1̄11)[110]	C2 (1̄1̄1)[011]	(1̄01)[121]	A3 (111)[101]	(011)[2...
C1 (1̄1̄1)[101]	D6 (1̄1̄1)[110]	(011)[2̄11]	A4 (111)[011]	(110)[...
D6 (11̄1)[110]	C1 (1̄1̄1)[101]	(01̄1)[211]	A4 (111)[011]	(101)[...

Material initially oriented for slip on two systems may be represented by the pairs of systems shown in Table. 5. It is possible for material to be oriented for slip on pairs of systems not represented in this table.

In table 6, all possible pairs of slip systems which might operate together from the onset are listed.

TABLE 6.

Initially equally favoured slip systems		End position when the tensile axis is initially in the 001, 111,011 unit triangle.	End position when the compression axis is initially in the 001, 111,011 unit triangle.
A3	A4	(110) [001]	(112) [1̄11]
A3	B1	(100) [001̄]	(011) [110]
A3	C1	(110) [001]	(001) [11̄0]
B1	B6	(2̄11) [111]	(011) [100]
B1	B4	(11̄0) [001]	(11̄2) [111]
B6	D6	(1̄1̄2) [111]	(112) [11̄1]
A3	B6	(100) [011]	(011) [21̄1]
A4	C2	(110) [001]	(001) [11̄0]
A4	D6	(010) [101]	(101) [12̄1]
A5	B1	(011) [100]	(011) [2̄11]
B1	D2	(11̄0) [112]	(001) [11̄0]
C1	D6	(01̄1) [211]	(100) [011̄]

Tables 5 and 6 show that most of the material will rotate to orientations of the type $\{100\}\langle 112\rangle$ but that small amounts will take up orientations of the following types; $\{100\}\langle 010,\rangle$ $\{100\}\langle 011,\rangle$ $\{110\}\langle 001,\rangle$ $\{112\}\langle 111,\rangle$ all of which have been considered [37,38] as stable end orientations.

Tucker[44] has suggested that the stability of an ideal orientation is not determined by simple considerations of symmetry alone, but is determined by whether or not the slip rotation will tend to return the material to this orientation if fluctuations of the positions of the stress axes take it away from the ideal orientation. This criterion of stability is applied to the 'stable' orientations obtained from Tables 5 and 6.

In rolling, the most likely displacements of the stress axes due to external circumstances are (a) both compression axis and tensile axis displaced along the great circle joining them and (b) the tensile axis displaced around the great circle 90° away from the compression axis. Any orientation which is permanently removed by such displacements can be considered as unstable. It can be readily shown that under displacement (a), a $\{110\}\langle 011\rangle$ orientation rotates to a $\{211\}\langle 111\rangle$ orientation, while under displacement (b) a $\{011\}\langle 100\rangle$ orientation rotates to a $\{011\}\langle 211\rangle$ orientation, a $\{100\}\langle 011\rangle$ orientation rotates to a $\{100\}\langle 010\rangle$ orientation and a $\{112\}\langle 111\rangle$ orientation rotates to a $\{110\}\langle 112\rangle$ orientation. It may be noted here the other multiple slip orientations not listed in Tables 5 or 6, $\{111\}\langle 112\rangle$ and $\{011\}\langle 011,\rangle$ would be permanently removed by either displacement.

The $\{100\}\langle 001\rangle$ orientation is not permanently removed by these displacements and is found experimentally to be stable up to quite high deformations[46]. Displacements which will destroy the $\{100\}\langle 001\rangle$ texture are those which move the tensile axis and the compression axis asymmetrically, so that both axes are displaced into unit triangles for which the single slip systems are the same. Such a displacement depends on random chance since it can only arise from the build-up of intercrystalline constraints. If such a displacement did occur, it need only be small in order to cause the material to rotate away to a $\{110\}\langle 112\rangle$ orientation.

The $\{110\}\langle 112\rangle$ orientation is the only truly stable end orientation since a displacement of either stress axis or both stress axes together of at least 30° would be required to remove this orientation

The foregoing considerations show that all material must finally, under primary and conjugate slip rotations, reach a $\{110\}$ $\langle 112 \rangle$ orientation. This should, therefore, be a reasonable description of the pole-figures of f.c.c. metals rolled by large amounts and it is in fact found to be so for α- brass (figure 37), silver and many f.c.c. alloys. It is not, however, a good description of the rolling texture for most of the f.c.c. pure metals, and this leads to the conclusion that the deformation processes in the two groups are different.

(b) Rotations due to cross-slip.

In figure 39 the orientation $(0\bar{1}1)$ $[21\bar{1}]$ is considered. It is assumed for simplicity that the material has initially rotated to the end position of primary and conjugate slip rotations before cross-slip commences. This assumption is not a basic requirement of the theory; in fact the only pre-requisite is that slip is occurring on the two systems leading to the $(0\bar{1}1)$ $[21\bar{1}]$ orientation before cross-slip commences in the body of the grain.

The two slip systems operating at the orientation $(0\bar{1}1)$ $[21\bar{1}]$ are Cl $(\bar{1}\bar{1}1)$ $[\bar{1}01]$ and D6 $(\bar{1}\bar{1}1)$ $[\bar{1}10]$. The two systems have the same cross-slip plane B $(\bar{1}11)$ and when cross-slip becomes an important mode of deformation, the compression axis will start to move along the (211) great circle towards B. Since the slip directions are not altered there is no tendency for the tensile axis to move. The compression axis will try to take up a position such that the cross-slip rotations and the normal slip rotations balance, but any rotation along the (211) great circle decreases the resolved shear stress on D6 faster than that on Cl, so that Cl will operate to a greater extent than D6. The equilibrium position of the tensile axis is now upset and the tensile axis will start to move towards (101) while the compression axis moves under the influence of slip on Cl and its cross-slip system Bl towards the (101) great circle. These rotations will stop when a position has been reached where the stress on D6 has been increased to the same value as that on Cl.

Increasing the incidence of cross-slip will move the compression axis further away from $(0\bar{1}1)$ and repeatedly upset the balance of stresses on D6 and Cl. The tensile axis will oscillate on the $(\bar{1}11)$ great circle between $[21\bar{1}]$ and $[\bar{1}01]$ but will stay fairly close to $[21\bar{1}]$ since movement towards $[\bar{1}01]$ rapidly increases the stress on D6.

Figure 5 shows the path on which the tensile axis liew and the region containing the compression axis, which lies between the (211) great circle and a line drawn to satisfy the two equations

$$(k + 1) h_1 + kk_1 + 11_1 = 0 \qquad (2)$$

and $\qquad a_1 b_1 - c_1 d_1 = a_2 b_2 - c_2 d_2 , \qquad (3)$

where $(k + 1, k, 1)$ are the indices of points lying on the $(\bar{1}11)$ great circle and $(h_1 k_1 1_1)$ are the indices of , compression axis $90°$ away from $(k + 1, k, 1)$. a and b are the direction cosines of the compression axis with respect to the slip plane normal and slip direction, and c and d are similar direction cosines of the tensile axis. The suffix 1 refers to the slip system C1 and 2 to D6.

The line (PQ in figure 38) is thus drawn through orientations of the compression axis which are $90°$ away from tensile axes lying on the $(\bar{1}11)$ great circle, for which the resolved shear stresses on C1 and D6 are equal. Some orientations satisfying equations 2 and 3 are $(0\bar{1}1)$ $(21\bar{1})$, $(\overline{20}, \overline{35}, 64)$ $(\overline{945})$, $(\bar{8}, \overline{12}, 23)$ $(\overline{734})$ and $(\overline{32}, \overline{10}, 60)$ $(\overline{523})$.

For a given rate of incidence of cross slip, a dynamical equilibrium will be set up with the orientation oscillating, the compression axes between the line defined by equations 2 and 3 and the (211) great circle and the tensile axis along the $(\bar{1}11)$ great circle. At increasing stresses, the rate of incidence of cross-slip will increase and the centre of equilibrium of the compression axis will move further in a general direction towards $(\bar{1}11)$. At the same time the amplitude of oscillation of the tensile axis will increase.

It must now be considered that as the compression axis moves away from $(0\bar{1}1)$ the resolved shear stresses on both C1 and D6 decrease, and there is a possibility that other systems will become operative. An analysis shows that the likely systems are C2 and D3. In Table 7 the resolved shear stress on each of the four slip systems C1, C2, D3 and D6 are shown expressed as a proportion of the stress on the most favourable system for four orientations in the region indicated above. The fifth orientation listed will be considered below.

TABLE 7.

Slip System	$(\bar{1}46)$ (211)	$(\bar{1}35)$ (211)	$(\overline{20},\overline{35},64)$ (945)	$(\bar{8},\overline{12},23)$ (734)	$(\overline{18},\overline{24},51)$ (
C1	1	1	1	1	1
C2	.52	.58	.66	.67	.83
D3	.79	.75	.81	.60	.72
D6	.90	.89	1	1	.9

Close to $(0\bar{1}1)$ (211), D3 is the most likely third system, but any rotations due to slip on D3 would increase the resolved shear stress on C1 and D6 faster than on D3. As cross-slip accounts for more and more of the deformation, and rotation of the compression axis proceeds towards $(\bar{1}11)$, C2 will become a more likely alternative system and any rotations on C2, which could cause the orientation to move to somewhere near $(\overline{18},\overline{24},51)$ $(\bar{3}22)$, would increase the stress on C2 faster than on C1 and D6 and would thus continue to favour C2 as an alternative system. Any fluctuations of the positions of the stress axes would favour one of the three systems C1, D6 or C2. These favouring C1 or D6 would lead to a return of the orientation to a balance between these two systems, but any favouring of C2 would cause the tensile axis to move towards $(\bar{1}11)$. As the compression axis is close to $(1\bar{1}2)$ after large amounts of cross-slip, it is likely that the material will gradually take up the $(1\bar{1}2)$ (111) orientation. The spread of orientation expected from cross-slip rotations is illustrated in Fig.39, where the orientations considered in the text are plotted.

2. 3. Experimental.

The materials used for the majority of the experiments were commercial purity aluminium and crown silver. Rolling was carried out on a Robertson two high cold rolling mill with 14 in. diameter rolls, the sheet being passed through the rolls in the same direction for each pass.

Pole figures were obtained by the Schulz reflection method using a Siemens texture goniometer. For all deformations except those exceeding 99% reduction in thickness, half of the thickness of the rolled sheet was removed by machining and etching, and pole figures were obtained from the

Corrections for absorption and defocussing towards the periphery of the pole figure were made by plotting intensity levels as multiples of the intensity from a random powder specimen at the same radial position.

The pattern of slip markings on longitudinal edge sections of aluminium and silver was observed on sections which had been polished after known amounts of deformation and subsequently given a light pass to reveal the operative slip planes.

2. 4. Results.

$\{111\}$ pole figures for commercial purity aluminium rolled at room temperature with reductions in thickness of 0,45,60,70,80,95 and 99.8% are shown in Fig.40. A similar series of pole figures for silver with reductions of 50,90,95 and 99.6 is reproduced in Fig. 41.

The pole figures for aluminium suggest that initial rotations after small reductions are towards orientations of the type $\{110\}$ $\langle 112 \rangle$ After heavier reductions, the familiar "pure metal" type of texture develops, but after 99.8% reduction, a strong component of texture corresponding to the ideal orientation $\{112\}$ $\langle 111 \rangle$ is apparent.

Pole figures for silver rolled with reductions up to 95% illustrate the gradual development of the $\{110\}$ $\langle 112 \rangle$ texture, but after 99.6% reduction there is a definite indication that rotations away from this orientation are occurring.

Photomicrographs of the slip traces developed on longitudinal edge sections of aluminium after 60 and 70% reduction and silver after 60% reduction are shown in Figs. 42a,b and c respectively. After 60% reduction two sets of markings are visible on both metals, the markings being consistent with deformation occurring on the systems predicted in Section 2a. After greater amounts of deformation, a difference is observed between the two metals. While silver continues to show two sets of marking, single sets of strongly developed markings appear in most of the deformed grains of aluminium giving rise to a "herring-bone" appearance, (Fig.42c).

A similar observation [47] was made on two other f.c.c. metals, copper behaving similarly to aluminium and 70/30 brass behaving similarly to silver, although in this experiment, the longitudunal edge sections had been polished and etched to reveal "latent slip lines".

2. 5. Discussion.

The development of two different types of rolling textures in f.c.c. metals, referred to qualitatively as the "alloy" type of texture and the "pure metal" texture is well-established experimentally, and some attempts[41,48] have been made to provide a theoretical basis for this observation.

In addition to explaining how the two types of texture arise, a complete theory of texture development in f.c.c. metals must also take into account the following experimental facts:-

1. Slip rotations in all f.c.c. rolled metals are initially towards the $\{110\}$ $\langle 112 \rangle$ orientations. In addition to the evidence obtained in the present work, this statement is consistent with previous observations on copper and brass by Braybrook and Calnan[49]. These workers, however, did not determine complete pole figures after different reductions.

2. In deviating from the $\{110\}$ $\langle 112 \rangle$ orientation, one of the active slip systems is preferred over the other.

3. The deformation processes and texture development in different f.c.c. metals depend on the level of internal stress. Present results are consistent with the interpretation that the behaviour of silver after very heavy deformation is similar to that of aluminium after smaller strains.

4. The textures cannot be described by simple ideal orientations, and account must be taken of the spread of orientation.

5. There is a strong correlation between the stacking fault frequency and the type of texture developed after heavy deformation[50,51]. In general, metals with a high stacking fault frequency develop the "alloy" type of texture, while metals with a low stacking fault frequency develop the "pure metal" texture.

The theory proposed in Section 2.2. has been evolved in order to account for these facts, and it should also be discussed in relation to existing theories. A recent theory to account for the formation of textures in f.c.c. metals is due to Haessner[41], who gives good reasons why earlier theories are inadequate. A list of phenomena which could possibly influence texture formation is presented and Haessner concludes that many of these can be eliminated, leaving twinning and slip on non-octahedral planes as factors which he considers to be important in addition to normal $\{111\}$ $\langle 011 \rangle$ slip. Twinning is considered in low stacking fault energy metals only, and is said to assist the formation of the $\{110\}$ $\langle 112 \rangle$

texture and to account for a weak $\{110\}\langle001\rangle$ component. * The "pure metal"
texture is considered to be due to slip on $\{100\}$ and $\{111\}$ planes, and
a Calnan and Clews analysis is performed assuming that slip systems of
the type $\{100\}\langle011\rangle$ and $\{111\}\langle011\rangle$ operate.

The direct experimental evidence that slip occurs on $\{100\}$ planes
in f.c.c. metals is open to alternative interpretation.   An example is
the observation of slip markings in polycrystalline aluminium by
Hartmann and Macherauch. [52].   Trace analysis indicated that about half
the markings correspond to $\{111\}$ planes, and the remainder could be
due to slip on $\{100,\}$ $\{110,\}$ $\{311\}$ and $\{331\}$ It seems most
improbable that all of these planes should be regarded as alternative
slip planes, and a more likely explanation is that slip is occurring on $\{111\}$
planes with varying amounts of cross slip on a fine scale giving the
appearance of traces corresponding to different planes.   A similar view
regarding slip systems in b.c.c. metals has also been expressed [10], in
which $\{112\}\langle111\rangle$ and $\{123\}\langle111\rangle$ slip systems are composed of
specific amounts of slip on non-parallel $\{110\}\langle111\rangle$ systems.
In f.c.c. metals, cube-plane slip has been reported most frequently in
aluminium, in which the activation energy for cross slip is very low.
There is also a strong orientation dependence of the appearance of " $\{100\}$ "
slip, which is observed in single crystals when the tension axis is nearly
parallel to $\langle111\rangle$.   The resolved shear stress on primary and cross slip
plane in this orientation is roughly equal and dislocations which are not
dissociated such as those in aluminium would cross slip readily.   Equal
amounts of primary and cross slip would give a trace parallel to a
$\{100\}$ plane.   The extremely fine scale on which cross slip may occur
is illustrated by some experiments of Washburn, Kelly and Williamson [53]

* Footnote: The $\{110\}\langle001\rangle$ orientation is also predicted as a
         minor texture component in the present theory following rotations
         due to primary and conjugate slip, as indicated in Tables 5 & 6.

on magnesium oxide examined by transmission electron microscopy.   Glide
was observed on irrational slip planes, and it was suggested that this was
due to unresolved cross-slip.

It thus appears that the observations of slip traces in f.c.c. metals
might be interpreted solely in terms of primary slip on $\{111\}$ planes
with varying amounts of unresolved cross-slip.   Analysis of slip
rotations in terms of $\{100\} \langle 011 \rangle$ slip is then equivalent to a special
case of primary and cross slip with equal amounts of slip on each system.

Haessner also considered the possibility of cross slip as a
contributory factor to texture development in f.c.c. metals, but he
dismissed this mechanism on the grounds that the internal stresses in a
rolled metal are generally much greater than $\tau_{\mu\eta}$ the stress at which
stage III of the single crystal stress-strain curve commences.   He
therefore concludes that in the rolling of polycrystalline material, cross
slip should always be possible.

It seems to us that this argument is not valid, because the amount of
cross slip required to cause deviation from the linear hardening stage,
Stage II, of the single crystal stress-strain curve may be quite small.
On the other hand, the amount of cross slip required to contribute
significantly to crystal rotations must be large and must correspond to
very much higher stresses than those required to initiate cross slip.

It is on the assumption that the deformation mode in f.c.c. metals is slip
on octahedral planes with varying amounts of cross slip depending on the
stress, stacking fault energy and temperature of deformation that the
analysis presented in Section 2.2. is based.   Rotations due to slip on the
two systems bearing the highest resolved shear stresses due to the biaxial
stress system imposed by rolling to the development of the $\{110\} \langle 112 \rangle$
rolling texture.   This texture becomes progressively stronger with
increasing rolling reductions provided that large amounts of cross slip
do not occur.

When extensive cross slip does occur, rotations away from $\{110\} \langle 112 \rangle$
take place, leading to the spread of texture shown in Fig.39 and
eventually to the orientation $\{112\} \langle 111 \rangle$.

The relationship between stacking fault frequency and type of
texture is readily explicable in terms of cross slip.   Indeed, Brown[54]

has suggested that wire textures in f.c.c. metals may be related to ease
of cross slip, although no details of the rotations due to cross slip
were considered. At a particular deformation temperature and stress level,
the amount of cross slip will be dependent on the stacking fault energy of
the metal. If the stacking fault energy is very low, cross slip will be
difficult, and so at low temperatures, the "alloy" type of texture will be
formed. As the deformation temperature is raised, thermal activation
aids cross slip and the texture may transform to the "pure metal" type.

In all f.c.c. metals, it is suggested that the rolling textures varies
with increasing amounts of rolling according to the pattern:-

$$\text{"alloy" type} \longrightarrow \text{"pure metal" type} \longrightarrow \{112\} \langle 111 \rangle$$

With low stacking fault energy metals rolled at room temperature, it will
not be possible to achieve sufficient reduction to develop the "pure metal"
texture, but evidence is presented to show that after 99.6% reduction in
thickness at room temperature, the texture of silver is beginning to change
from "alloy" type towards "pure metal" type. After a similar heavy
reduction, the texture of aluminium is beginning to change from
"pure metal" type towards $\{112\} \langle 111 \rangle$ Thus when the internal stresses
caused by rolling are great enough, metals of low stacking fault energy
cross slip and behave similarly to metals of higher stacking fault energy
under the influence of smaller internal stresses.

A possible criticism of the present theory is that in the $\{110\} \langle 112 \rangle$
orientation, the cross slip plane lies perpendicular to the transverse
direction and it will have no component of the applied stress acting on it.
A f.c.c. single crystal with the tension axis parallel to $\langle 112 \rangle$ would
similarly have no component of applied stress acting on the cross slip plane,
but it is generally agreed that in this case, the onset of Stage III is due
to the commencement of cross slip. In polycrystalline material, intergranular
constraints would tend to promote cross slip by changing the effective stress
direction within each crystal by causing a higher dislocation density
at a given strain.

The presence of $\{112\} \langle 111 \rangle$ orientation in the deformation texture
after heavy reductions can have a strong influence on the subsequent
recrystallization behaviour of sheet. Verbraak[55] has shown that the
formation of cube texture on annealing is most probably related to the

presence of this orientation in the deformed metal. He has further suggested that a certain proportion of material in the $\{112\}$ $\langle 111\rangle$ orientation is necessary to nucleate the cube texture in polycrystalline material. If this is so it may be seen why a small amount of solute in copper suppresses the cube recrystallization texture but a large amount is required to prevent the "pure metal" deformation texture being formed. It is known that increasing the solute content progressively reduces the stacking fault energy, thus making cross-slip more difficult and reducing the probability of material reaching the $\{112\}$ $\langle 111\rangle$ orientation, but much solute will be required to reduce cross slip sufficiently to prevent the formation of the "pure metal" texture.

The conditions laid down by Cook and Richards[56] for the production of strong cube texture in copper sheet may also be rationalised since cross slip commences earlier the finer the initial grain size.

2.

6. Texture development in b.c.c. metals.

Following the earlier discussion on slip systems, it will be assumed that the operative slip system in b.c.c. metals are of the type $\{110\}$ $\langle 111\rangle$, It is then possible to apply the ideas of Section 2.2. to predict rolling textures. Figures 34 and 35 a-d may be used when considering the operative slip systems in b.c.c. metals when the figures 1-6 refer to slip plane normals and the letters A-D refers to slip directions. It can then be shown that most of the material will rotate under the influence of primary and conjugate slip to orientations of the type $\{112\}$ $\langle 110\rangle$

Considering now the orientation (211) $[0\bar{1}1]$, it will be assumed that cross slip starts after this orientation has been reached. This assumption merely makes the description of the rotations simpler. Each slip system in b.c.c. metals has two possible cross slip systems, at least one of which will have some component of the applied stress acting upon it. For the primary and conjugate slip systems 6D and 1C, in the notation of Fig.34, the possible cross slip systems are 2D and 3D, and 2C and 5C respectively. The component of the applied stress is twice as large on 5C as on 2C and on 3D as on 2D, so that cross slip will occur on 5C and 3D. Under the influence of cross slip, the position of the rolling direction is not affected but the rolling plane normal moves around the $(0\bar{1}1)$ great circle towards $[\bar{1}00]$. With equal amounts of primary and cross slip, the stable position will be (100) $[0\bar{1}1]$ and any mixture of the two will give a spread of orientation from (211) $[0\bar{1}1]$ through (100) $[0\bar{1}1]$ to $(\bar{2}11)$ $[0\bar{1}1]$. The

orientation (111) $[0\bar{1}1]$, which is included in the orientation spread
given by Gensamer and Mehl[57] is not represented in the spread expected
from the present theory. $\{110\}$ and $\{222\}$ pole figures of 95% cold
rolled vanadium have been plotted and are shown in Figs. 43 a and b.
From these it may be seen that some of the (111) $[0\bar{1}1]$ positions correspond
to regions of low intensity on the pole figures and this is generally
true for other b.c.c. metals [58], the rolling textures of which are
adequately described by the spread from (100) $[0\bar{1}1]$ towards (211) $[0\bar{1}1]$.

3.   The Rolling Texture and Stacking Fault energy of Thorium, Cerium
     and Thorium-Cerium Alloys.

3.   1.   INTRODUCTION.

By studying the transition from the rolling texture near the ideal
orientation $\{153\}$ $\langle112\rangle$, characteristic of pure copper heavily rolled at
room temperature so that characteristic of α-brass near the ideal orientation
$\{110\}$ $\langle112\rangle$, in a series of alloy systems of known stacking energy, γ , it
has recently been shown [59,60] that there is a correlation between the change
in rolling texture and the decrease in stacking fault energy on alloying.
Moreover, the $\{110\}$ $\langle112\rangle$ texture is not confined specifically to alloys but
is a feature of any material with γ less than about 35 ergs/cm^2, rolled at a
temperature not higher than 0.25 T_m.   It has also been demonstrated in the
previous section   that the dependence of the rolling texture on stacking
fault energy arises from the increased difficulty of cross-slip as the dislocations
become more widely dissociated in materials of low γ.   However,
cross-slip is a thermally activated process, and therefore the
critical stacking-fault energy at which the texture transition occurs
depends on the rolling temperature.   Thus of the common pure f.c.c. metals
only silver has a low stacking fault energy[61] of about 25 ergs/cm^2 and
accordingly has an "alloy texture" when rolled at room temperature[62].
Silver can be made to exhibit a "pure metal" texture by rolling at temperatures
above room temperature[62,63] when the relatively difficult cross-slip process
becomes thermally-activated.

Recently, McHargue[64,65] has reported that thorium shows a stacking
fault frequency similar to that of silver but this has been questioned by
Arunachalam and Tangri[66] who obtained a low value for the stacking fault
frequency.   The values of the stacking fault frequency were determined by an
X-ray diffraction technique, and this parameter has been shown[59] to be inversely
proportional to the stacking fault energy γ.   From the work described above
one would therefore expect that if thorium has a low stacking fault energy then
it should exhibit an "alloy-type" of texture when it is rolled at room temperature.
The rolling texture of thorium has been determined previously by Smallman[67]
and shown to be of the pure-metal type, and hence this work indicates a high
stacking fault energy metal.   In addition, some thorium rich Th - Ce alloys
were examined and also shown[62] to have a pure-metal texture which further
suggests that a high γ is involved, since cerium, which undergoes a transformation
at temperatures just below room temperature, is thought to be a low stacking fault

energy metal. (Thorium and cerium form a continuous solid solution
at room temperature). To resolve the differences between these
conflicting results, the texture of thorium has been redetermined at room
temperature and determined at $-196^{o}C$, and the results of Smallman[67] on the alloys
of thorium with the low stacking fault energy metal cerium have been extended into
the cerium-rich range.

2. EXPERIMENTAL.

Iodide thorium*, supplied by the Atomic Energy Research Establishment and high
purity stocks of cerium* , supplied by Johnson-Matthey, were used in the investigation.

In making the alloys the weighed out pieces of thorium and cerium were placed on
the hearth of an arc furnace which was evacuated to 10^{-5} mm.Hg. and argon was admitted
to a pressure of about 150 mm. Hg. An arc was struck from a large piece of
zirconium and the molten pool was maintained for several minutes to further purify
the argon atmosphere. The weighed out pieces were then fused and the resulting
buttons inverted and re-melted six times to eliminate segregation. These arc-cast
ingots were then squeezed in a vice to cold work them, wrapped in tantalum foil,
and homogenised for one week in a fused silica tube evacuated to 10^{-6}mm.Hg.
The homogenisation temperatures varied from 700° to $1000^{o}C$ depending upon the alloy
composition.

The compositions of the homogenised buttons were checked by measuring their
lattice-spacings and comparing them with previously determined values[68], since
a linear relationship between lattice-spacing and composition has been found for
cerium-rich alloys.

The homogenised buttons and the pure metals were forged approximately 50%
and then annealed for two hours, the temperature of the anneal depending on the
composition (thorium was annealed at $1000^{o}C$, cerium at $630^{o}C$). A further deformation
of approximately 50% by rolling was required to bring the material to the starting
thickness and this was followed by a one hour anneal at the same temperatures as
ios us previously.

* The iod.ie thorium contained less than 0.10 wt% metallic impurities,
    <0.02 wt.% C, <0.01 wt.% N_2 and <0.10 wt% O_2.
    The cerium contained less than 0.01 wt.% other rare-earths,
    <0.02 wt.% other base metals and tantalum was not spectro-
    graphically detectable.

Deformations of 95% were achieved on a hand operated mill using very small passes and without reversing end for end between passes. Rolling at approximately -196°C was carried out by precooling the material in liquid nitrogen and re-immersing in liquid nitrogen between passes.

The immediate surface layers from the rolled strip were removed by etching and the $\{111\}$ polefigure was plotted from reflection data obtained using a Siemens "Texturgoniometer".

3. 3. RESULTS AND DISCUSSION.

The textures obtained from rolled thorium at room temperature and at -196°C were both of the 'pure-metal' type, as shown by Fig.44 which is a $\{111\}$ pole figure from the thorium rolled 95% at -196°C. It has been reported [69,70], that copper of comparable purity to that of the thorium, shows an alloy texture after rolling at -196°C, on which basis it would appear reasonable to suggest that thorium has a stacking fault energy considerably higher than that of copper ($\simeq$ 70 ergs/cm^2). This may be particularly so since the melting point of thorium is much higher than that of copper.

Further indication is found in the textures produced in the thorium-cerium alloys that thorium has a high stacking fault energy. Smallman[62] showed that alloys containing up to 50% cerium have a 'pure-metal' texture and the present work has shown that even with cerium contents as high as 90% the texture still indicates a stacking fault energy higher than that of silver. The $\{111\}$ pole figure of the 90% cerium alloys reproduced in Fig.45 shows a texture intermediate between the 'pure-metal' and 'alloy' textures.

The pole figure of pure cerium, reproduced in Fig. 46 shows a weakly developed texture of the type obtained from hexagonal metals of near ideal $^c/a$ ratio. This indicates that the γ (f.c.c.) to β (hexagonal) transformation has been promoted by deformation, forcing the remaining f.c.c. material to slip in the three $\langle 110 \rangle$ directions parallel to the $\{111\}_\gamma$ // $\{00.4\}_\beta$ habit plane.

Diffractometer traces on cerium rolled 50, 60, 70, 80 and 90% showed the β phase to separate out at above 70% deformation, thus verifying the above observations.

McHargue and Yakel[71], who studied the γ and β tranformation on thermal cycling found that more β-phase was formed in annealed material than in material which had been pre-deformed by surface peening, suggesting that stress inhibits the γ to β transformation.   This result does not appear to be compatible with the present observations and further experiments were conducted in which lightly scratched cerium was thermally cycled between room temperature and -196°C.   It was found that the β-phase was in fact nucleated at scratches as indicated in the electron micrograph given in Fig. 47.

The technique of surface peening has been criticised previously[66] and no further comments are necessary here.   It is clear, however, that the conclusion that cerium has a very low stacking fault energy is correct.

It may also be concluded that thorium has a high stacking fault energy, as indicated by the fact that it shows a 'pure-metal' texture after rolling at -196°C and by its marked effect in stabilising the f.c.c. structure in cerium.   The addition of only 10% thorium to cerium suppresses any tendency to form the β-phase during deformation   (and in thermal cycling as shown by Gschneider, Elliott and McDonald[72], and raises the stacking-fault energy so effectively, certainly above 40 ergs/cm^2, that the separation of partial dislocations is severely restricted, and as a consequence, cross-slip can readily occur at only moderately high stress levels.

4. **A Determination of the Stacking Fault Energy of some pure f.c.c. metals.**

4. 1. <u>INTRODUCTION.</u>

The most widely accepted valued of stacking fault energy are those determined from the node radius measurements of Howie and Swann[73] corrected by Thornton et al[74]. to allow for the interaction between partial dislocations. These values are at variance with results obtained from plasticity measurements by Seeger et al.[75], and by Wolf[76], who determined the temperature and strain-rate variation of the onset of cross-slip from single crystal stress-strain curves. Thornton et al. have critically compared the two methods and have concluded that the discrepancies may be attributed to the cross-slip model used by Seeger et al., which, although predicting the correct form for the relationships between the onset of cross-slip and temperature and strain rate, nevertheless requires an activation energy which is far too high. .It is possible that different cross-slip processes are rate determining at different temperatures in the same material.

Recent work in the deformation texture of f.c.c. metals and alloys (Hu and Goodman[77], Haessner[60]; Smallman and Green[59] has shown that a correlation exists between the deformation texture and the stacking fault energy. For example Smallman and Green have measured the variation of rolling texture with composition in those alloy systems for which the stacking fault energy has been determined and show that the $\{110\}\langle 112\rangle$ texture is exhibited by copper, silver and gold alloys having a γ-value less than about 35 ergs/cm^2, or γ/Gb less than about 4.

From the rotations for crystals of various orientation, it has been demonstrated in Section 2 that when extensive cross-slip occurs the 'alloy-type' rolling texture $\{110\}\langle 112\rangle$ transforms into the 'pure-metal' type texture which may be represented by the indices $\{531\}\langle 112\rangle$. Using a single crystal analogue of the process it may be concluded that the $(110)[\bar{1}12]$ orientation is broken up at some point in the deformation process after the onset of stage III. This orientation was used in Section 3 to indicate that thorium has a relatively high stacking fault energy, not a low one as previously suggested (McHargue[64].)

It is clear from our own observations (section 2) and from the measurements of Braybrook and Calnan[49] that the later the stage in the deformation process at which cross-slip becomes sufficiently extensive to affect the orientation, the greater will be the amount of material with the $(110)[\bar{1}12]$ orientation. If a measure of the amount of $(110)[\bar{1}12]$ orientation present in the textured material could be obtained, this would provide an indication as to the stage reached in the deformation process, and whether cross-slip has become sufficiently extensive to affect the orientation. In Fig. 48 (a) is shown a $\{111\}$ pole figure from 70 - 30 brass

which may be described by two components of the ideal $\{110\}\langle112\rangle$ orientation; the texture of copper is reproduced in Fig. 48(b) and may be described by four equivalent orientations close to $\{531\}\langle112\rangle$. Smallman (62) characterised these two textures by an intensity ratio determined from the central region of each pole figure. However, a more sensitive intensity ratio characteristic of each texture is that derived from the periphery. It can be seen from figure 48 (a) and (b) that as the texture changes from the $\{110\}\langle112\rangle$ type to the $\{531\}\langle112\rangle$ type, the intensity peak on the 'equator' of the pole figure moves towards the centre, whilst that at 20° to R.D. remains stationary within the scatter of the ideal orientation. A convenient measure of the proportion of $\{110\}\langle112\rangle$ orientation present at any time may thus be obtained from the ratio of intensities of $\{111\}$ poles at the transverse direction (I_{TD}) to that 20° from the rolling direction (I_{20}).

From a study of the texture exhibited by a given metal it should be possible to estimate the stacking fault energy. Such a method of estimating the stacking fault energy is related to the method proposed by Seeger et.al. (75) in that the parameter obtained by measuring the pole-figure is related to the onset of stage III in the single crystal stress-strain curve. The method differs, however, in that no arbitrary cross-slip mechanism is assumed and, moreover, it is essentially the value of strain corresponding to cross-slip operation which is measured, not the stress value. The validity is dependent on the assumption that the single crystal stress-strain curves of metals of the same γ/Gb with equivalent thermal activation and for the same orientation are identical when the stress is measured as fractions of the shear modulus. It seems likely that this is a reasonable assumption and it may be justified by reference to current theories of work-hardening. Thus, under ideal conditions the length of stage I depends only upon specimen dimensions, orientation and purity, (Kuhlmann-Wilsdof(35), the slope of stage II is the same for all f.c.c. metals regardless of almost any variable except orientation and the onset of stage III occurs at stress values (γ_{III}) which fit the relationship of Seeger et al.(75) at several different temperatures and strain-rates, namely

$$\ln\left(\frac{\gamma_{III}/G}{\gamma_{III(0)}/G(0)}\right) = \frac{kT\left(1+\frac{n}{900}\right)\left(1+\frac{180\gamma}{Gb}\right)}{Gb^3}$$

where G is the shear modulus, k Boltzmann's constant, T the absolute
temperature, b the Burgers vector and γ the stacking fault energy.
From this it may be seen that since n, whatever significance is
assigned to this parameter, is dependent on γ/Gb, then materials of
equal γ/Gb will cross-slip at the same value τ_{III}/G when the thermal
aid to cross-slip is the same. Gb^3 is the work done in moving the
atomic length of dislocation through one Burgers vector and kT is the
thermal energy available at temperature T so that materials must be
compared at equal values of kT/Gb^3.

In a polycrystalline sample possible variations in Stage 1
due to non-ideal conditions are eliminated and the only point in
question is whether the strain at which cross-slip becomes sufficiently
frequent to affect the orientation differs between materials of the
same γ/Gb under similar conditions of thermal activation. This
possible source of difference is minimised in practice by obtaining
materials of closely similar grain size.

4. 2. Experimental.

Of the 16 pure metals which have a stable f.c.c. structure at
temperatures in the range $-196^{\circ}C$ and $+50^{\circ}C$ eleven have been examined.
Silver, gold, copper, aluminium, ytterbium and cerium were obtained from
Johnson-Matthey and were of highest purity available. Platinum, rhodium,
palladium and nickel were kindly loaned by Mond Nickel Ltd and iodide thorium
was obtained from the United Kingdom Atomic Energy Research Establishment,
Harwell. The purity of all these metals is given in table 8.

TABLE 8.

Purity of f.c.c. Metals.

Metal	Purity
Ni	Total impurity 350 ppm, with 180 ppm Fe, 75 ppm Si and 50 ppm S
Th	Iodide thorium. Impurities 0.10 wt% other metals, 0.02 wt% C, 0.01 wt% N_2 and 0.10 wt% O_2.
Ce Yb	0.01 wt% other rare earths and 0.02 wt% base metal.
Rh	0.01 Pt, 0.006 Pd; 0.03 Pu; 0.03 Ir; 0.0001 Au; 0.002 Ag; 0.036 Fe; 0.003 Si; 0.004 Ca.
Pt.	0.0004 Pd; 0.0001 Rh; 0.01 Ru; 0.01 Ir; 0.0002 Ag; 0.0001 Sm; 0.02 Fe; 0.0005 Cr.
Pd.	0.001 Pt; 0.002 Ru; 0.05 Ir; 0.001 Au; 0.004 Ag; 0.002 Pb; 0.001 Fe; 0.002 Cr.
Au Ag Cu Al	Johnson-Matthey spectroscopically standardised materials.

All materials were given a penultimate 50% deformation

by rolling or compression and a final anneal of two hours at two thirds of the melting point on the absolute scale of temperature.

All annealing was carried out in a vacuum of 10^{-5}mm. Hg. The final grain size was found in all cases to be between 10 and 30 grains/mm^2.

Copper, silver and gold were deformed 95% at a number of standard temperatures and the variation of the intensity ratio with the relative amount of thermal activation, $\frac{kT}{Gb^3}$, was plotted for these materials. Other materials were rolled 95% at only one or two temperatures and the value of the intensity ratio plotted at the appropriate value of $\frac{kT}{Gb^3}$.

From this plot calibration curves of Υ/Gb versus I_{TD}/I_{20}, were obtained for constant kT/Gb^3. The value of Υ/Gb for gold was determined using interpolated values of copper and silver and the value for nickel. Subsequent calibration curves used the three metals copper, silver and gold for which the variation of I_{TD}/I_{20} with kT/Gb^3 was known.* For ytterbium no data were available on the variation of elastic constants with temperature and this metal was deformed only at $20^{\circ}C$. The value obtained was outside the range of the calibration curves but clearly indicated a very low value of Υ/Gb, and hence of Υ, since Gb is very small for ytterbium.

Except for rhodium, the deformation was standardised at 95% deformation. For rhodium it was found impossible to deform to this extent and a deformation of 90% at $20^{\circ}C$ was used. In this case the result was normalised to 95% deformation in an approximate comparison with copper deformed 90% and 95% at a temperature such that approximately the same value of the measured intensity ratio at 90% deformation as for rhodium was obtained.

---

* It is assumed that Υ for Cu, Ag and Au does not vary significantly with temperature.

TABLE 9.

Measured values of the intensity ratio I_{TD}/I_{20} and estimated γ values for various F.C.C. metals.

$T^{o}K$	77		196		293		323		
Metal	$\dfrac{I_{TD}}{I_{20}}$	$\dfrac{\gamma}{Gb} \times 10^3$	$\dfrac{I_{TD}}{I_{20}}$	$\dfrac{\gamma}{Gb} \times 10^3$	$\dfrac{I_{TD}}{I_{20}}$	$\dfrac{\gamma}{Gb} \times 10^3$	$\dfrac{I_{TD}}{I_{20}}$	$\dfrac{\gamma}{Gb} \times 10^3$	γ
Ag.	1.18		1.28		1.31		1.16		25 *
Au.	.98	5.05	.78		.75		.74		45
Cu.	.85		.73		.71		.67		70 *
Ni					.49				225 *
Pt					.94	4.3			75
Pd	.55	10.2			.50	10.5			130
Th					.67	7.5			330
Th	.82	6.2							70
Yb					1.31	< 3			< 10
Al	.42	>20							>150

* Asterisk indicates fitted γ-values.

In all cases rolling was carried out on a hand driven mill with 3" diameter steel rolls and the material was not reversed ent to end between passes. After rolling the metals were etched or electropolished until thin enough to transmit X-rays, and then intensity measurements were made on a Siemens texture-geniometer using Mo, $K\alpha$ radiation, with the specimen oscillated parallel to its own plane during measurement. The intensities were corrected for the background count, but no other corrections were necessary since both intensity measurements were made with the plane of the specimen bisecting the angle between incident and diffracted beams.

4. 3. RESULTS.

The intensities I_{20^o} and I_{TD} which were measured are indicated on the
{111} pole figures shown in Fig. 48; the values of I_{20^o} were averaged for
the two peaks either side of the rolling direction. The observed ratios
of the intensities $\frac{I_{TD}}{I_{20^o}}$ are shown in table 9 for the various materials and
temperatures used.

In plotting figure 49 the intensity ratios have been fitted to values
of γ/Gb taken from the results of Howie and Swann (73) modified as
suggested by Thornton et al. (74). The values of γ after modification
are Ag $\simeq$ 25, Cu $\simeq$ 70 and Ni $\simeq$ 225 ergs/cm^2. Shear moduli were
corrected for temperature variation using the results of Köster (30)
for the variation of Young's modulus with temperature. Curves are fitted
to these calibration points at constant values of $^{kT}/Gb^3$ and the remaining values
taken from the curves.

To determine whether the small differences in penultimate grain size
have any appreciable effect on the results, the variation in the parameter
$\frac{I_{TD}}{I_{20^o}}$ with initial grain size has been examined for copper deformed at room
temperature. The results are summarised in table 10. It is evident that
grain-size has little effect on the intensity ratio.

TABLE 10.

Variation of the Intensity Ratio I_{TD}/I_{20^o}

with Grain Size for copper rolled 95% at Room Temperature.

Grain Size g/mm^2	Intensity Ratio I_{TD}/I_{20^o}
10	0.72
50	0.65
400	0.66
1500	0.69

4. Discussion.

The results shown in table 10 indicate that grain size variation is not very important, at least for copper. This may be due to the rapid fragmentation of large grains due to deformation banding and cell formation in the early stages of deformation. A greater dependence on grain size might be found for low stacking fault energy materials.

The results obtained from figure 49 and listed in table 9, can only be compared with previous estimates of γ for Au and Pt. The value of Thornton and Hirsch (78) for platinum, 120 ergs/cm^2, (corrected to compare with a value of 70 ergs/cm^2 for copper rather than the 40 ergs/cm^2 used by Thornton and Hirsch) is somewhat higher than the value of 75 ergs/cm^2 found in the present work. For gold the present result is also lower than the corrected Thornton and Hirsch value. It is clear however, that $\gamma_{Cu} > \gamma_{Au} > \gamma_{Ag}$ and this is not in agreement with the order of increasing stacking fault energy: gold, silver and copper inferred by Silcox and Hirsch (79) and Smallman et al. (80) from observations on vacancy agglomeration and also found by Thornton and Hirsch. The value also indicates that gold has a stacking fault energy somewhat lower than that of copper rather than slightly higher as suggested by Smallman and Green (59).

No values are available from the present work for the stacking fault energy of lead or iridium. Lead recrystallises at room temperature, so no measurements coul be made with the present technique, while iridium was found to be too difficult to deform at temperatures below about 1000°C. It is generally thought that metals which can exist in more than one allotropic modification have a low stacking fault energy. Three metals with allotropic modifications, namely Yb, Ce and Th, have been examined in the present work. Ytterbium normally transforms to the b.c.c. structure at 798°C or at 20°C with 40 kilobars pressure and is found to have a stacking fault energy of less than 10 ergs/cm^2. Cerium was shown in section 3 to transform to a hexagonal structure under stress and from the texture results clearly has a low stacking fault energy, about 0 to 5 ergs/cm^2. Thorium transforms to b.c.c. at about 1400°C, but this metal exhibits a moderately high stacking fault energy at -196°C as indicated both by the present results and the previous results on its alloying behaviour with cerium, (Smallman[62]). The low γ for ytterbium is commensurate with its chemical similarity to calcium for which Spreadborough[81] has calculated a value of γ of 15 ergs/cm^2.

4. 5. <u>Conclusions.</u>

The method described here for determining γ is rapid and particularly suitable
for application to materials for which the stacking fault is too large for
extended dislocation nodes to be observed in the electron microscope.

Where previous estimates are available the present results are generally in
agreement except for the metal platinum.   In this case the present results are
probably more reliable, since the method is essentially empirical and relies on
no arbitrary assumptions.   Values of 70 ergs/cm^2 for thorium, 130 ergs/cm^2 for palladium
330 ergs/cm^2 for rhodium, 45 ergs/cm^2 for gold, 75 ergs/cm^2 for platinum and less than
10 ergs/cm^2 for ytterbium are new values of γ estimated here.

The determination of γ from mode radii are liable to some error and the
correction procedures adopted leave much to be desired.
In the event of more accurate values of becoming available for the
metals used in the calibration, the present results may be modified accordingly.

5. Crystallographic texture variations through rolled aluminium
and copper sheet.

1. Introduction

A surface texture corresponding to the ideal orientation (100) [011] was
first reported by v. Vargha and Wassermann[82] in cold-rolled aluminium sheet. They
suggested that it was associated with thick sheet, a conclusion also reached by
Lucke.[83] On the other hand, Hu, Sperry, and Beck[84] found that a (100) [011] texture
occurred in the surface of thin aluminium sheet that had been reversed between
passes, but not in sheet rolled unidirectionally. In sheet rolled unidirectionally
Hu et al. found merely a slight tilt of the normal centre texture about the
transverse direction, although it was in unidirectional rolling only that Lucke
obtained any (100) [011] surface texture.

In the same investigation Hu et al. found that α-brass and copper showed no
distinctive surface texture under either unidirectional or reverse-rolling conditions;
they again noted a slight tilt of the normal centre texture about the transverse
direction at the surface.

No indication of the mechanism of formation of the (100) [011] surface texture
was provided by the work noted above, and no explanation of the contradictory results
of Lucke[83] and of Hu et al.[84] was available.

2. Experimental.

Work was carried out on two metals, commercial-purity aluminium and oxygen-free
high-productivity copper, and the variables considered were: (1) friction between metal
surface and rolls, (2) draught, (3) temperature of rolling, and (4) unidirectional or
reverse rolling.

In every case the starting material was 0.5 thick and rolling was carried out
on a two-high Taylor and Challen mill with 10-in-dia steel rolls. In studying the
effects of temperature, the rolls were heated by means of a gas burner placed beneath
the lower roll. The lower roll was maintained at a temperature of $200^{\circ}C$ and the
upper roll at $100^{\circ}C$.

At room temperature four different frictional conditions were obtained. The values
of the coefficient of friction chosen to represent these conditions are, in the absence
of any direct method of measuring the coefficient of friction in rolling, only
approximate estimates but there is no doubt of the order in which they are placed.

At the two lower levels estimates were made by determining the limiting draught, while the two higher values were placed in order by subsequent examination of the surface state. The conditions used and the estimates of the coefficient of friction were as follows:

(a) Rolls cleaned but not degreased; $\mu = 0.1$
(b) Paraffin applied to the rolls: $\mu = 0.2$
(c) Rolls cleaned and degreased and dusted with MgO powder; $\mu \simeq 0.5$.
(d) Both paraffin and MgO powder applied to the rolls; $\mu \simeq 0.35$

The combinations of variables examined are indicated in Table 11 Full sets of $\{111\}$ pole figures showing the variation in texture through the thickness of the sheet were obtained for certain conditions, as indicated in the table. For the other conditions diametral scans through the rolling direction and sheet normal of the $\{111\}$ pole figures were sufficient to reveal the variation of texture with depth of section.

The pole-figure work was carried out on a Siemens "Texturgoniometer" with CuKα radiation. Successive layers of the sheet were etched away and X-rays were reflected from the surface using the Schulz reflection method.

5. 3. Description of Textures.

Sets of $\{111\}$ pole figures for cold-rolled aluminium, obtained from sections at various depths from the sheet surface, are reproduced in Figs.50 and 51. When the coefficient of friction is fairly low ($\mu = 0.2$) (Fig. 1.) the surface texture is mainly (100) [011]. After 0.001 in. has been removed, the original (100) [011] texture has rotated about the transverse direction through 15° towards the rolling direction and a new peak has appeared at 25° from the rolling plane. As further layers are etched away, the (100) [011] texture continues to rotate towards the rolling direction until [111] poles lie at $\sim 25^{\circ}$ from the sheet normal and close to the rolling direction. The peak near to the rolling direction tends to split and the orientation then corresponds to the centre texture.

Under conditions of very high friction between the strip and the rolls, another texture is observed in the surface in addition to the (100) [011] (Fig.51). In this new texture, $\{111\}$ planes lie parallel to the sheet surface but because it is a relatively small component, it is difficult to state with certainty which direction lies parallel to the rolling direction. The tentative indices (111) [110] will be assigned to this component.

TABLE 11

Variables Examined.

Uni direct- ional or Reverse (U or R)	Draught, in.	Material						
		Aluminium				Aluminium and Copper		
		Rolling Temperature, $^{\circ}$C						
		20				200	300	400
		Coefficient of Friction (μ)						
		0.1	0.2	0.35	0.5	0.5	0.5	0.5
U	0.01		*		*			
U	0.02		*		*			
U	0.04	*	*†	*	*†	*†	*	*
U	0.08		*		*			
R	0.02				*			
R	0.04		*					

Conditions examined are indicated by an asterisk
† indicates that full sets of pole figures throughout the thickness of the sheet were obtained.

Poles of $\{111\}$ planes for the ideal orientations are indicated in Fig 52.
It can be seen that the two orientations mentioned above are related to components
of the centre texture by a rotation about the transverse direction. (100) $[011]$ is
related to (211) $[\bar{1}11]$ by a 35° rotation about the transverse direction and (111) $[\bar{1}\bar{1}0]$
is related to an orientation near to (153) $[\bar{2}\bar{1}1]$ by a 27° rotation.

4.   Effects of the Main Variables.

Friction.

The depth of penetration of the (100) $[011]$ surface texture increases as the
coefficient of friction increases.   This is shown in Fig.54 for aluminium cold rolled
unidirectionally with passes of 0.04 in.   Under conditions of very low friction, no
(100) $[011]$ texture is formed.

Draught.

Under the high friction conditions and for a range of draughts from 0.01 in., to 0.10:
appreciable layer of the surface texture (100) $[011]$ was formed, but the depth of
penetration varied erratically with draught, and no simple relation between the two
variables existed under these conditions.

At low friction ($\mu = 0.2$) the angle of tilt between the surface texture and the
centre texture was determined from diametral scans and plotted against draught (Fig.54)
for aluminium cold rolled unidirectionally.   The curve shows an increasing angle of
tilt with increasing draught up to an angle of 35°, at which angle the surface texture
is (100) $[011]$ Further increasing the draught beyond that required to give the 35°
relative displacement increases the depth of penetration of the   (100) $[011]$ surface textur

Temperature.

Penetration of the surface texture for unidirectionally rolled aluminium increases
with rolling temperature up to $300^{\circ}C$ but then falls back to zero at $400^{\circ}C$ (Fig.55).
As shown by Fig.55 there is a difference between the depth of penetration of the
surface texture on either side of the sheet, the side that had been against the cooler
roll showing the greater penetration.   The difference is attributed to dissimilar
frictional conditions, possibly arising from the fact that the lower roll was enveloped
in a reducing flame which may have acted to prevent the formation of abrasive oxide
layers.   Subsequent examination of the sheet surfaces confirmed that the friction
was higher against the cooler roll.

Copper at room temperature did not show any distinctive surface texture under
any conditions of rolling, but at elevated temperatures exhibited the same behaviour
as aluminium, showing a peak in the curve of temperature vs. penetration of (100) $[011]$

surface texture at 300°C and a subsequent fall to zero at 400°C. A specimen of copper rolled at 500°C, however, showed appreciable penetration of the (100) $[011]$ texture. This suggests that the drop in surface penetration at 400°C is in some way associated with the roll surface. It was possible that some of the effects observed at elevated rolling temperatures might have been due to the occurrence of re-crystallization in the time intervals between passes. To check this possibility the surface structure of aluminium rolled at 400°C to the penultimate stage of the normal sequence, held for a few seconds amd quenched, was examined. A finely collimated beam of CrKα radiation was reflected from the surface of the sheet. Continuous Debye rings were obtained, and it was concluded that recrystallization had not taken place.

In all warm-rolling experiments the sheet was passed rapidly through the rolls, back over the top roll, and through again in continuing sequence. The sheet was in no case reheated between passes and temperature determination in the case of the alumini m rolled at 400°C indicated that the maximum temperature drop was only 30 deg.C. The whole process took $\sim \frac{1}{2}$ min and the sheet was quenched into water after the final pass.

Reversal of Rolling Direction.

Aluminium sheet was rolled with the direction of rolling reversed after each pass under two frictional conditions, with a pass sequence which, on unidirectional rolling gave the (100) $[011]$ surface texture. With a low coefficient of friction (μ= 0.2) no (100) $[011]$ surface texture was produced in the reverse-rolled sheet, whereas with a high coefficient of friction (μ= 0.5) the (100) $[011]$ component was stronger in the reverse-rolled sheet than in the unidirectionally rolled material.

5. Discussion.

It has been shown above that the surface and centre textures are related to each other by a rotation about the transverse direction. If it were simply a matter of rotation from one orientation to the other, the surface texture would be expected to be predominantly (111) $[1\bar{1}0]$, which is related by rotation to (153) $[2\bar{1}1]$. This latter orientation describes the centre texture better than (211) $[\bar{1}11]$, which is the central component related by rotation to the surface component (100) $[011]$. The observation recorded is that the surface texture is usually (100) $[011]$, except when the friction between sheet and rolls is very high.

It is proposed below that the surface texture is formed by precisely the same processes as the centre texture, but under the influence of differently oriented stress axes. This accounts for the rotational relationship between the textures. In addition, however, there are other conditions of stability that determine whether or not a surface texture is formed.

The orientation of the stress system in a material undergoing deformation is conveniently illustrated by means of the slip-line field, in which the directions of maximum shear stress through the material are plotted. In the derivation of the slip-line field for a particular type of deformation, the material is considered to behave as an ideal rigid/plastic solid and is assumed to be isotropic. No slip-line-field solution for rolling has yet been calculated. As an approximation to the case of rolling we have therefore chosen, merely as a device to illustrate the orientation of the stress axes in rolling, the plane-strain compression test, but this cannot be considered completely satisfactory. It has been chosen, however, because it exhibits a neutral point across which the velocity between material and platen changes direction, in common with rolling.

In Fig.56 the slip-line field solutions for extreme friction conditions are shown. The solution due to Hill, Lee, and Tupper[85] for the slip-line field under conditions of plane strain between perfectly rough platens, is represented in Fig.56(a) In fig.56(b) the slip-line field for perfectly smooth platens is shown for the case where the platen breadth is an integral multiple of the sheet thickness. The plane-strain slip-line field cannot apply to rolling under conditions of sticking friction, since the position of the neutral point varies through the thickness and also lies at all points along the metal/roll interface. For the purpose of discussion this complication is avoided by assuming high, but not sticking, friction, where necessary.

The angles at which the slip lines meet the platen are given by:

$$\cos 2\Theta = \frac{\mu q}{k} \qquad \qquad \ldots (1)$$

where q is the pressure and k is the shear stress. For the Tresca criterion q/k = 2 and equation (1) becomes $\cos 2\Theta = 2\mu$.

From this it follows that under conditions of zero friction $\Theta = + 45°$, while under sticking-friction conditions $\Theta = 0°$ and $90°$. Values of friction between zero and sticking give the full range of values of Θ between these extremes.

Two principal stress axes lie at ± 45° to the slip lines and are indicated in the surface and centre in Figs.56(a) and (b).

It is readily seen that the slip lines always cross the centre line of the material at 45° to the centre line, so that the centre texture is always formed under the same stress system regardless of the external conditions, and regardless of position relative to the neutral point.

Under both these extreme conditions of friction the stress system at the surface is not altered on passing through the neutral point, but for material between the surface and the centre the stress system on the exit side of the neutral point is a mirror image of the stress system on the entry side. This will also be the case when values of the coefficient of friction between the two extremes obtain.

It is clear that under zero friction the same texture would be expected throughout the material, since the positions of the stress axes do not vary through the material. At high friction the surface texture should be different from the centre texture, but since at values of friction close to sticking negligible changes in the stress system occur on passing through the neutral point, there will be no additional stability conditions determining the surface textures. The surface texture under these conditions would thus be expected to be capable of direct rotation to form the centre texture. It is seen from Fig.51 that the immediate surface texture does, in fact, show a predominance of the orientation related by simple rotation to the orientation that predominates in the centre.

The intermediate layers in the material rolled under high-friction conditions, the stress system for which does change appreciably on passing through the neutral point, have a texture similar to that in the surface of aluminium rolled at intermediate friction values (Fig50), viz. the (100) $[01\bar{1}]$ texture.

(1) When the stress system does change on passing through the neutral point, the additional stability condition is imposed upon the texture formed that it must beb stable under both orientations of the stress system. This means that it must be symmetrical about the transverse direction and both the (100) $[01\bar{1}]$ and the (111) $[1\bar{1}0]$ textures satisfy this condition. The (111) $[11\bar{2}]$ orientation does not satisfy this condition and for this reason it is thought that (111) $[\bar{1}\bar{1}0]$ probably describes the texture associated with a central (111) peak better than (111) $[11\bar{2}]$

Considerations of stability show that the (100) [01Ī] surface texture is more likely to endure than the (111) [1Ī0] texture, although in the case of high friction when there is a pure shear in the surface this will favour the (111) [1Ī0] texture.

It has been shown (section 2) that heavy cross-slip in f.c.c. metals will lead eventually to a (211) [Ī11] texture. Cross-slip is more likely to occur in the surface than the centre of the material, and it is therefore probable that the surface will exhibit a component related to the (211) [Ī11] centre texture. (100) [01Ī] is such a component.

It has recently been found that silver rolled at 150°C with warm steel rolls exhibits a surface texture described by (112) [1Ī0][86]. This is related to the central (Ī01) [121] texture by a rotation of 30° about the common (111) pole in the transverse direction. Th: surface texture can be explained in the same way as the (100) [01Ī] surface texture described above.

On the basis of the general principles outlined here, it is now possible to give a detailed account of the factors affecting the production of surface textures:

Friction.

The angle between the stress axes at the surface and the centre is a function of friction, as indicated by equation (1) and is equal to $(45 - \theta)^{o}$.

It will be recalled that the angle between the (100) [01Ī] surface texture and the (211) [Ī11] centre texture is 35° and the stress-system orientation difference should be the same. However, it is found (Fig.53) that a (100) [01Ī] texture is formed even with the friction as low as $\mu = 0.2$. It is clear that, since the (100) [01Ī] texture is stable under the changed stress system on passing through the neutral point, a region of (100) [01Ī] orientation arising on the entry side of the neutral point will persist after passing through the neutral point. An increase in the coefficient of friction brings the stress system nearer to the position most favourable for the formation of (100) [01Ī] , and so increases the depth of penetration of the texture. At very low values of friction there will be very little tendency to form (100) [01Ī] and this condition holds for the lowest friction used in rolling aluminium. It would appear that in copper rolled at room temperature it was not possible to obtain a sufficiently high coefficient of friction to develop a surface texture.

Draught

At low to intermediate values of the coefficient of friction there is not a very strong tendency to form the (100) [011] component, but it will be more likely to form the greater the amount of deformation with the stress axes in one position.

This is related to the amount of deformation occurring on either side of the neutral point, which can be calculated as a function of draught and friction from the following approxmate theoretical relationships.

$$\psi = \sqrt{\frac{\Delta h}{2D}} \quad \frac{1}{\mu} \quad \frac{\Delta \cdot h}{2D} \quad \quad \dots\dots(2)$$

where ψ is the neutral angle. Δh is the draught, μ is the coefficient of friction, and D is the roll dia.;

$$p = \frac{D\psi^2}{\Delta h} \quad \times 100 \quad \quad \dots\dots(3)$$

where p is the percentage of the deformation per pass occurring in forward slip, i.e. after the neutral point.

Combining (2) and (3) gives

$$p = 50 - 100\left[\frac{1}{\mu}\left(\frac{\Delta h}{2D}\right) - \frac{1}{\mu^2}\frac{\Delta h}{4D}\right] \quad \dots\dots(4)$$

This relationship is plotted in Fig.57 for D = 10 in. and the values μ = 0.1, 0.2, and 0.5.

It is shown that increasing the draught increases the amount of deformation before the neutral point is reached for all values of the coefficient of friction, but the effect is greater at low values of friction. This provides the explanation of Fig.54, in which the angle between the centre and surface texture becomes larger with increasing draught. Two effects are operative when the draught is increased. First, the amount of deformation due to one set of stress axes rises with the total deformation per pass, and secondly, the proportion of the deformation per pass due to one set of stress axes also increases. Both conditions are conducive to the formation of a (100) [011] surface texture.

Temperature.

It is thought that the effect of varying the temperature of deformation may be explained mainly in terms of variation of the coefficient of friction. In the absence of reliable measurements of the coefficient of friction, this explanation cannot be supported by direct experimental evidence.

Reversing between Passes.

It was pointed out above that the amount of deformation occurring with the stress axes in one position would be important in determining whether the (100) [011] texture was formed. In reverse rolling the amount of consecutive deformation occurring with the stress axes in the same position is increased, because the position of the stress system on leaving the rolls is maintained by turning the material end for end before it re-enters the rolls. Hence, on taking small passes with a fairly high coefficient of friction, there is approximately double the chance of the (100) [011] surface texture being formed in reverse rolling as compared with unidirectional rolling. This may well account for the results of Hu et al.[3] and it will explain why the aluminium reverse-rolled under conditions of high friction in the present work showed greater penetration of the (100) [011] component than did the unidirectionally rolled material.

Under conditions of low friction more deformation occurs in advance of the neutral point than after it, and from the point of view of texture development the deformation occurring after the neutral point may be considered to be negligible. The texture thus develops under the same stress system throughout in unidirectional rolling and there is a high probability of the (100) [011] texture being formed. Reversing between passes ensures that the two orientations of the stress system operate for equal amounts of deformation, and thus lessens the chance of formation of the (100) [011] surface texture. This could account for the results of Lucke[2] and also for the fact that in the present work reverse rolling under low-friction conditions produced no surface texture.

5. 6. Drawing and Extrusion.

The conical texture observed in drawn and extruded rods by Schmid and Wassermann[87] may also be explained by the concepts outlined above, and preliminary experiments on drawing copper rod through dies of various apical angles indicate that it is the frictional variation which is important rather than the conicity of the die as suggested by Schmid and Wassermann.

It may be noted that in drawing operations the complications inherent in the rolling process, due to the existence of a neutral point, are avoided and the texture formed is solely a function of the orientation of the stress system.

It is possible that, with a knowledge of drawing loads and die pressures, it may be possible to determine values for the coefficient of friction from measurements of the texture variation through the material thickness.

7. Conclusions.

The texture variations through the thickness of rolled sheet have been accounted for in terms of the variations in the stress system, both through the sheet thickness and across the neutral point. The concepts involved are capable of more general application to working processes.

ure!

6. Unifying Concepts.

Throughout this work the idea of cross-slip has consistently arisen to account for the features which have been observed. In the first section, one of the major differences between the deformation at high and low strain-rates was found to be the greater incidence of cross-slip at the high strain-rate. In the second section, cross-slip was invoked in describing the texture development in f.c.c. metals. It is concluded that cross-slip is a most important concept which is at the root of many of the deformation characteristics of f.c.c. metals.

This work has been concerned with deformation, with textures and with the application of texture studies to deformation. The development of deformation theory in terms of dislocations and of texture theory in terms of slip rotations have until now been relatively unrelated. It is felt that the introduction of the ideas of dislocation theory to texture development has now produced some unity between them, and has transformed texture theory into a useful tool of deformation studies. This is demonstrated by the determination of stacking fault energies from texture measurements.

An implication of texture theory which may be important to work-hardening theory, particularly in its application to polycrystalline materials, is that the observed effects can be explained by invoking the occurrence of cross-slip. Slip on third or fourth preferred slip systems cannot account for these effects which are observed.

REFERENCES.

1. L.E. Samuels, J.Inst.Met. (1955), 83, 359.

2. M. Hatherley, J.Inst.Met. (1960), 89, 60.

3. D. Kuhlmann-Wilsdorf and H.G.F. Wilsdorf. Acta.Met. (1953) 1 394.

4. T.H. Blewitt, R.R. Coltmann and J.K. Redman, J. Appl. Phys. (1957), 28, 651.

5. C.S. Smith, Trans. A.I.M.E. (1958), 212, 574.

6. J.A. Venables, Phil. Mag. (1961), 6, 379.

7. C.S. Barrett, "The Structure of Metals" 2nd.Ed. (1952), Mc.Graw-Hill.

8. R.W.K. Honeycombe. J.Inst.Met. (1951), 80, 39.

9. K. Lücke and H. Lange, Z.Metallk. (1952), 43, 55.

10. R. Maddin and N.K. Chen, Prog. Met. Phys. (1954), 5, 65.

11. J. Sawkill and R.W.K. Honeycombe, Acta Met. (1954), 2, 854.

12. E.N. da C. Andrade and A. Aboav, Proc. Roy. Soc. (1957), A24, 304.

13. W.A. Wood, Proc. Roy. Soc. (1939), 172, 231.

14. P.B. Hirsch and J.N.Kellar, Acta Cryst. (1952), 5, 162.

15. P. Gay and A. Kelly. Acta Cryst. (1953), 6, 165.

16. P. Gay, P.B. Hirsch and A. Kelly, Acta Met. (1953), 1, 315.

17. P. Gay, P.B. Hirsch and A. Kelly, Acta Cryst. (1954), 7, 41.

18. M.J. Whelan, P.B. Hirsch, R.W. Horne and W. Bollman, Proc.Roy.Soc. (1957), A240, 524.

19. D.H. Warrington, Proc. European Regional Conf. on Electron Microscopy, Delft, Holland (1960), Vol. I.

20. A. Howie,   Ibid.

21. W. Steeds, Phil. Mag. (1963) 8.

22. F. Rohm and A. Kochendorfer, Z. Metallk. (1950), 41, 265.

23. N.F. Mott, Phil. Mag. (1952), 43, 1151.

24. C.J. Ball, J. Iron and Steel Inst. (1959), 191, 232.

25. G.V. Smith, P.M. Kranzlein and M.S. Burton, Trans. A.S.M. (1963), 56, 701.

26. T.H. Blewitt. R.R. Coltmann and J.K. Redman, Report of Conf. on Defects in Crystalline Solids, Phys.Soc. (London) 1955.

27. J.E. Bailey and P.B. Hirsch, Phil. Mag. (1960), 5, 485.

28. P.A. Jacquet, Rev. Met. (1945), 42, 133.

29. A. H. Cottrell and R.J.Stokes, Proc. Roy.Soc. (1955), 233, 17.

30. W. Köster, Z. Metallk. (1948), 39, 1.

31. F.P. Bullen and M.M. Hutchison, Phil. Mag. (1962), 7, 557.

32. G.E. Dieter, "Response of Metals to High Velocity Deformation", Interscience (London, New York) 1960, p. 409.

33. P.B. Hirsch and D.H. Warrington, Phil. Mag. (1961), 6, 735.

34. A. Kelly, Acta Cryst. (1954), 7, 554.

35. D. Kuhlmann-Wilsdorf, Trans. A.I.M.E. (1962), 224, 1047.

36. F. Weaver and W.E. Schmid, Zeit. Metall., (1930) 22, 123.

37. M.R. Pickus and C.H. Mathewson, J. Inst. Met., (1939) 64, 237.

38. W.R. Hibbard and M.K. Yen, Trans. A.I.M.E. (1948) 175, 126.

39. E.A. Calnan, and C.J.B. Clews, Phil. Mag. (1950) 41, 1085.

40. E.A. Calnan and C.J.B. Clews, Phil. Mag. (1951) 42, 616.

41. F. Haessner, Z. Für Metallk. (1963) 54, 98.

42. W. Boas and M.E. Hargreaves, Proc. Roy. Soc., (1948) A193, 89.

43. M.E. Hargreaves, J. Aust, Inst. Met. (1956) 1, 125.

44. G.E.G. Tucker, J. Inst. Met. (1954) 82, 655.

45. G.E.G. Tucker, Acta Met. (1961) 9, 275.

46. W.H. Baldwin, Trans. A.I.M.E. (1946) 166, 591.

47. W.T. Roberts. J. Inst. Met. (1954) 82, 654.

48. E.A. Calnan, Acta Met. (1954) 2, 865.

49. R.F. Braybrook and E.A. Calnan, J. Inst. Met., (1956) 85, 11.

50. Hu, H., R.S. Cline, and S.R. Goodman, J. Appl. Phys. (1961) 32, 1392.

51. R.E. Smallman and K.H. Westmacott, Phil. Mag. (1957) 2, 669.

52. R.J. Hartmann and E. Macherauch, Naturwiss. (1958) 45, 540.

53. J. Washburn, A. Kelly and G.K. Williamson, Phil Mag. (1960) 5, 192.

54. N. Brown, Trans. A.I.M.E. (1961) 221, 236.

55. C.A. Verbraak, Thesis, Delft Technische Hoeschool, 1959 and Acta Met. (1958) 6. 580

56. M. Cook and T. Ll. Richards, J. Inst. Met., (1940) 66, 1.

57. M. Gensamer and R.F. Mehl, Trans. A.I.M.E. (1936) 120, 270.

58. G. Wassermann and J. Grewen, "Texturen-Metallischer Werkstoffe", Springer-Verlag, Berlin 1962.

59. R.E. Smallman and D. Green, Acta. Met. (1964) 12, 145.

60. F. Haessner, Z. Metallk., (1963) 54, 61.

61. P.R. Thornton & T.E. Mitchell, Phil. Mag., (1962) 7, 1349.

62. R.E. Smallman, J. Inst. Met. (1955) 84, 10.

63. H. Hu and R.S. Cline, J. Appl. Phys. (1961) 32, 760.

64. C.J. McHargue, Acta Met. (1961) 9, 851.

65. J.O. Steigler and C.J. Mc. Hargue, Acta Met., (1963) 11, 225.

66. V.S. Arunachulam and K. Tangri, Acta Met., (1963) 11, 223.

67. R.E. Smallman, J. Inst. Met. (1954) 83, 408.

68. J.T. Waber, I.R. Harris and G.V. Raynor, In the Press.

69. H. Muller, Ostert, Akad. Wiss. Math-Naturw Kl. Aus., (1958) 7, 117.

70. H. Hu, R.S. Cline and S.R. Goodman, Private Communication.

71. C.McHargue and L.Yakel, Acta.Met., (1960) 8, 637.

72. K.A. Gschneider, R.D. Elliott and R.R.McDonald, J.Phys.Chem. Solids,
    (1962) 23, 1191.

73. A. Howie and P.R. Swann, Phil. Mag., (1961) 7, 1215.

74. P.R. Thornton, T.E.Mitchell and P.B. Hirsch, Phil. Mag. (1962) 7, 1349.

75. A. Seeger, R. Berner and H. Wolf, Z. Phys. (1959) 155, 247.

76. H. Wolf, Z. Naturf., (1960) A15, 180.

77. H. Hu and S.R. Goodman, Trans. A.I.M.E., (1963) 227, 617.

78. P.R. Thornton and P.B. Hirsch, Phil. Mag., (1958) 3, 738.

79. J. Silcox and P.B. Hirsch, Phil. Mag., (1959) 4, 72.

80. R.E. Smallman, K.H. Westmacott, and J. Coiley, J. Inst. Metals. (1959) 88, 127.

81. J. Spreadborough, Phil. Mag., (1958). 3, 1167.

82. G. von Varga and G. Wasserman, Z. Metallwirtschaft, (1933) 12, 511.

83. K. Lucke, Z. Metallkunde, (1954) 45, 86.

84. H. Hu. P.R. Sperry and P.A. Beck, Trans. Amer. Inst. Min. Met. Eng.,
    (1952) 194, 76.

85. R. Hill, E.H. Lee and S.J. Tupper, Ministry of Supply Armament Research Dept.,
    Theoretcial Research Rep. (28/45).

86. D. Green, M. Met. Thesis, Univ. Sheffield, (1963)

87. E. Schmid and G. Wassermann, Z. Metallkunde, (1927) 19, 325.

88. Z.S. Basinski. Phil. Mag. (1959) 4, 393.

GRANT ASTIA NO. AF.EOARDC - 61 - 6
United States Air Force, Aeronautical Systems Div.AFSC.
European Office, Aerospace Research, Brussels, Belgium
Final Technical Report: RESEARCH ON HOT WORKING OF METALS,
with particular reference to microstructure, mechanical
properties & texture. by I.L. Dillamore & W.T. Roberts
Date April, 1964.
75 pages, 57 illustrations.
DEPARTMENT OF INDUSTRIAL METALLURGY, UNIVERSITY OF
BIRMINGHAM.

ABSTRACT: The structure and stress-strain behaviour
of O.F.H.C. copper deformed at temperatures in the
range $-196^{\circ}C$ to $600^{\circ}C$, and at two strain rates,
5×10^{-3} and 5×10^2 sec^{-1}, have been studied. A
correlation has been made between the structures
observed optically and by transmission electron
microscopy. It was found that at the low

strain-rate the deformation processes varied considerably over the temperature range, but at the high strain rate the variation was small. Indications of deformation twinning were found at the high strain rate at temperatures up to 450°C. Cross-slip was favoured by the high strain-rate. The effect of deformation temperature on the preferred orientation produced by rolling a number of pure f.c.c. metals has been studied. Variations in the rolling texture could be related to the ease of cross slip in the metal, and this concept has been used to estimate the stacking fault energy of some f.c.c. metals.

The rolling textures developed in f.c.c. and b.c.c. metals have been explained in terms of realistic stress systems, and the variation in texture through the thickness of rolled sheet has been related to rotations of the effective stress system which are governed by friction between the sheet and rolls.
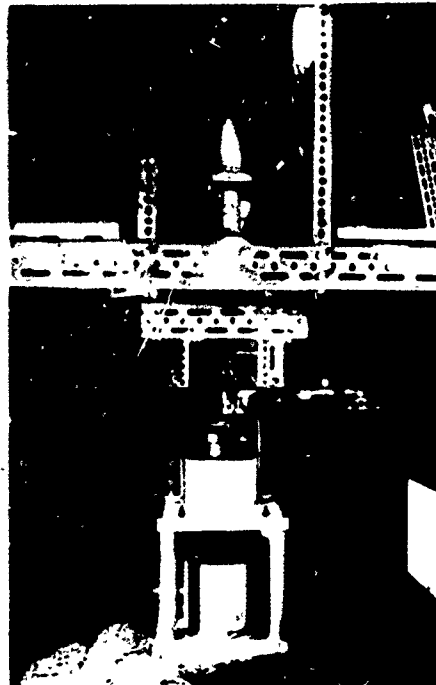
Fig. 1. The drop hammer, showing the weight supported by an electromagnet above the punch assembly.
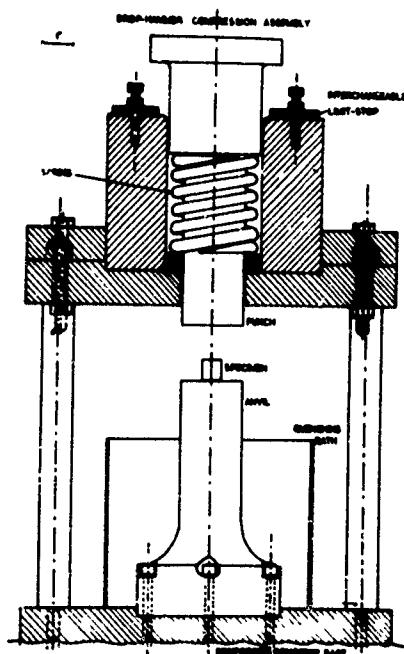
Fig. 2. Scale drawing of the punch assembly on the drop hammer.

Fig. 3.   The slow compression apparatus.
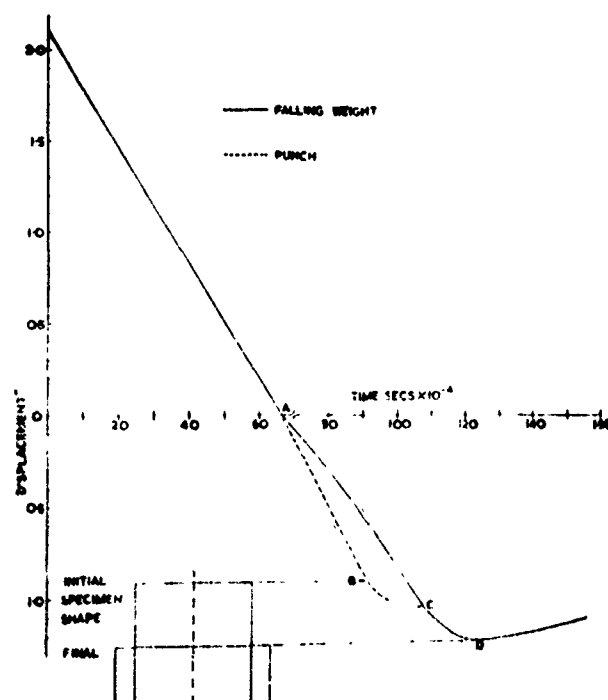
Fig. 4.   Displacement-time plot showing the weight-punch specimen interactions from the cine film of the specimen deformed at room temperature.
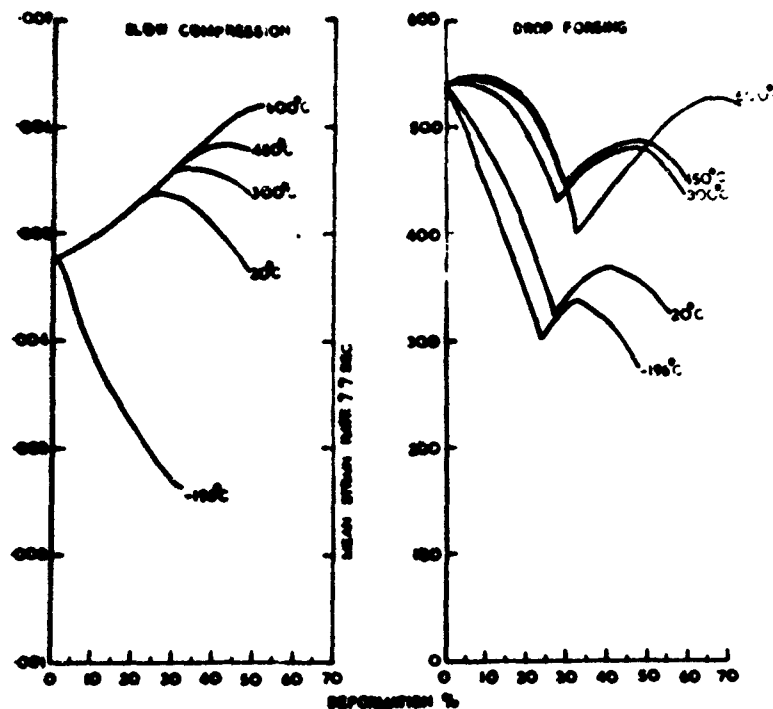
Fig. 5.   Strain-rate versus deformation curves for both slow compression and forging.
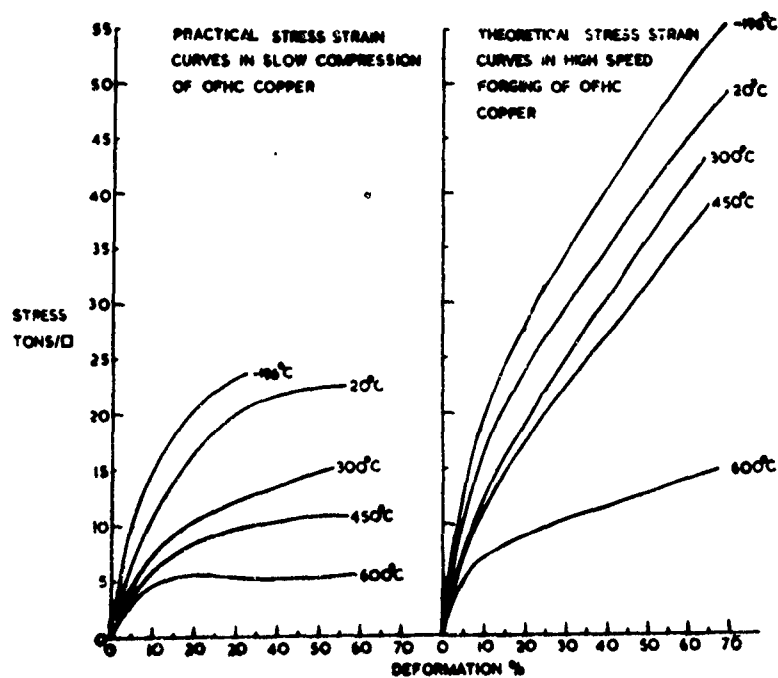
Fig. 6.   Stress-strain curves .   The slow compression curves were obtained directly and the forging curves by calculation from the displacement-time plots.
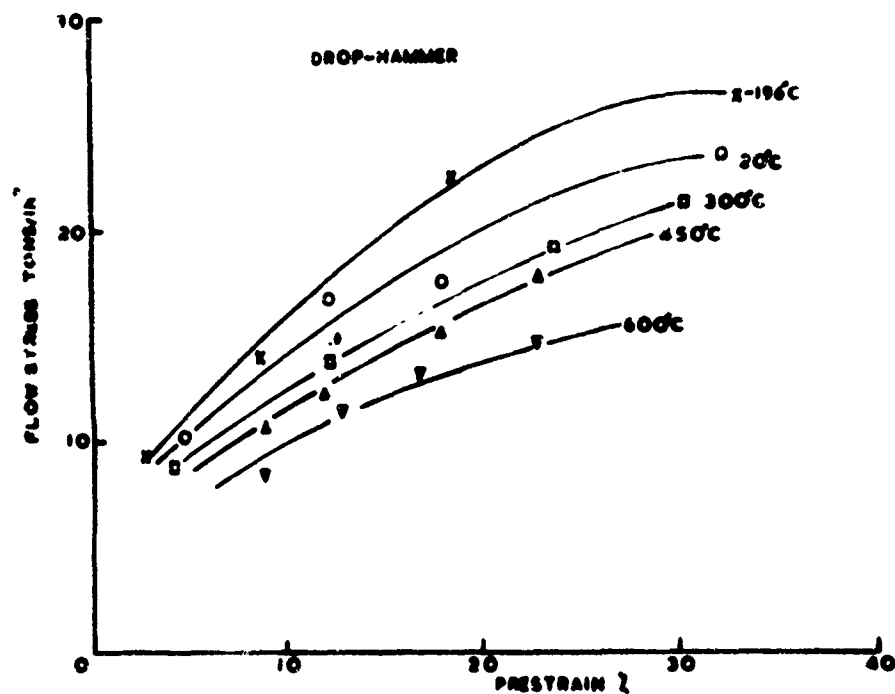
Fig. 7.   Flow stresses of specimen prestrained on the drop-hammer
versus prestrain.
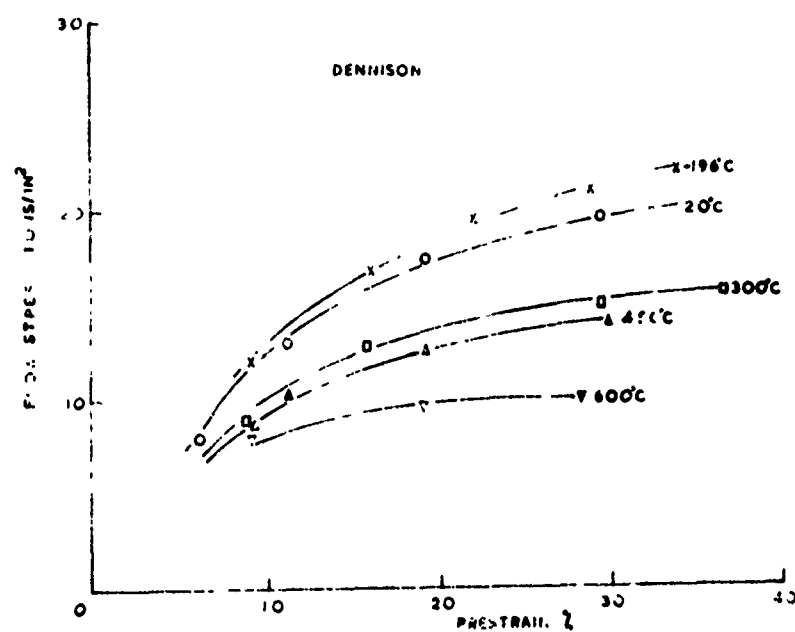
Fig. 8.   Flow stresses of specimens prestrained at the slow strain rate
versus prestrain.
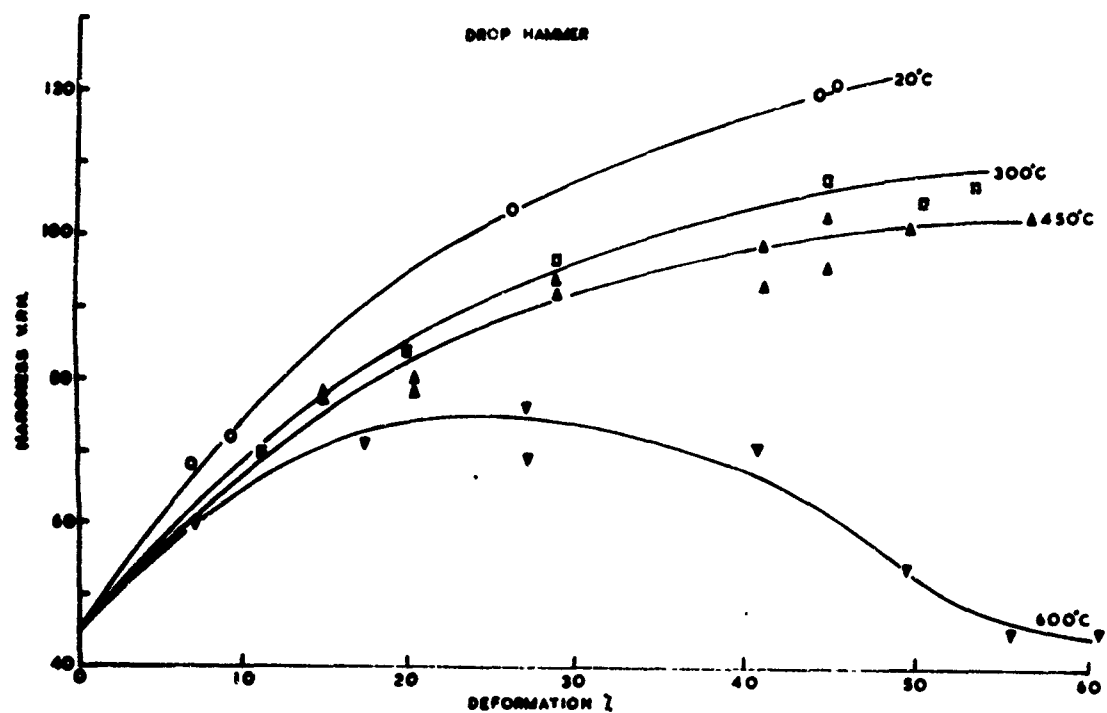
Fig. 9.   Indentation hardness versus deformation for the high strain rate.
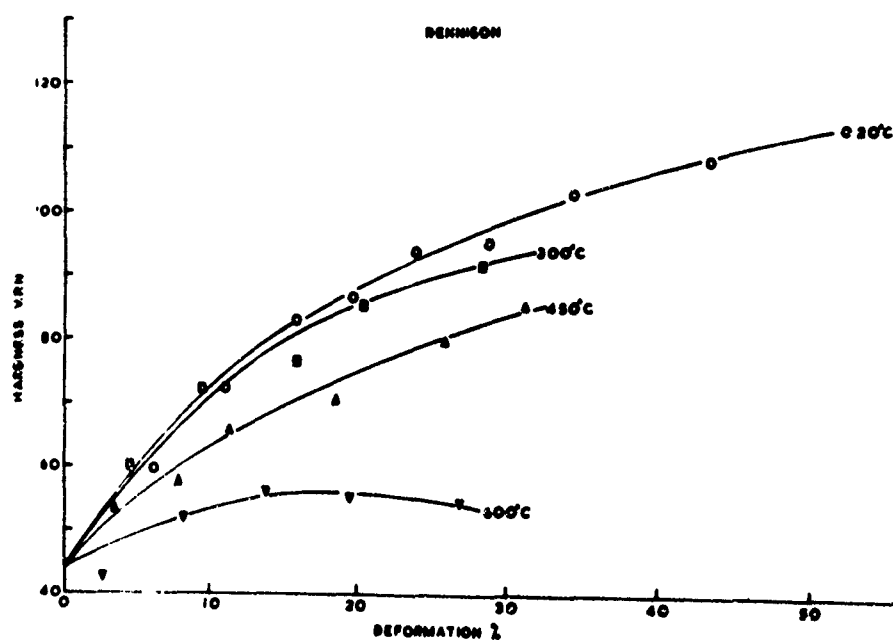
Fig. 10.   Indentation hardness versus deformation for the slow strain rate.
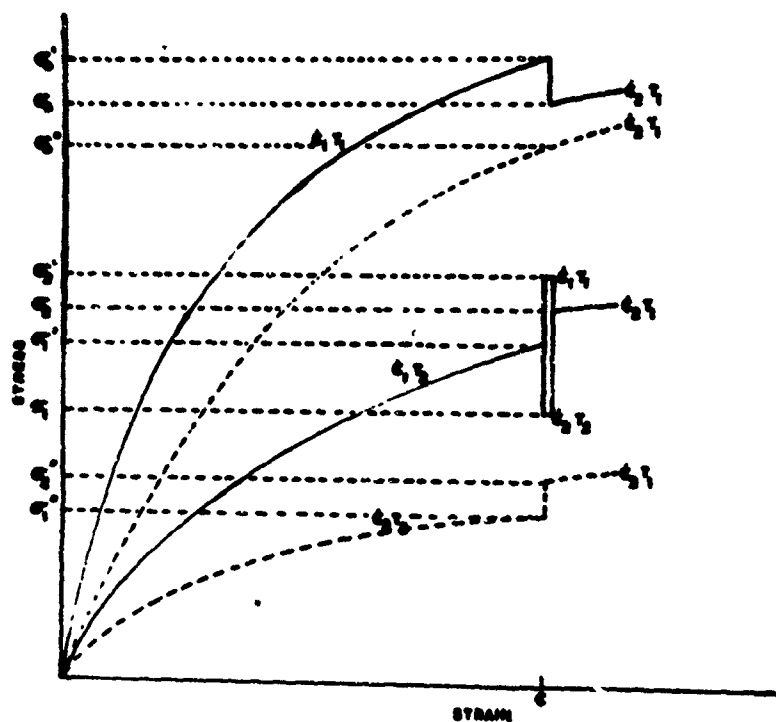
Fig. 11.   Schematic definition of the stress levels discussed in the text.
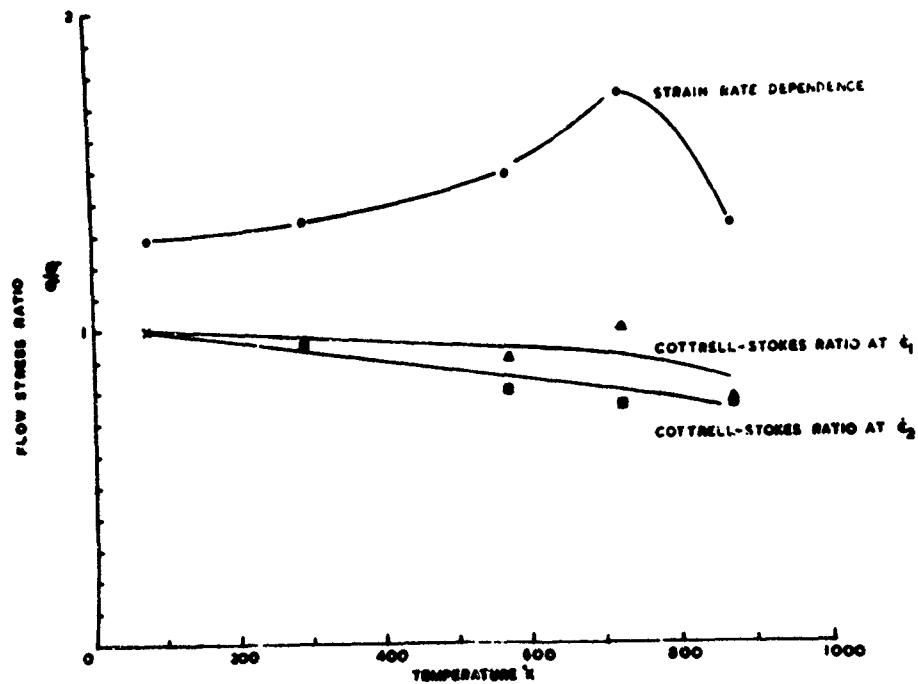
Fig. 12.   Flow stress ratios plotted against temperature.
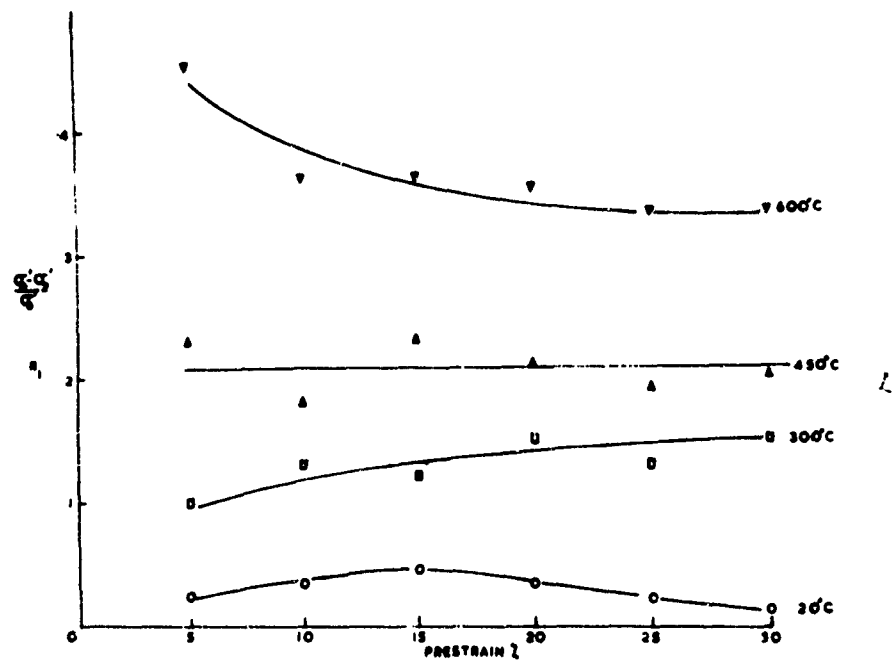
Fig. 13.   Recovery ratio R_1 ($= \dfrac{\sigma_o' - \sigma_2'}{\sigma_o'}$) versus prestrain.
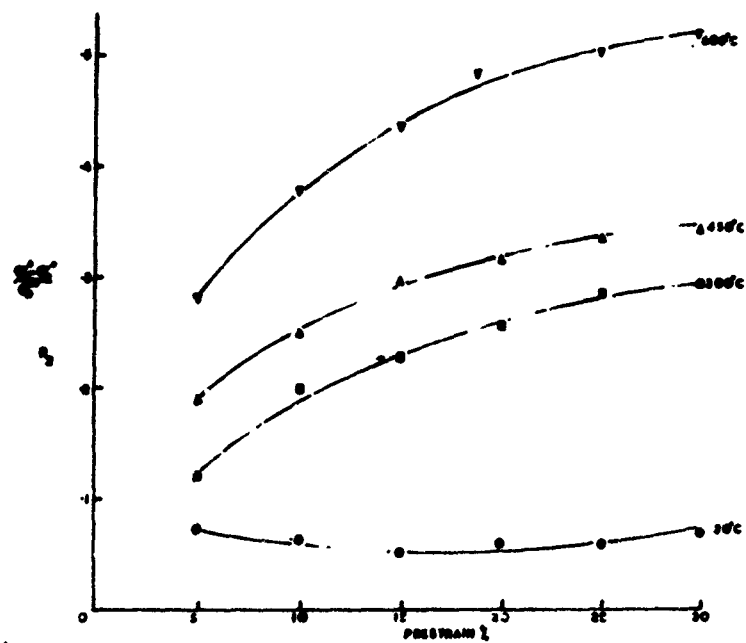
Fig. 14.   Recovery ratio R_2 $\left(= \dfrac{\sigma_o^{''} - \sigma_1^{''}}{\sigma_o^{''}}\right)$ versus strain.
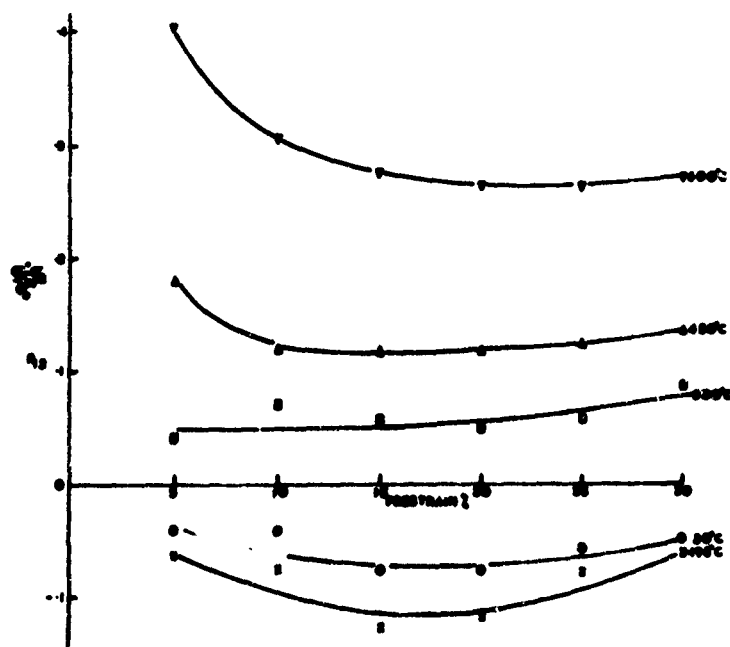
Fig. 15.   Recovery ratio R_{12} $\left(= \dfrac{\sigma_o^{''} - \sigma_2}{\sigma_o^{''}}\right)$ versus strain.

Fig. 16. Optical Micrograph of specimen forged 11% at 300°C. X70.

Fig. 17. Micrograph of sample slow-compressed 10% at 300°C. X70.

Fig. 18. Micrograph of specimen forged 20% at room temperature showing a typical 'step-ladder' structure of deformation bands between annealing twins. X70.
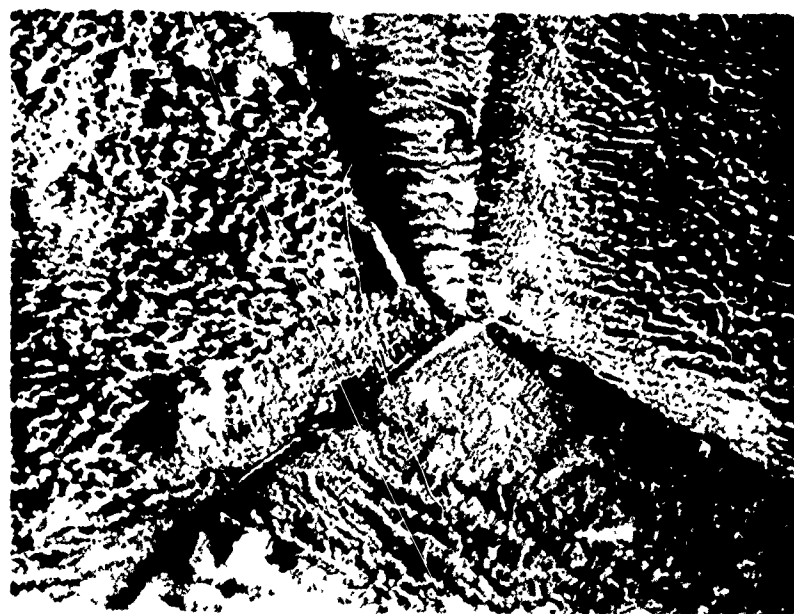
Fig. 19. Micrograph of sample forged 12% at 600°C. X1000.

Fig. 20.   Micrograph of a sample forged 41% at -196°C.   Showing
            deformation twins.   X70.

Fig. 21. Micrograph of specimen forged 14% at 600°C. X70.

Fig. 22. Micrograph of sample slow-compressed 14% at 600°C. X70.
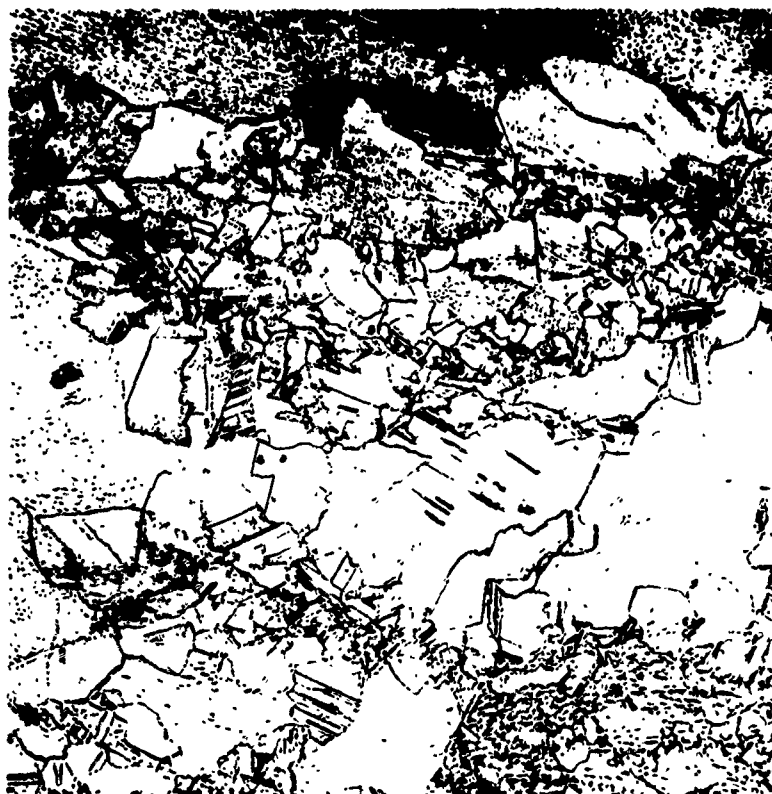
Fig. 23.   Micrograph of partially recrystallised specimen forged 55%
at 600°C.   X210
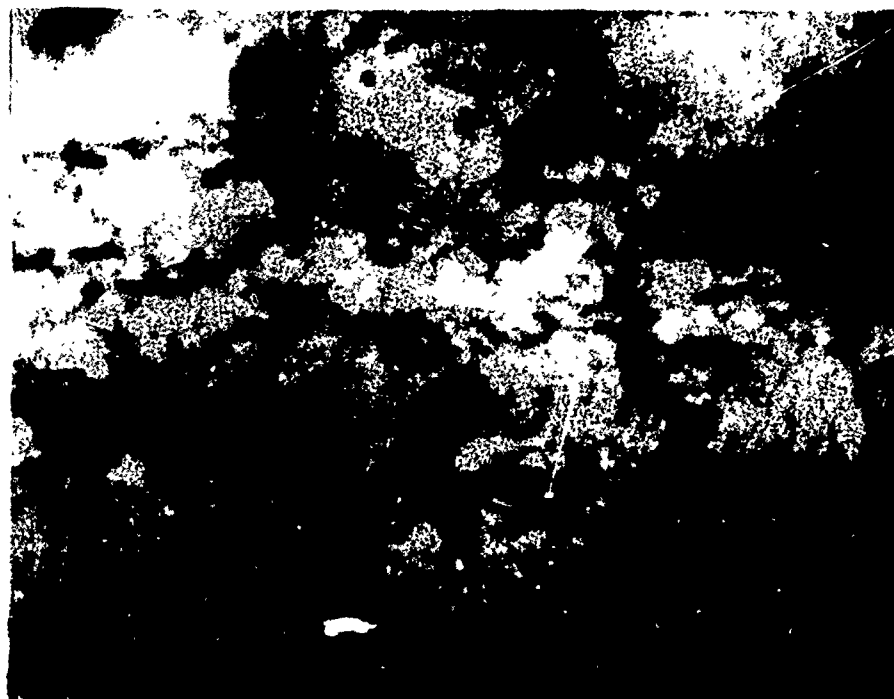
Fig. 24. Electron micrograph from specimen forged 9% at 20°C. X20,000.

Fig. 25. Electron micrograph from specimen forged 24% at 20°C. X20,000.
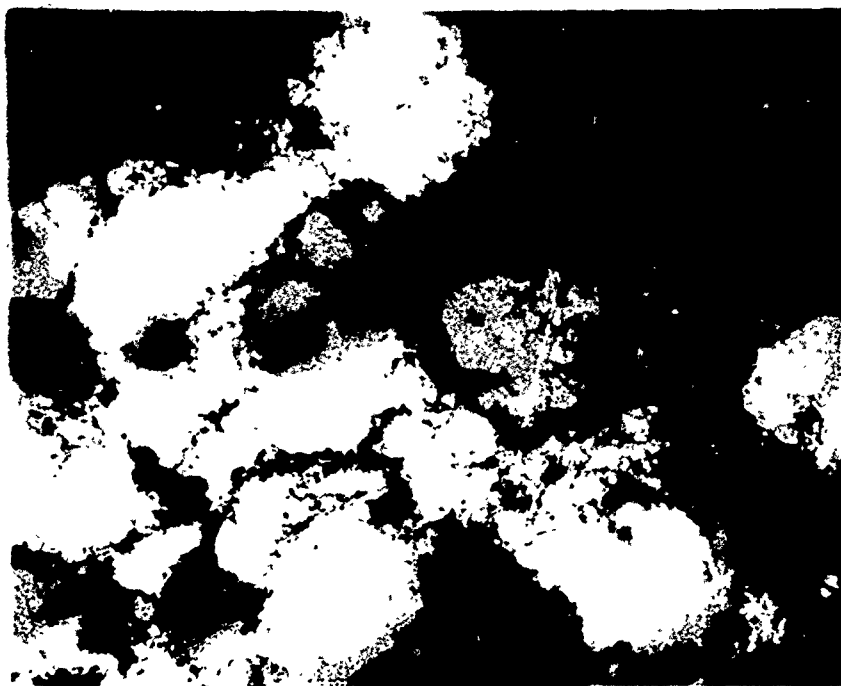
Fig. 26. Electron micrograph from sample forged 12% at 600°C. X20,000.
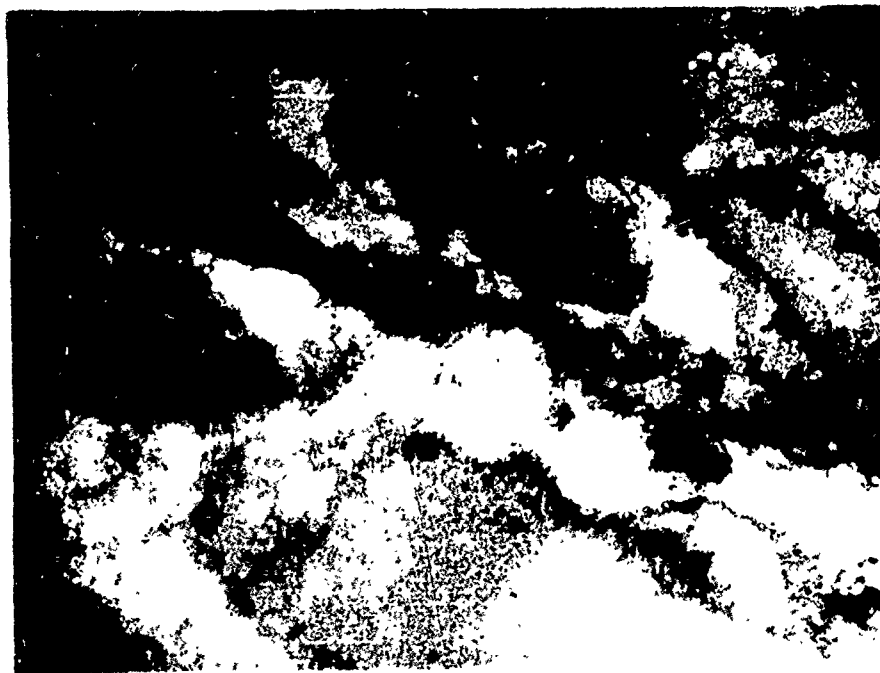
Fig. 27. Electron micrograph from specimen forged 25% at 600°C. X20,000.
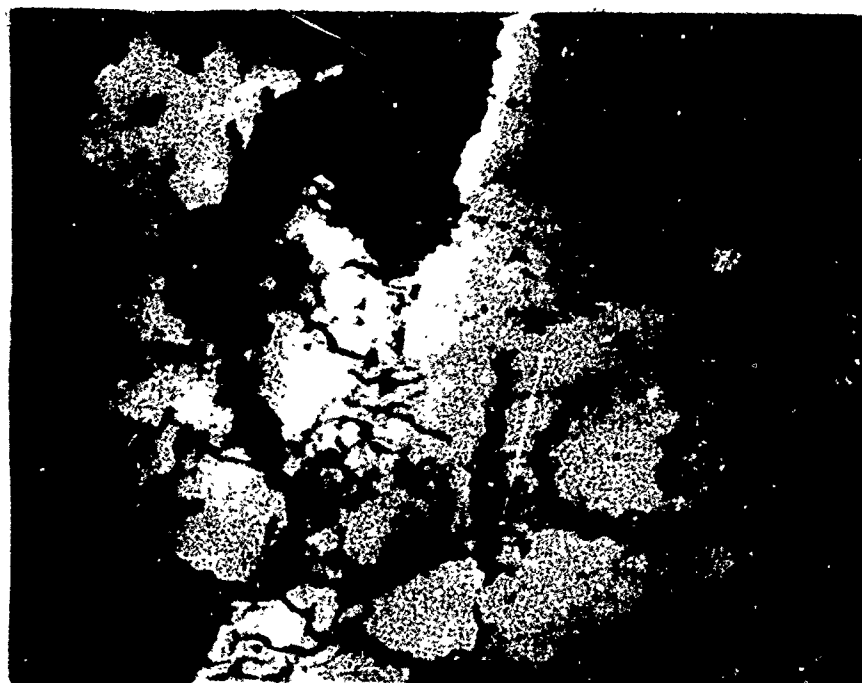
Fig. 28.   Electron micrograph from a sample slow-compressed 2% at 600°C.   X20,000.
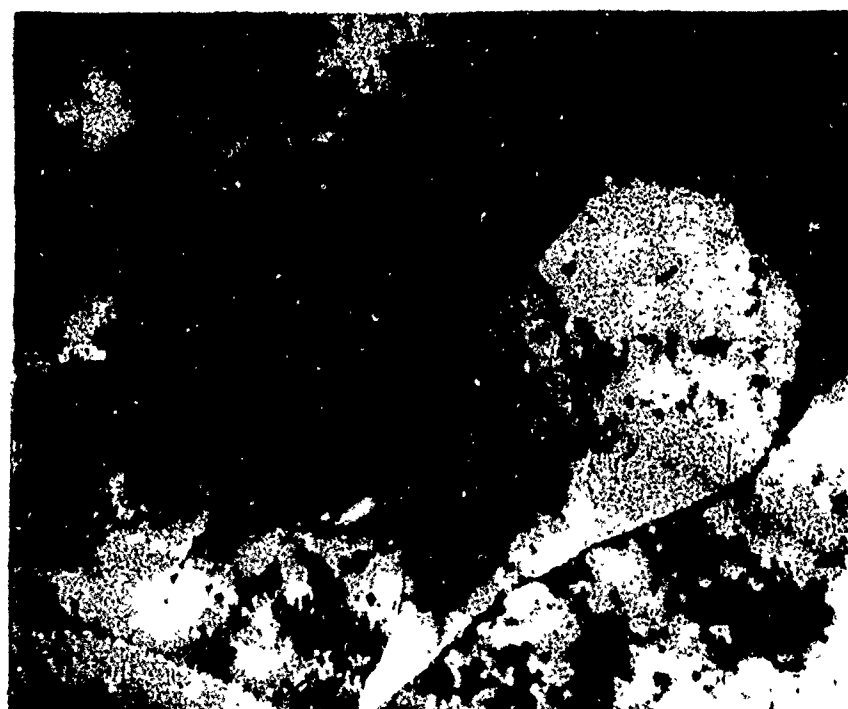
Fig. 29.   Electron micrograph from a sample slow-compressed 2% at 600°C,   X20,000.

Fig. 30. Electron micrograph from a sample forged 50% at 300°C. Showing a stacking fault. X40,000.
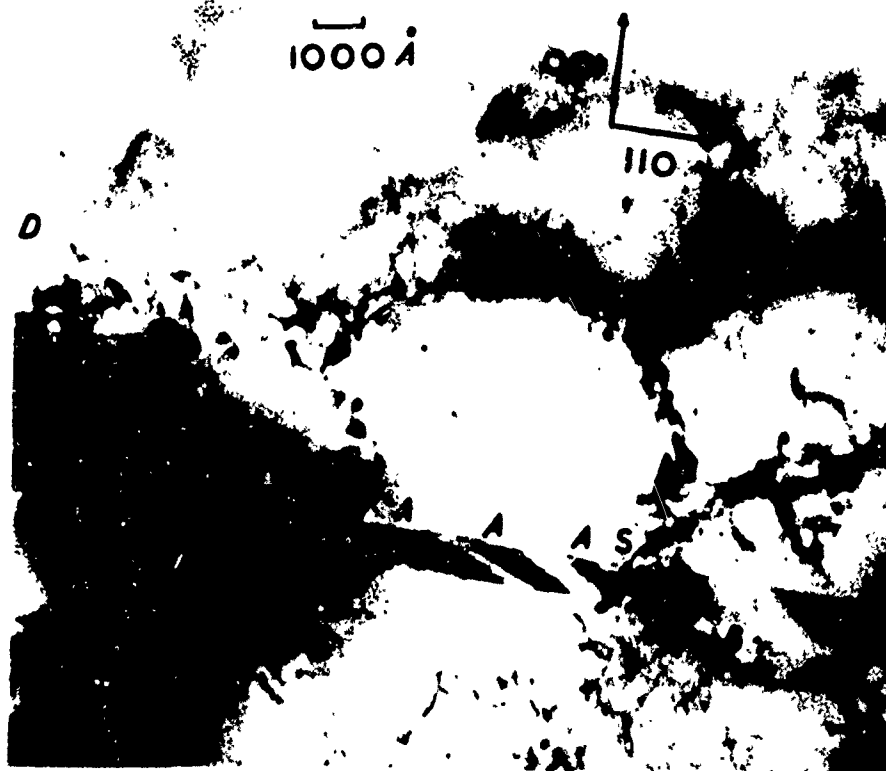
Fig. 31. Electron micrograph from a sample forged 24% at 20°C. Showing a pile-up of extended edge dislocations against a sub-grain boundary. X50,000.
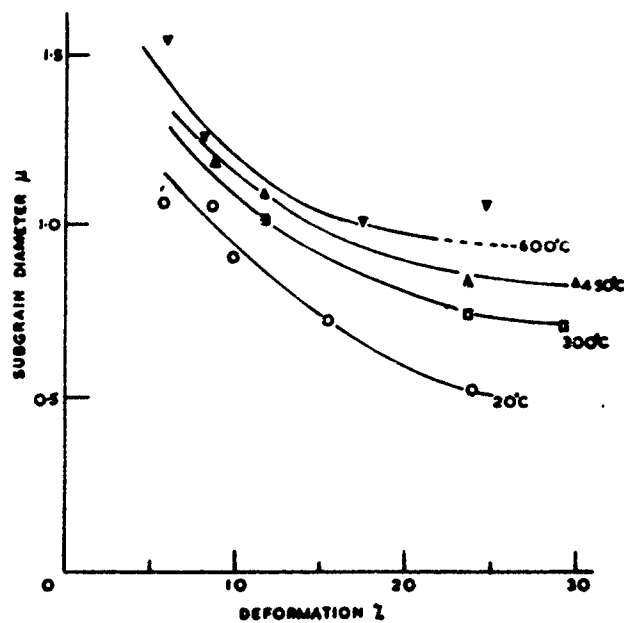
Fig. 32. Sub-grain diameter versus prestrain.
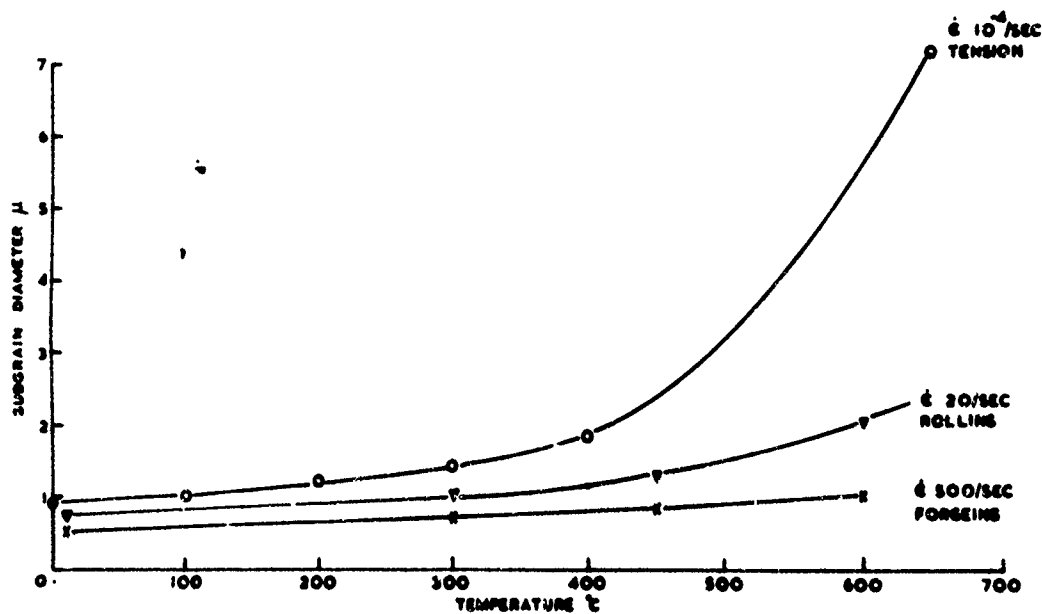
Fig. 33. Limiting sub-grain size plotted against temperature.
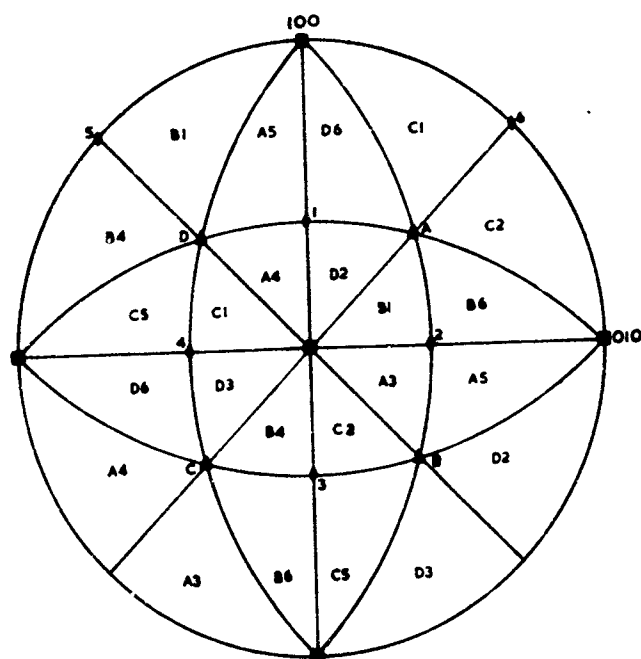
Fig. 34. Standard (001) Stereographic Projection for cubic crystals showing the slip system of maximum resolved shear stress for a uniaxial applied stress in any one of the unit triangles. Slip plane normals A-D, slip directions 1-6.
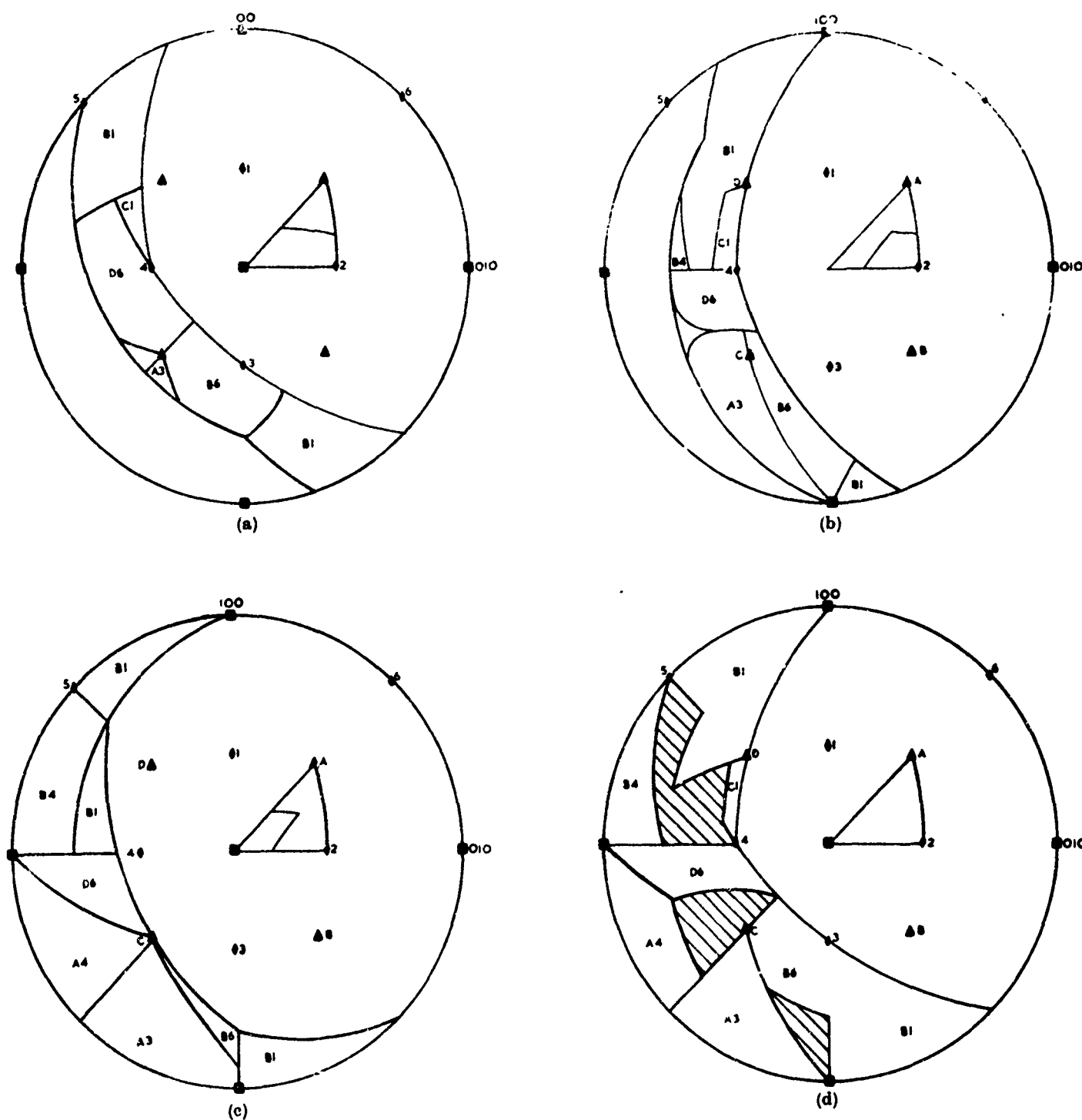
Fig. 35. (a)-(c). Standard projection showing systems of maximum resolved
shear stress for a biaxial stress system, with one stress
axis in three different areas of the unit triangle 001,
111, 011. Area bounded by (a) 113,111,133,123; to
(b) 013,123,133,011, (c) 001,113,123,013.

Fig. 35(d). Regions in which the system of maximum resolved shear stress
is independent to the position in 001,111,011.

Fig. 36.   Standard projection showing rotations towards (110) 112 .
Primary and conjugate slip on A3 and C2.

Fig. 37.   {111} pole figure for 70/30 brass cold rolled with 95% reduction
in thickness.
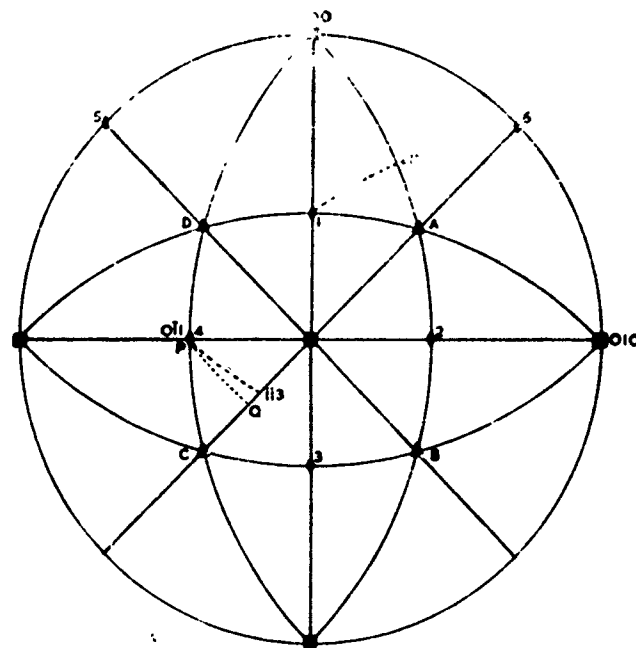
Fig. 38. Standard projection referring to cross slip. Primary and conjugate slip initially on C1 and D6.
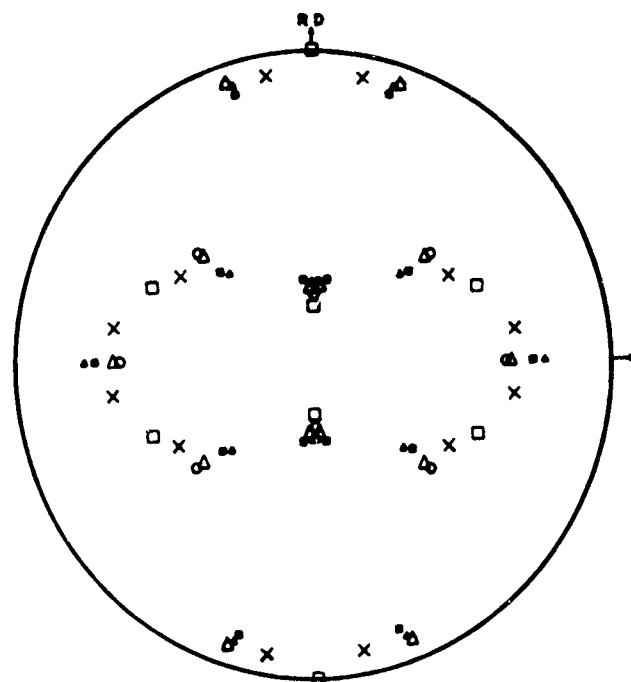
Fig. 39. {111} pole figures showing orientation spread predicted from rotations due to cross slip.

▫	$\{112\} \langle 111 \rangle$	△	$\{20,35,64\} \langle 945 \rangle$
✗	$\{18,24,51\} \langle 322 \rangle$	■	$\{135\} \langle 211 \rangle$
○	$\{8,12,23\} \langle 734 \rangle$	▲	$\{146\} \langle 211 \rangle$

(a)

(b)

(c)

(d)
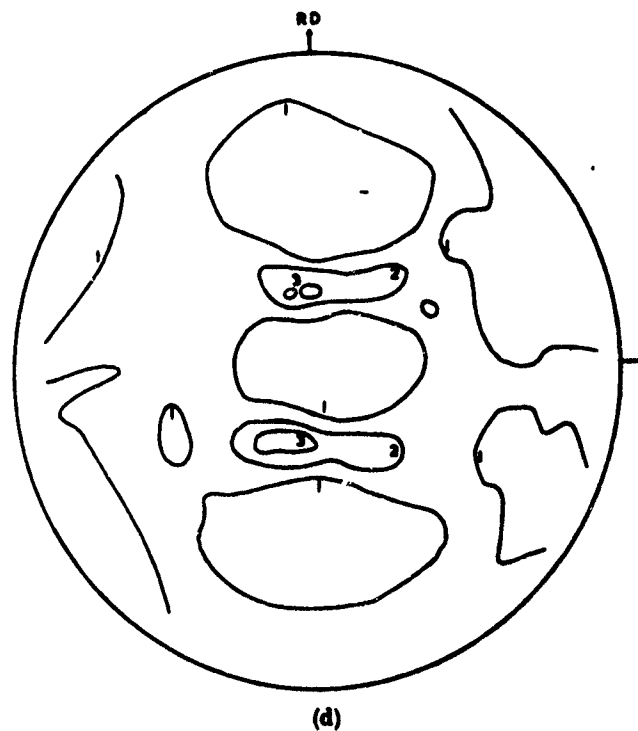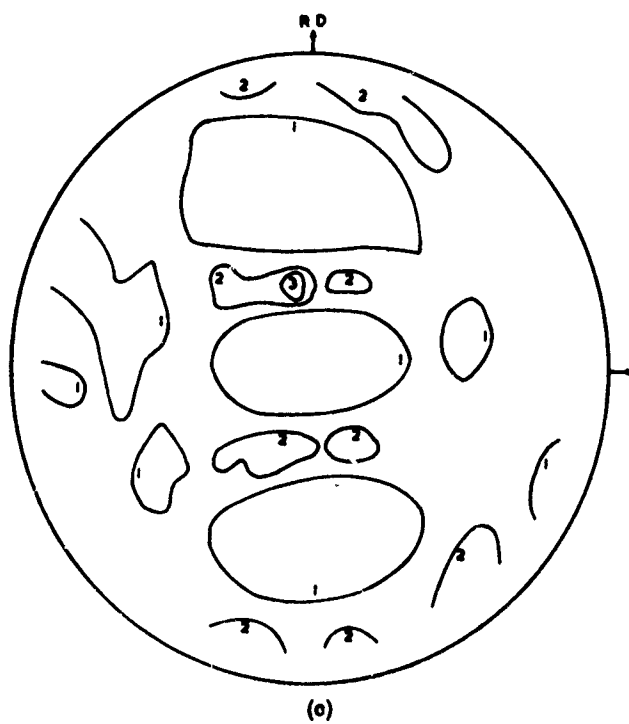
Fig. 40. (a-d).
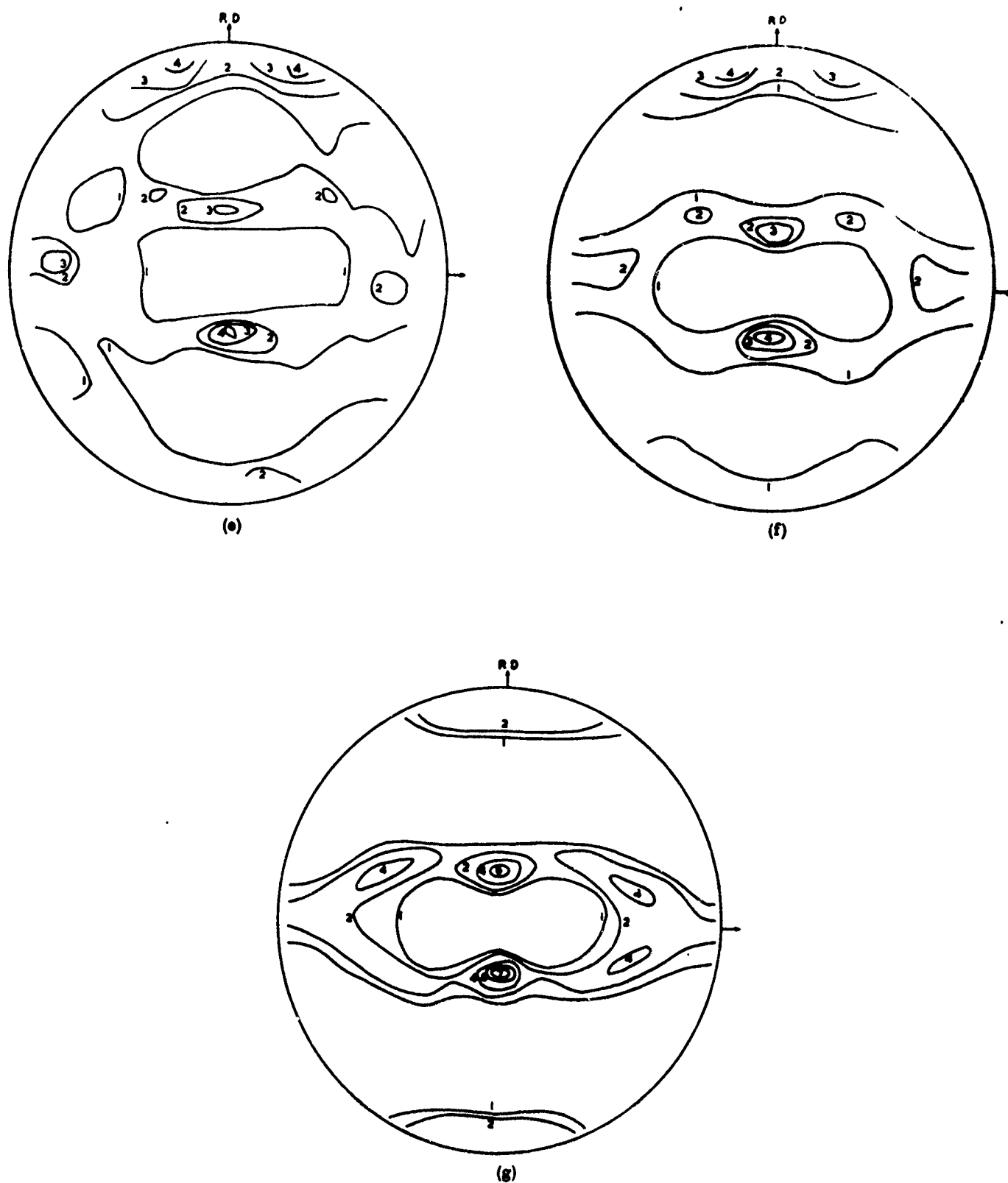
Fig. 40.   {111} pole figures for aluminium cold rolled with the following reductions: (a) 0, (b) 45%, (c) 60%, (d) 70%, (e) 80%, (f) 95%, (g) 99.9%.
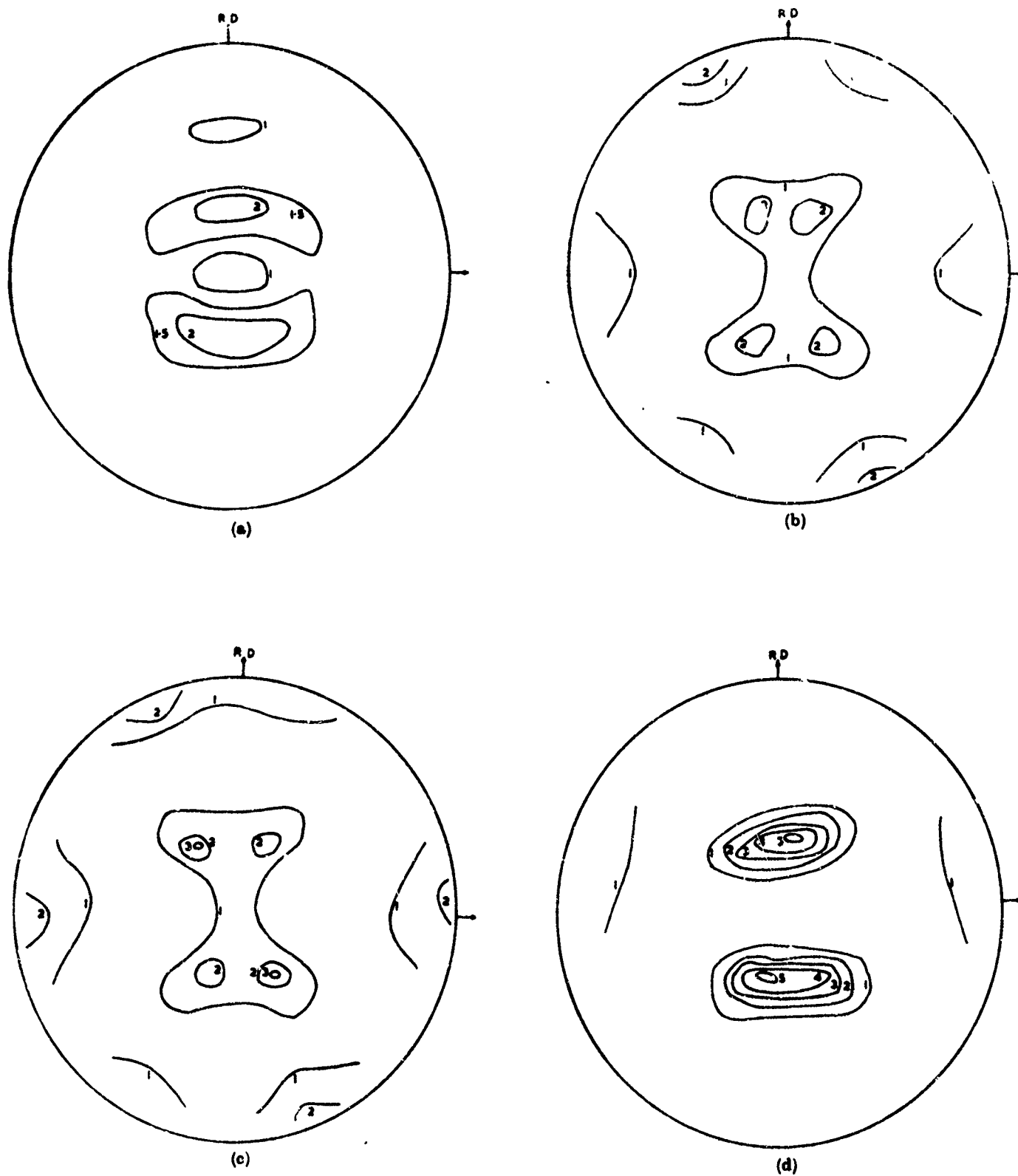
Fig. 41.   {111} pole figures for silver cold rolled with the following
             reductions: (a) 50%, (b) 90%, (c) 95%, (d) 99.6%.

(a)
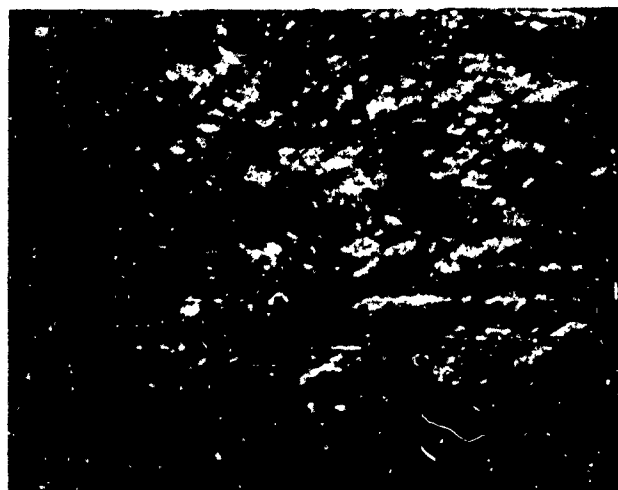
(b)

(c)

Fig. 42. Photomicrographs of longitudinal edge sections of rolled sheet:-
(a) Aluminium-60% reduction, (b) aluminium-70% reduction,
(c) silver-60% reduction.   Rolling direction parallel to long
edge.   X410.
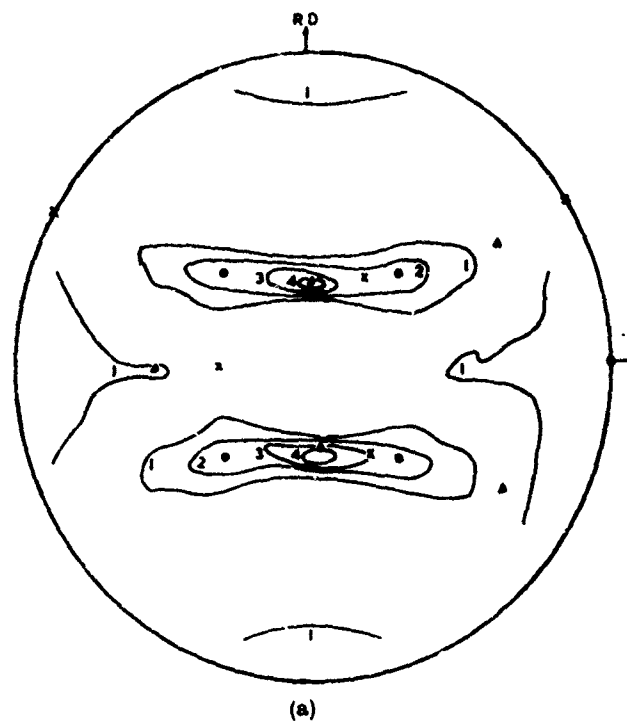
(a)
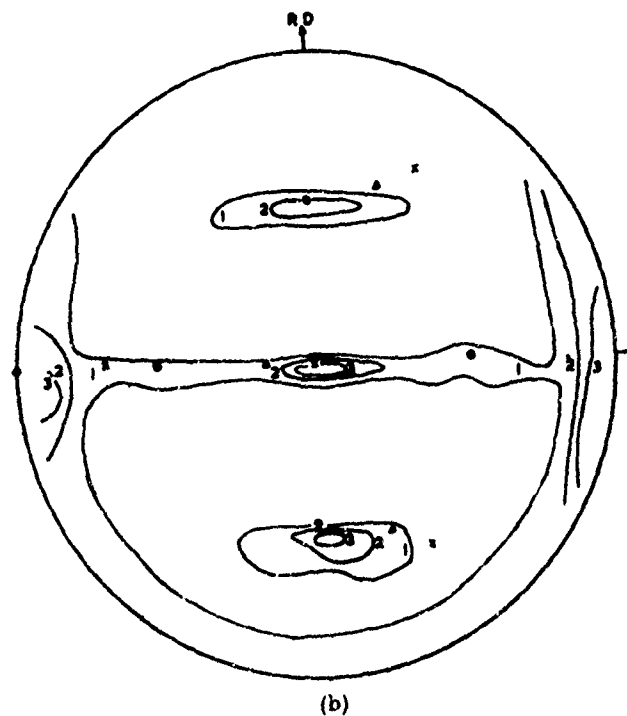
(b)

Fig. 43.   Pole figures for vanadium cold rolled 95%.

        (a)   {110} pole figure.   (b)   {222} pole figure.

      ✕ (111) [0$\bar{1}$1]   ● (100) [00$\bar{1}$]

      ▲ (112) [1$\bar{1}$0]
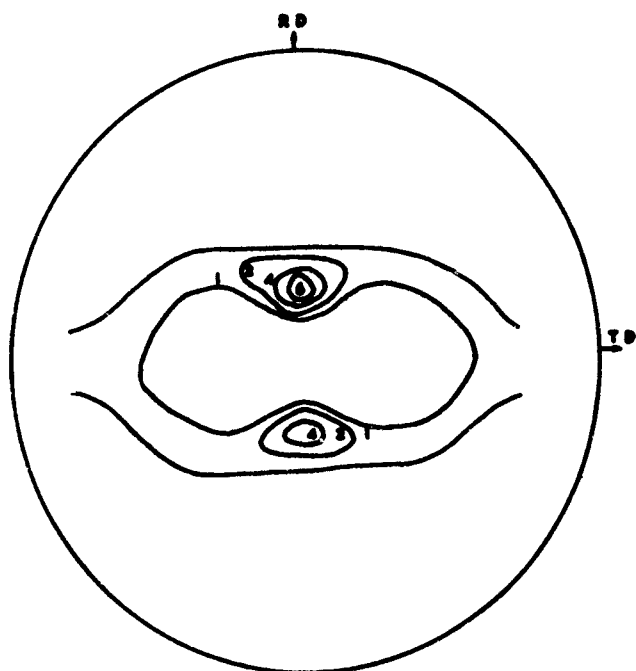
Fig. 44. {111} pole figure for thorium
rolled 95% at -196°C.
Intensities in arbitrary units.
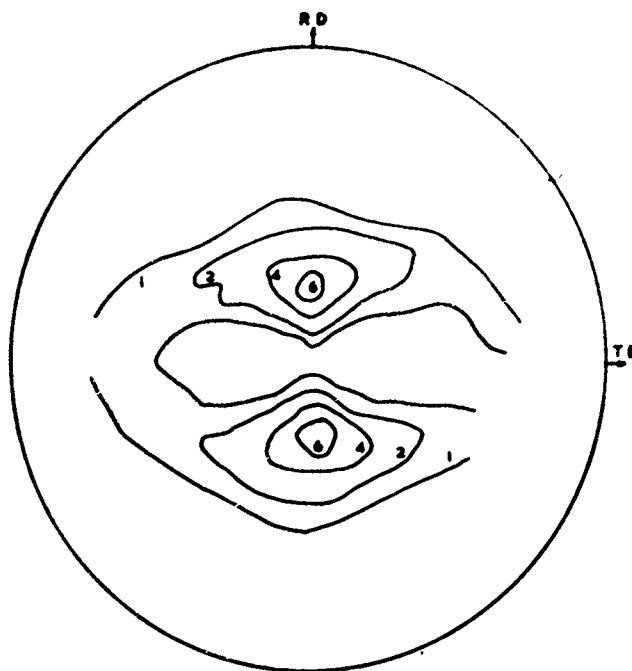
Fig. 45. {111} pole figure for
Carium rolled 95% at
room temperature.
Intensities in arbitrary
units.
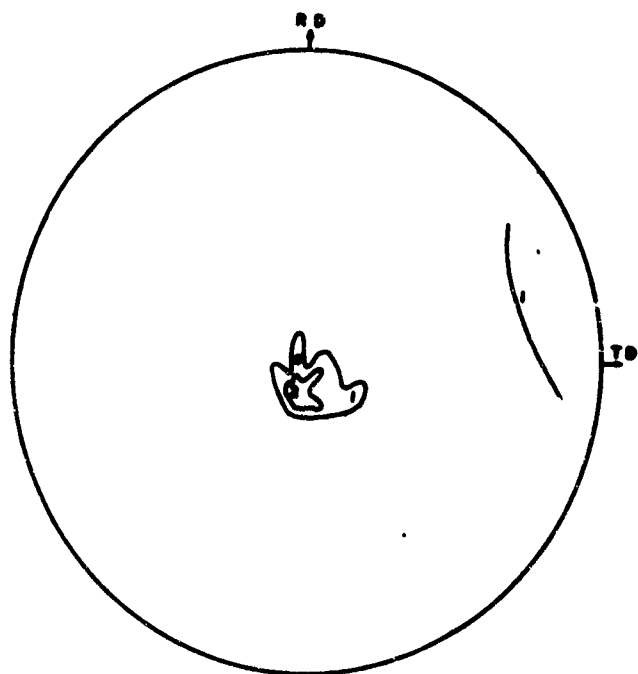
Fig. 46. {111} pole figures for 90%
cerium 10% thorium alloy
rolled 95% at room temperature
Intensities in arbitrary units.

Fig. 47. Electron Micrograph of
shadowed carbon replicas
taken from the surface of
annealed arium after
lightly scratching and
thermally cycling between
room temperature and -196°C.
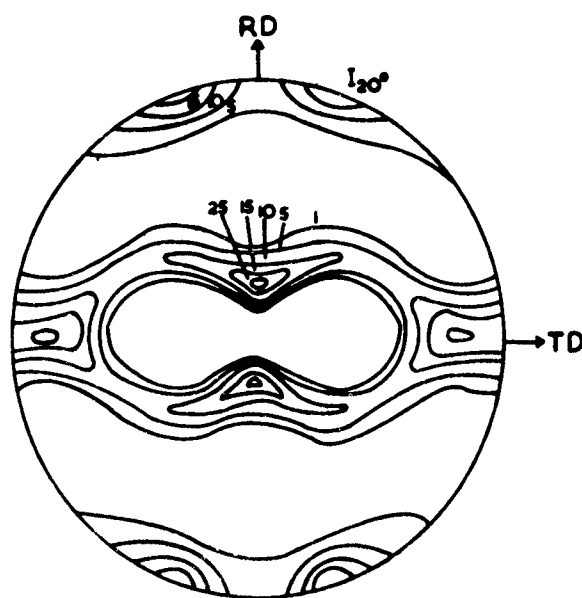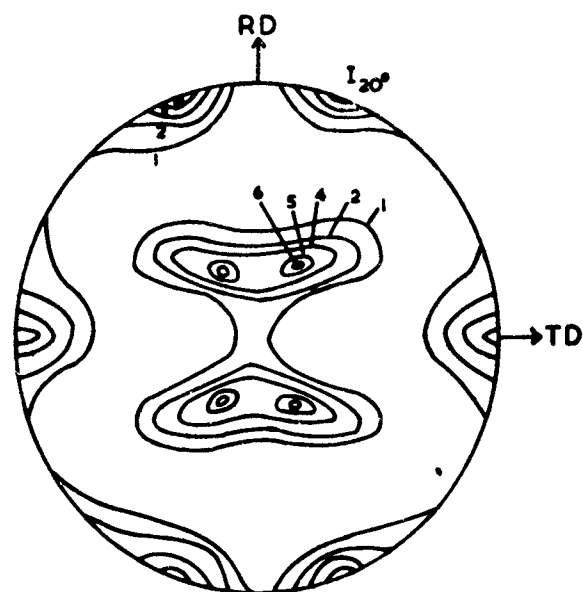
Fig. 48.   {111} pole figure of (a) 70/30 brass and (b) pure copper.
Intensities in arbitrary units.
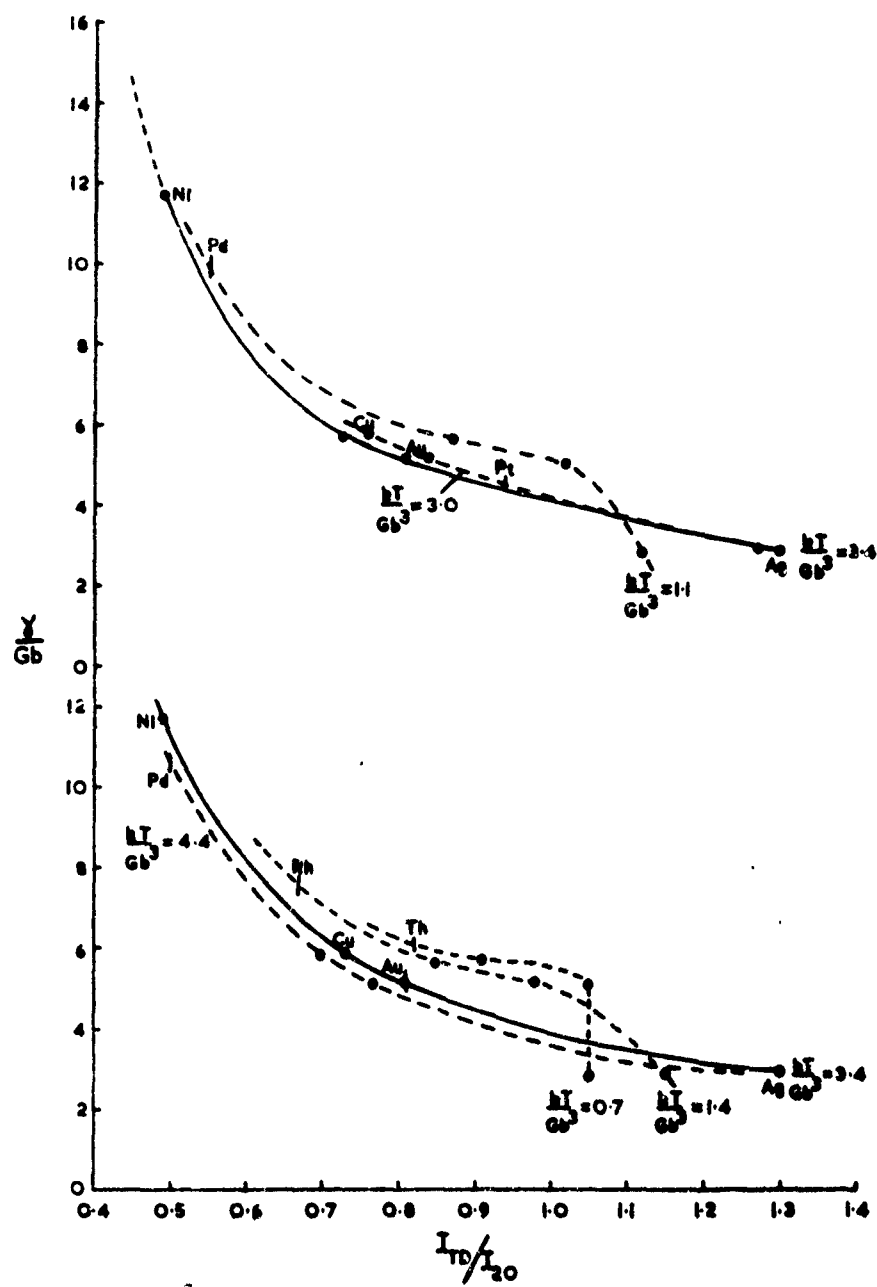
Fig. 49.   The variation of γ/Gb with the texture intensity ratio I_{TD}/I_{20}
measured at various values of kT/Gb^3.
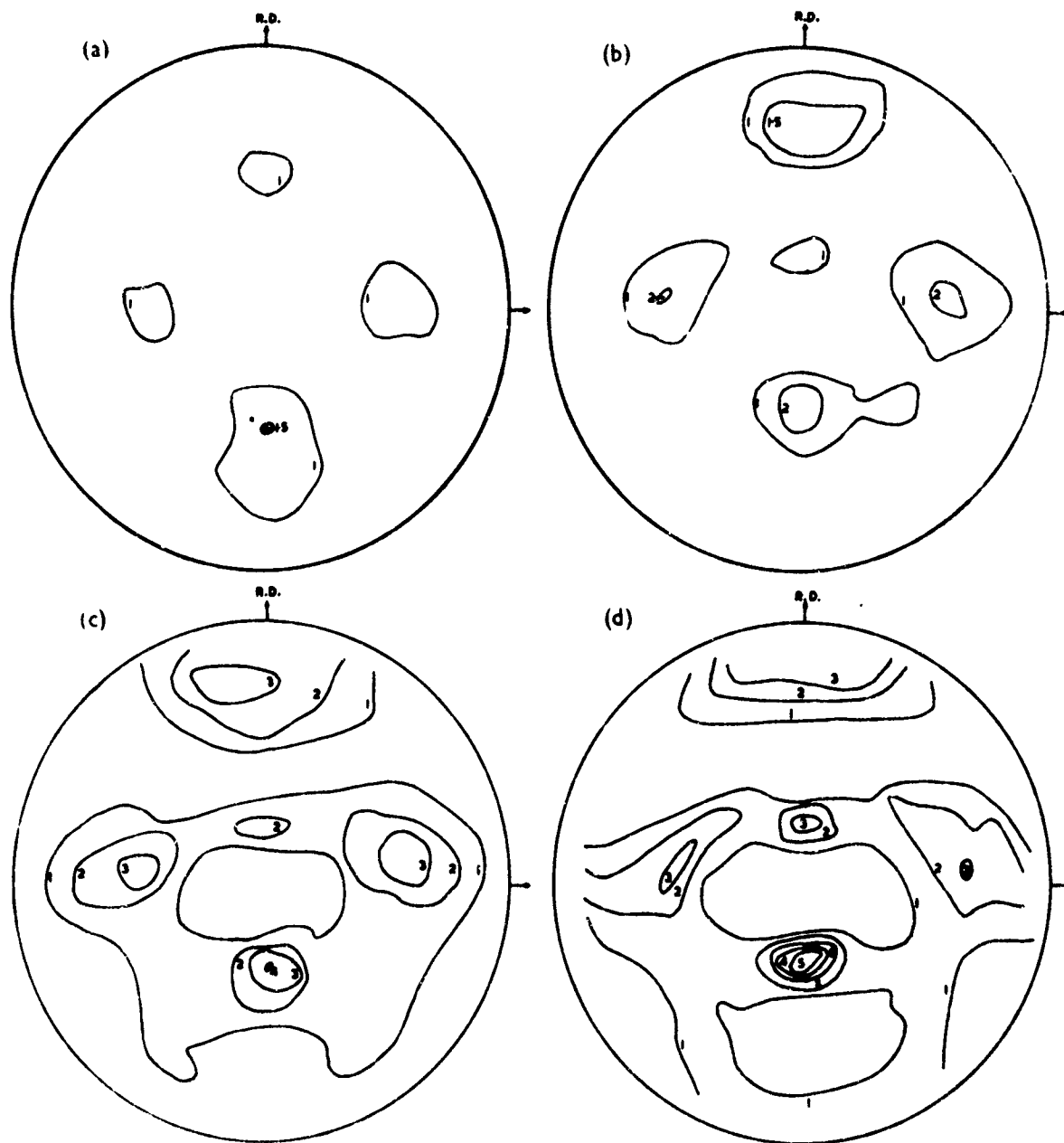
Fig. 50. (a-d).
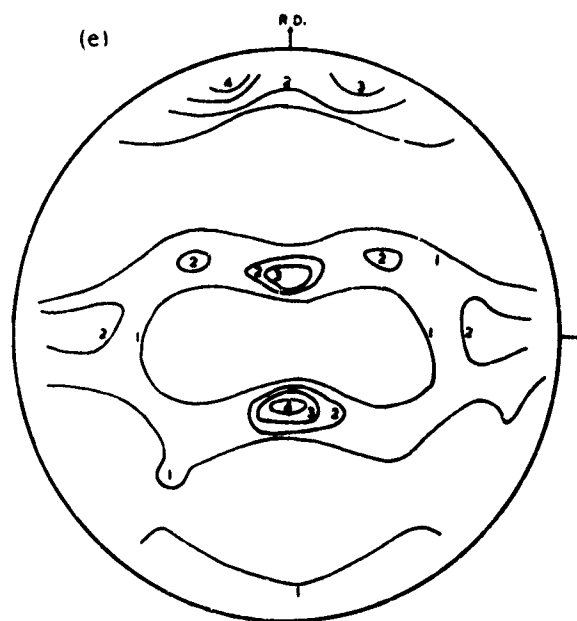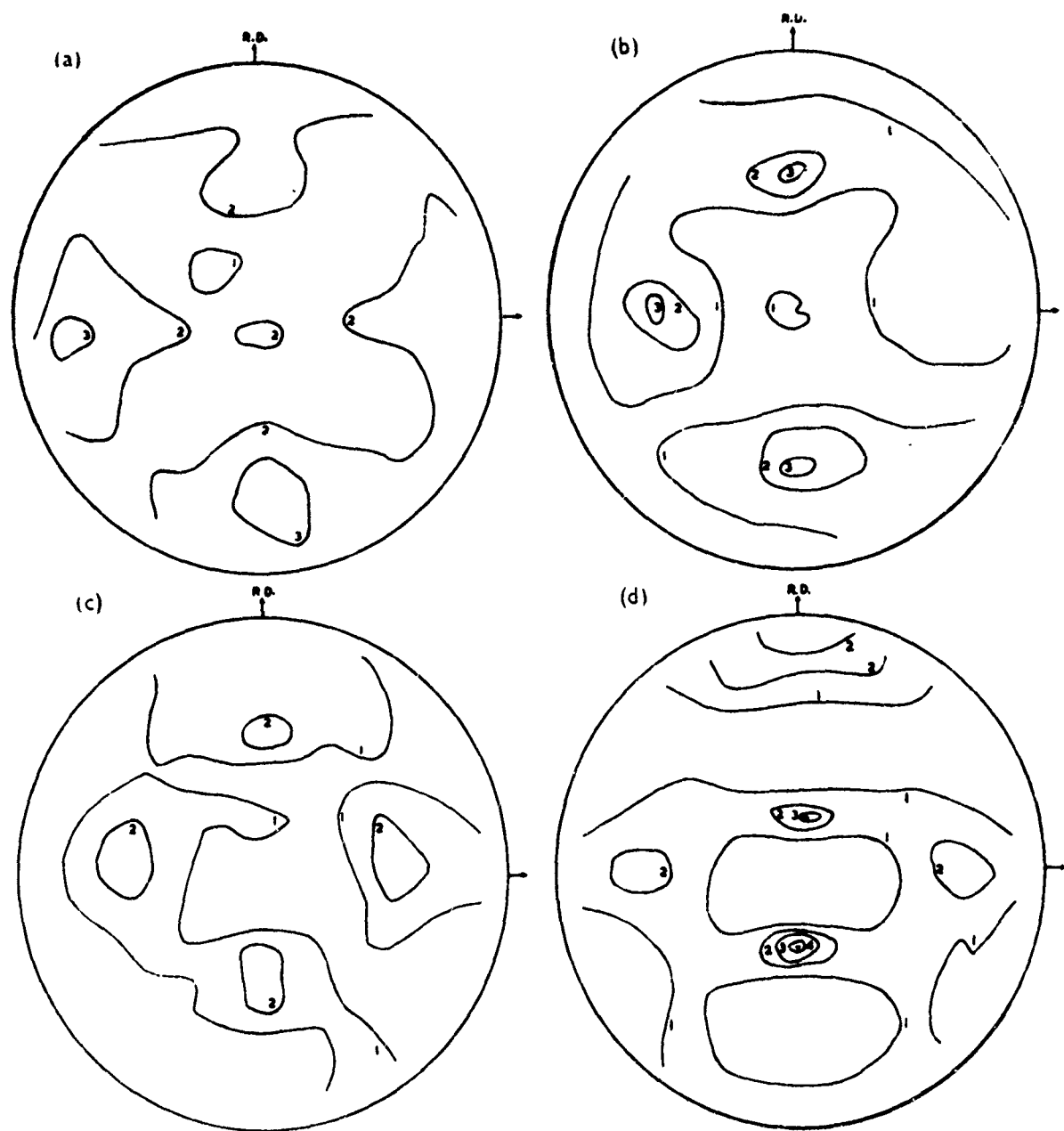
Fig. 50.   The {111} pole figures of aluminium rolled 92% unidirectionally at
           room temperature taking 0.04 in. passes, with paraffin in the rolls.
           The immediate surface texture is shown in (a) and the other
           figures relate to various distances below the surface:
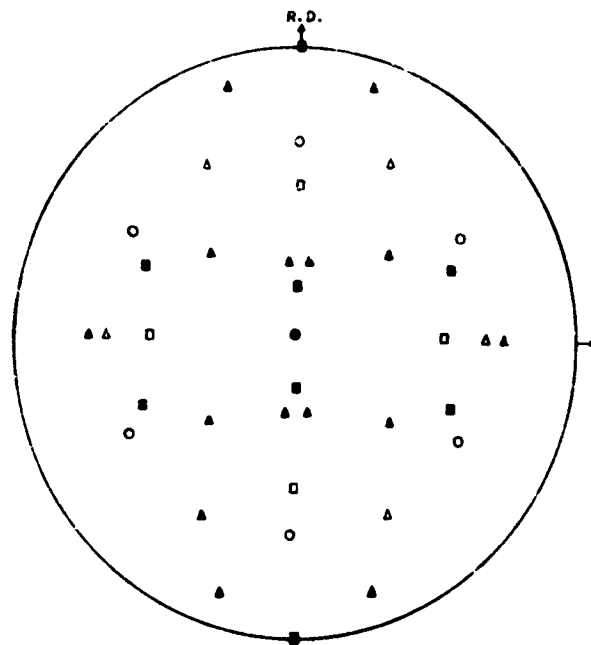   (b) 0.001 in.;   (c) 0.003 in.;   (d) 0.005 in.;   (e) centre texture.

Fig. 51. (a-d). The {111} pole figures of aluminium rolled 92% unidirectionally at room temperature taking 0.04 in. passes, with the rolls degreased and MgO applied to them. The immediate surface texture is shown in (a) and the other figures relate to various distances below the surface: (b) 0.005 in.; (c) 0.009 in.; (d) 0.013 in.

Fig. 52.   The {111} poles of ideal orientations:

◻ {100} ⟨01⟩   △ {111} ⟨011⟩

■ {112} ⟨111⟩   ▲ {135} ⟨211⟩

○ {111} ⟨112⟩

Open symbols denote surface components.
Cloud symbols denote centre components.
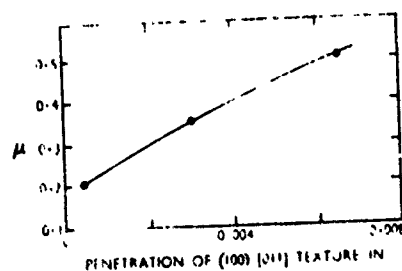
Fig. 53.   Coefficient of friction (μ) vs. the penetration of the (100)[011]
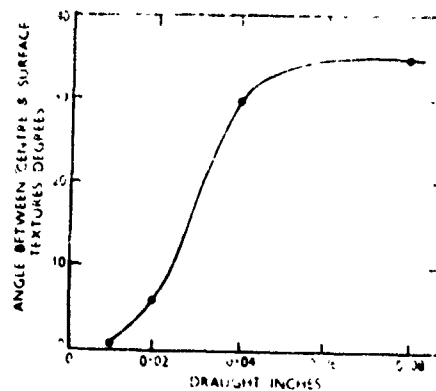texture for aluminium rolled 92% at room temperature.

Fig. 54.   Angle between centre and surface texture vs. drought for aluminium rolled 92% at room temperature μ = 0.2.
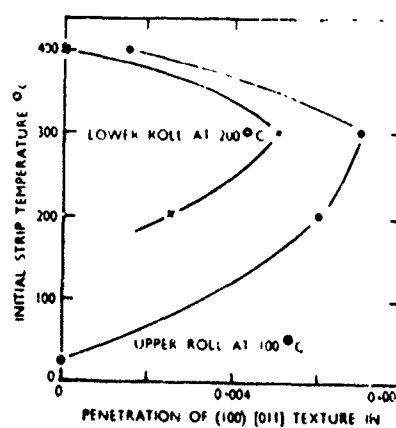

Fig. 55.   Penetration of the $(100)[011]$ texture vs. rolling temperature for aluminium rolled to 92% reduction in thickness.
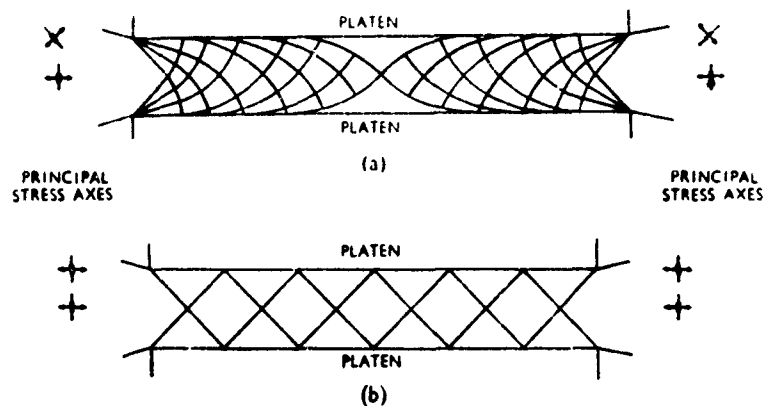
Fig. 56.   Slip-line fields for (a) completely rough platens; strip thickness:
platen breadth 1:6.6;   (b) zero friction; strip thickness; platen
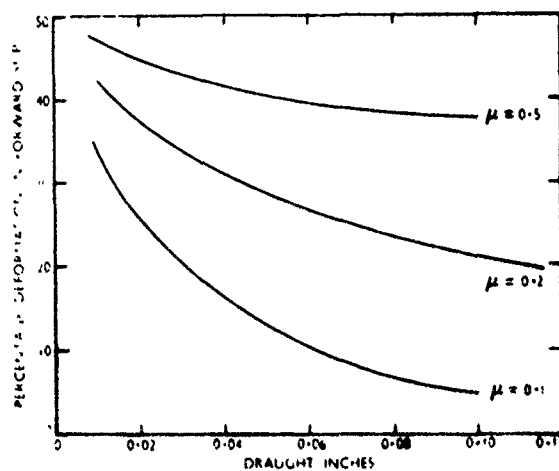breadth 1:6.

Fig. 57.   Plot of p vs.   h for three values of the coefficient of friction.
From equation (4).